The art of texturing glass for Photovoltaics

Processing and optical characterisation

Matthias Criel

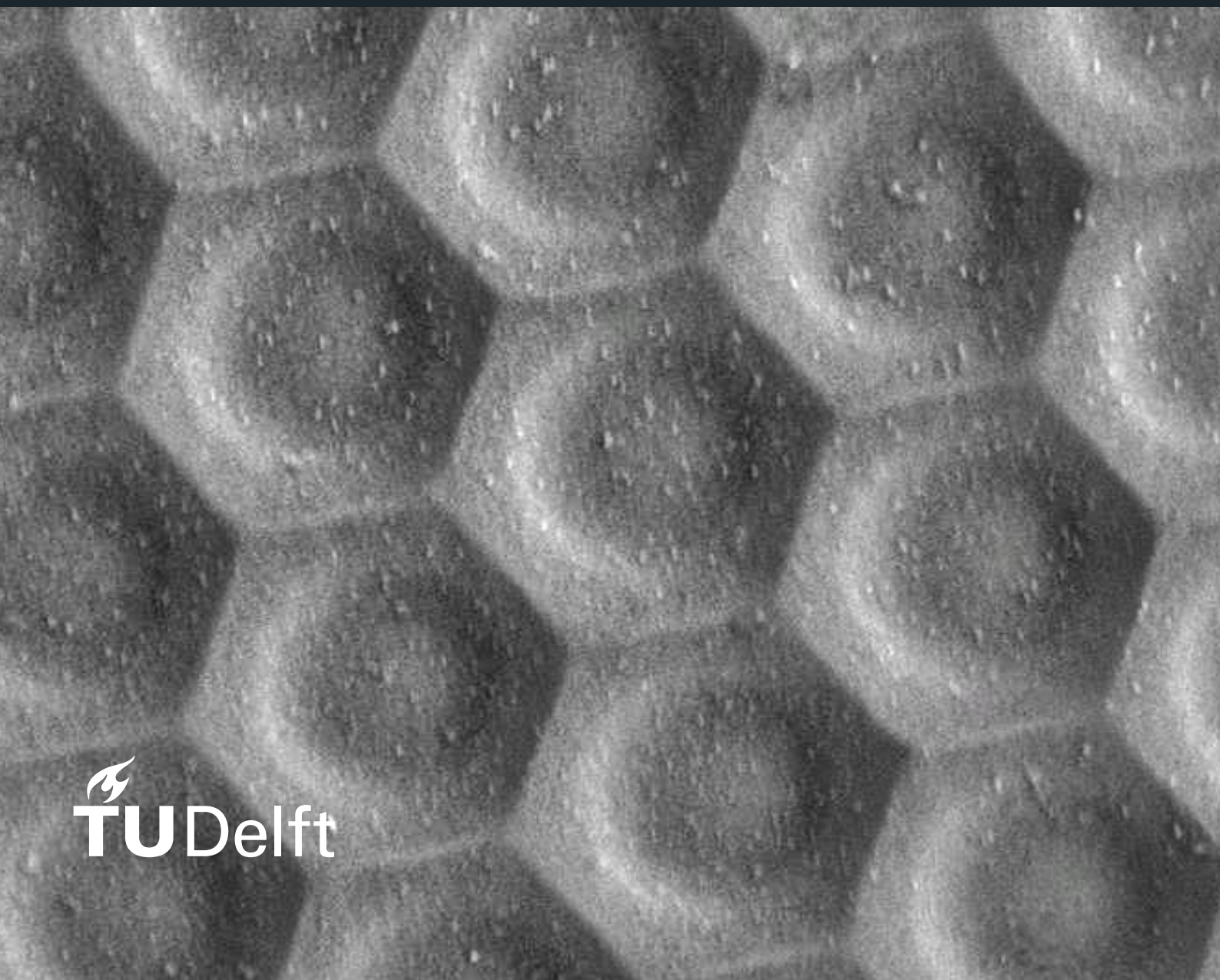

TU Delft

The art of texturing glass for Photovoltaics

Processing and optical characterisation

Thesis report

by

Matthias Criel

to obtain the degree of Master of Science
at the Delft University of Technology
to be defended publicly on June 27, 2023 at 14:00

Thesis committee:

Chair:	Prof. Dr. Ir. Arno Smets (PVMD)
Supervisors:	Prof. Dr. Ir. Arno Smets (PVMD)
	Ir. Govind Padmakumar (PVMD)
External examiner:	Dr. Malte Ruben Vogt (PVMD)
	Dr. Simon Tindemans (IEPG)
Place:	Faculty of Electrical Engineering, Mathematics & Computer Science, Delft
Student number:	5524156

An electronic version of this thesis is available at `http://repository.tudelft.nl/`.

Preface

Before you start to read my work, I want to thank you for taking the time to read through my report. I spend the last 8 months working on this thesis with the goal to contribute something to the academic community but hopefully also to companies that are interested in the results to see how they can improve their processes itself. Just like every production process in a company, there is always room for improvement. This is exactly the same for this work but I tried my best to present you the best possible result. Of course, I didn't manage to present you this work all by myself. I got an enormous amount of support these 2 years from my family and parents who always believed in my and where there every step on the way. My grandfather was a bit of an inspiration to start this program so I am happy I can say to him that I finished this masters. Lorena Hendrix was my pillar of strength (or as they say in dutch: "rots in de branding") and my sunshine through this whole period which will remain this way for a long period of time. Of course all my friends (which I can call my family in the end) that I made here had a tremendous amount of effect on my personal development which made me become like an improved version of myself. This resulted in a tremendous amount of determination to deliver something that I am proud of even more.

Even though I didn't see my friends back in Belgium so much, they are always there for a laugh or a tear so I am very glad after 2 years I can still call them friends/ family.

I can't forget of course my supervisors who helped me on every step of the way and always found time in their schedules to provide me with feedback or a laugh. I thank the people and not the title they have because this sounds more sincere to me. I want to thank Govind Padmakumar, Gianluca Limodio for their daily insights and time. I want to give a special thanks to Daniel van der Plaats, Silvana Milosavljevic and Johannes van Wingerden from the EKL team because without them I wouldn't have been able to process my honeycomb textures. I want to thank Arno Smets for his knowledge and insights. Last but not least, I would like to thank Malte Ruben Vogt and Simon Tindemans for being present at my defense and taking the time to objectively asses my report.

Abstract

Thin-film silicon technology creates electricity out of micrometer thick silicon absorber layers, which makes this technology less material heavy compared to classic crystalline technology. This advantage can be further exploited with the transition towards flexible thin-film technology, where the non-modular cost can be further reduced compared to traditional crystalline solar parks ect. However, thin films have limited absorption coefficients at higher wavelengths which means the optical pathlength must be maximised to overcome this limitation. In literature, the highest efficiencies are obtained with the creation of periodic textures resulting in 10.2%, 12.7% or 14% for nanocrystalline, micromorph and triple junction silicon technology. All these cells are made on silicon substrates which means the back of the cell is textured but if the front side of the solar cell is textured, efficiencies can outperform the current holding records. A methodology is designed to create periodic micro-textures on Corning glass to improve the total absorption of lower energetic wavelengths. However, the creation of random micro-textures (Aluminum Zinc oxide- and Indium Tin Oxide sacrificial texturing)(AZO-/ ITO textures) is also researched because different methodologies exist and limited knowledge exists on which methodology results in the highest amount of scattering. Second, a comparison between random and periodic textures must be made. Both types of textures undergo optical- and physical parametrisation after which both aspects are correlated to each other to gain a deeper understanding of light management. For random textures, Haze-values between 93-86% are obtained. These high values are obtained because the created craters are characterised by an increased depth for identical crater widths. Second, each methodology has its characteristic depth-width ratio which explains the optical superiority of one (ITO textures). For periodic textures, Haze-values lie between 50-3% with a maximum obtained aspect ratio of 0.18 but the optical response is not comparable to random textures because diffraction is the dominant light management technique. Therefore Angular Intensity Distribution measurements must be performed, which resulted in the conclusion that the created ITO textures stay superior (also compared to literature) while the AZO textures have a similar performance compared to the periodic texture. This translates itself in a superior external quantum efficiency (EQE) of ITO from 800nm on. Between 600-800nm, the periodic textures are superior.

Contents

Nomenclature

List of Abbreviations

a-Si	Amorphous Silicon
AID	Angular Intensity Distribution
AZO	Aluminum Zinc Oxide
c-Si	Crystalline Silicon
EQE	External Quantum Efficiency
HC	Honeycomb
ITO	Indium Tin Oxide
MST	Modulated Surface Texture
nc-Si	Nanocrystalline Silicon
PECVD	Plasma Enhanced Chemical Vapour Deposition
RMS	Root means square
Si	Silicon
TCO	Transparent Conductive Oxide
UCL	University College London
XRD	X-ray Diffraction

List of Symbols

λ	Wavelength
R_D	Diffuse reflection
S_{al}	Auto-correlation length
S_c	Average profile height
S_{ku}	Kurtosis
S_q	Root means square rouhness
S_{sk}	Skewness
S_{tr}	Aspect ratio
T_D	Diffuse transmission
E	Bandgap
n	Refractive index
P	Power
R	Total reflection
T	Temperature
T	Total transmission
t	Time

List of Figures

List of Tables

1

Introduction

Today, it is common knowledge that rising global CO2 concentration is accompanied with global climate change and increased average temperatures. Although, the effects will be severe, the cost accompanied by this still holds a lot of uncertainty. The European Commission [1] predicts the cost could lead up to 4% of the European GDP. In this model, mainly coastal and river floods are considered. For example, a country like the Netherlands would have up to 7 billion of climate cost since 29% of the surface area lies below ”Normaal Amsterdams Peil” (around sea level of the North Sea) and 59% is sensible to floods [2].

Since, climate change also includes droughts, failed harvests, increased occurrence of extreme weather events, these costs could even be greater than these predictions. University College London researchers [3] updated climate-economy models and concluded the climate cost could rise up to 37% of the GDP in 2100. If lasting damages are excluded (which is usually applied in cost estimates), the cost lowers to 31% of the GDP. Although both predictions are highly different, they show that climate change can’t be neglected. To switch from a fossil fuel based society towards an electrified/ renewable fuel society, sustainable energy sources must be massively deployed. Since around 173 PW of solar energy strikes the earth’s surface at any moment, the deployment of solar parks could provide society with sufficient electricity for industry, domestic and transport purposes [4], [5].

In general there are 4 types of solar cells: PERC, monocrystalline cells, polycrystalline cells, thin film solar cells. Although the crystalline technology is dominant in society, thin-film technology has the potential of being massively deployed (gigawatt scale) in remote areas in the form of flexible thin films since the non-modular costs of thin film technology is significantly lower for remote areas, the abundance is higher and non toxicity of the resource materials is obtained. A significant difference between both technologies is their difference in active layer thickness. While c-Si technologies have thicknesses of around 300µm, thin-film technology implement thicknesses of around 3µm. Although this makes this technology less material intensive, the main reason for this technology to be thin is because it cannot rely on a diffuse based charge collection. This means the energy absorbed cannot be collected if the thickness of the absorbent layer becomes larger than a couple of microns. Light penetrating the layer is not directly absorbed but is a function of the traveled distance, which means that thin-film technology finds itself at a disadvantage. This problem can be solved by applying textures on the substrates on which the cell is deposited. The light upon interaction with the texture deviates from its straight path and gets scattered in all directions, which makes it possible to increase the total absorption and efficiency in the end. If this texture is applied on the layer upon which the light falls in (glass superstrate), the texture is most defined and the light scattering is the most efficient [6], [7].

Not every type of texture is as efficient in scattering light due to their difference in shape, height, width etc. , which is why high optical performing textures must be created and compared with each other and create high efficiency solar cells with. This work has the goal of creating textures that can efficiently scatter light where the focus is put on the higher wavelengths to reach higher efficiencies for p-i-n technology. The compatibility with cell-growth is also considered. This leads to the following research questions:

1. Which process parameters create strong scattering random textures on glass superstates and how do these parameter influence the scattering performance?
2. Which profile parameters influence the light scattering performance of the sample?

3. Is it possible to create reproducible periodic textures on glass superstrates? And how can their scattering performance be increased?
4. How does a texture scatter light on an angular level? And how are they from each other?
5. Does periodic texturing lead to a higher optical- and/or electrical performance in comparison with random texturing?

This work is divided into 4 parts, which starts from theoretical principles. Afterwards, the experimental based approach is explained how these principles are implemented in reality and how an optimised texture can be obtained. Last of all, the results and conclusions are discussed. Chapter 2 discusses the theoretical principles required to understand the optical principles of textures and basic concepts of solar cells. It ends with a subsection discussing the physical- and optical parameters used in this work. Chapter 3 discusses the general methodology of this work that leads to an optimal texture from an optical- and electrical perspective. Chapter 4 discusses 2 approaches that lead to the creation of random textures due to the deposition of a sacrificial layer on top of it. These textures are optically and physically assessed and compared to each other. The section ends with a cell deposition that proves the created textures result in an improved cell performance. Chapter 5 discusses an approach to create a periodic texture that involves a photolithography step. Since this is a newly developed method of creating textures on glass superstrates, the focus lies mainly on controlling/ understanding the process and secondary on optimising the outcome. The textures are also optically- and physically assessed to discuss its performance. After this, an actual cell is created on top of the texture to prove its feasibility. This chapter ends with a part that compares random- and periodic textures to each other.

2

Background study

2.1. Material background study

2.1.1. Silicon substrates versus alkali aluminosilicate glass substrates

Processing on alkali aluminosilicate glass (also called Corning Gorilla glass) substrates is the focus of this work, which means it differs from classic silicon (Si) or aluminum processing. Si atoms have 4 valence electrons in the third shell (3s and 3p), which means the atom can only chemically bond with 4 other atoms. In an inert atmosphere, different Si atoms can form covalent bonds with 4 other Si atoms where the 2 3s-orbitals and 2 of the 3 3p-orbitals are filled. This creates a sp_3 hybrid, where all bonds are 109.5° apart. Multiple bonds than create the unit cell from which the entire crystal lattice is made up, which creates the so called crystalline Si (c-Si) substrates (shown in figure 2.1). Since the material often contains impurities (atoms different from Si) but concentrations are negligible, the material is also referred as intrinsic c-Si [6].

The properties of the crystalline structure are important when micro-/ nano-scale textures are processed in the substrate. The crystal properties determine in how many different processing steps a texture can be formed (or if it is even possible) and the quality or smoothness of the structure. The pyramidal surface textures often used in industry adjust the light management in the standard mono-crystalline Si technology. These textures are created via an anisotropic wet etching process that targets the orientations having lower activation energy (different crystal orientations require different amounts of energy to break the bonds between atoms). Therefore chemicals such as KOH-, NaOH- or a Tetramethylammonium hydroxide (TMAH)- alkine etch are used in industry [6] [8].

For alkali aluminosilicate glass (amorphous material), this unit cell symmetry from which the material is build up is lacking. The definition of a amorphous solid or glass substrate goes as follows: ”Glasses are solids with local arrangements like crystals, but lacking translational symmetry”. The choice for corning glass with a composition of 10-25% aluminum oxide, >10% alkali and SiO_2 is made because the network modifiers give it superior properties for solar cell applications (such as compressive strength etc.) over the classic silica (SiO_2) for example. The use of anisotropic etchant loses its purpose since there are no crystal orientations and these commercial textures cannot be formed in this way. In this case, a method

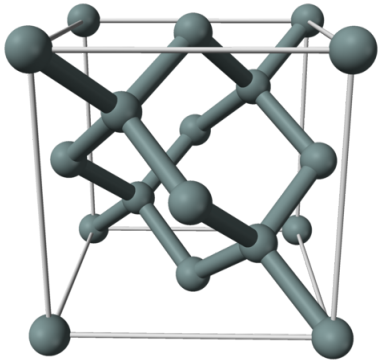

Figure 2.1: The unit cell of a pure single crystal silicon [6]

considering other chemicals involving HF or other processing steps such as photolithography must be opted for. This shows that processing steps must be adjusted to fit the material (as is seen in chapter) 5) [9] [8]. The datasheet of superstrates used in this work are included in the Appendix A.

2.1.2. a-Si:H versus nc-Si:H

The goal of a solar cell is to convert as much of the incident light into electricity. In this work, thin film solar cells are discussed which are implemented as a tandem stack of a nano-/ microcrystalline Silicon (nc-Si:H) layer and an amorphous silicon (a-Si:H) layer these days. This technology is not based on the classic p-n junction that makes use of diffusion principles to separate electron-hole pairs, but is a drift based technology introducing an intrinsic layer in which most light absorption takes place and the electron-hole pairs are generated. The separation of carriers is covered by the electric field generated by a nanometer thick n- and p-doped layer. To further ensure the separation is covered, a hydrogenation of the material is performed. Hydrogen atoms passivate the dangling bonds in the lattice, which gives separated carriers a lower chance to recombine before it gets collected.

a-Si is silicon with a continuous random network morphology. The bonds still form a tetrahedral coordination structure (identical to c-Si) but the angles differ from the perfect 109.5°, which makes it loses its crystalline lattice and creates dangling bonds. These dangling bonds create recombination centers and lead to a phenomena called ”Steabler-Wronski effect” that decreases the dark- and illuminated conductivity in function of the illumination time (until it stabilizes). Nevertheless, it remains an interesting material because of its high energy band of 1.7 eV (it leads to efficient absorption of the high energetic wavelengths). Plasma enhanced chemical vapour deposition (PECVD) is preferred as deposition technique and the material can’t make use of p-n type junctions for 3 reasons [10] [6]:

1. a-Si:H has a poor doping capability since the Fermi-level can only be partially pushed towards the valance or conduction band under heavy doping. For the c-Si technology, Fermi levels can be pushed towards both boundaries to make the comparison.
2. The doping of a-Si:H has a negative effect on the material quality since this introduces extra dangling bonds and increases the amount of recombination centers.
3. The diffusion length of the minority carriers is only 0.1 µm which makes it impossible to base the collection mechanism solely on diffusion.

Nc-Si has a morphology that exists out of grains with a crystal lattice of a couple nanometers big encapsulated by a-Si, which means it lies in between the crystalline and amorphous phase (in general around 60% crystallinity is taken as the nanocrystalline region). The advantage of this material is that it is not affected by the Steabler-Wronski effect, but the bandgap lies around 1.12 eV that leads to lower efficiency absorption. The reasons why nc-Si don’t work in a p-n junction, are similar to those of a-Si [10].

Since the focus lies on the glass substrate in thin film solar cells, the deposition follows a p-i-n configuration. To maximize the cells conversion efficiency, there must be as much light absorbed in the intrinsic layers so the conversion into electron-hole pairs is optimized. Therefore the cell must implement light management techniques, which help the light to be absorbed in the active layers. Second, this includes reducing absorption in neighboring layers and reflection losses for the cell simultaneously. Thin film technology relies heavier on effective light management techniques since the absorptive layers are thinner compared to classic c-Si technology (around 3 µm versus 300 µm). Second, thinner layers make the collection of carriers more efficient since the cell distances itself further away from the diffusion length. Before the characterisation of the possible texturing methods is performed, the theoretical background of the effect textures have on the optical performance of a surface is described [10].

2.2. Optical background study

2.2.1. Optical interaction at an interface

Electromagnetic waves traveling through space in all different directions can be described by the Maxwell equation:

$$(\frac{\delta^2}{\delta x^2} + \frac{\delta^2}{\delta y^2} + \frac{\delta^2}{\delta z^2})\zeta - \frac{n^2}{c_0^2}(\frac{\delta^2 \zeta}{\delta t^2}) = 0 \tag{2.1}$$

ζ describes the electric field, c_0 describes the speed of light in vacuum, n describes the refractive index and t describes the time. If the spectrum comes in contact with a solar cell, there exists an interaction of the

light with the interface of the cell, which can be described by the Snell's law. At the surface, the assumption of a non absorptive media is justified since the light is only able to be reflected or transmitted. Refractive indices of different layers can be considered as coefficients without an imaginary part due to this fact. In addition, the incident angle and reflected angle of the light are identical independent of the interfacing materials. Coefficients n_1, n_2 are refractive indices of interfacing layers and θ_i,θ_t are the refracted- and incident angles, which leads to Snell's law [6]:

$$n_1 sin(\theta_i) = n_2 sin(\theta_t) \tag{2.2}$$

Since the outcome is the refraction angle, the optical path in function of time/ angle can be determined for flat surfaces because the geometrical path length and refractive index are known and is described in the following equation:

$$l_o = \int_s n ds \tag{2.3}$$

For textured surfaces the refraction angle changes also for the lateral directions (changing incident angle) and interactions between light and textures could occur, causing scattering based on the size of the textures (which will be further discussed in 2.2.3.3). Apart from the equations defining the optical path, a fraction of the light gets reflected which decreases the photon flux entering the material. This is described by Fresnel equations that defines the reflectivity and transmittance at an interface of 2 different material while considering the type of polarisation the light contains (parallel polarisation= *p*, perpendicular polarisation= *s*) [6].

$$r_s = \frac{n_1 cos(\theta_i) - n_2 cos(\theta_t)}{n_1 cos(\theta_i) + n_2 cos(\theta_t)}, r_p = \frac{n_1 cos(\theta_t) - n_2 cos(\theta_i)}{n_1 cos(\theta_t) + n_2 cos(\theta_i)} \tag{2.4}$$

$$t_s = \frac{2n_1 cos(\theta_i)}{n_1 cos(\theta_i) + n_2 cos(\theta_t)}, t_p = \frac{2n_1 cos(\theta_i)}{n_1 cos(\theta_t) + n_2 cos(\theta_i)} \tag{2.5}$$

Solar irradiance is an unpolarized source of energy and implies the equation 2.4 is simplified to the quadratic average of both types of polarized light. From the reflectance, the transmission is calculated under the assumption no absorption occurs (which complies with the assumption at the interface) [6].

$$R = \frac{1}{2}(r^2_s + r^2_p) \tag{2.6}$$

$$T = 1 - R = \frac{n_2 cos(\theta_t)}{2n_1 cos(\theta_i)}(t^2_s + t^2_p) \tag{2.7}$$

If the interaction between the refractive indices is further observed, a decreased index creates a phenomena called "total internal reflection". For $\theta_i > sin^{-1}(\frac{n_2}{n_1})$, the values of equation 2.4 become complex which results in a total reflection R equal to 1. Nothing gets transmitted anymore and it is completely reflected in the medium. The light is than fully absorbed by the cell and it results in an increased photo-current density under the assumption no parasitic absorption occurs. The angle to which $\theta_i = sin^{-1}(\frac{n_2}{n_1})$ is called "critical angle". Notice if the refractive index increases, values of equation 2.4 remain positive for all angles and the phenomena doesn't occur [6].

2.2.2. Optical interaction in the active layer

Another aspect is the mechanism the active layers uses to absorb the light. This still requires the optical characteristics of the layer such as the refractive index which is defined by the complex electric permittivity. The link with the refractive index is made with a square root relation:

$$\epsilon_{complex} = \epsilon' + i\epsilon'' \tag{2.8}$$

$$n_{complex} = n + i\kappa \tag{2.9}$$

If the Maxwell equation for sole z-axis propagation is considered, including the complex refractive index, an electric field gets diminished exponentially in function of the depth. The electromagnetic field is also related to the electric field, which means the intensity of the incident light also gets diminished in function of traveling distance. This leads to the Lambert-Beer law that defines the attenuation of the intensity of light inside a medium [6]:

$$I(z, \lambda) = I_0(\lambda) \exp\{-\alpha(\lambda) z\} \tag{2.10}$$

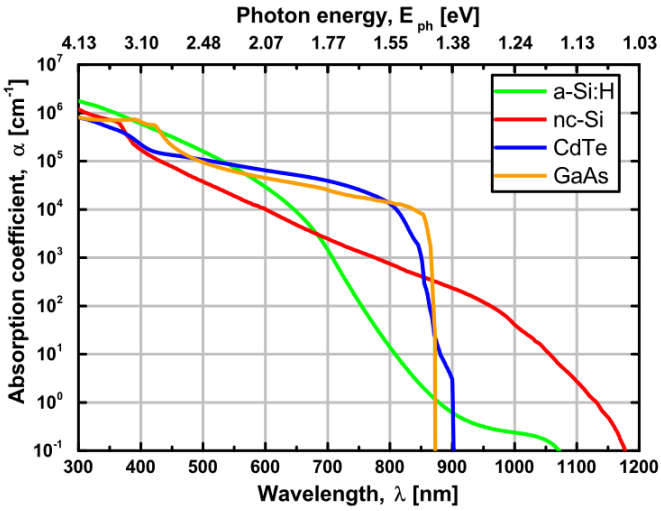

Figure 2.2: The difference between amorphous and nanocrystalline in terms of absorption coefficient and direct- (such as CdTe/ GaAs) or indirect bandgap materials (Silicon based structures [11])

In this formula, the absorption coefficient α defines the rate at which the light get absorbed and is correlated to the complex part of the refractive index. The inverse of α is defined as the penetration depth δ_p and defines the depth at which the light intensity is reduced to 1/e of its initial value. The absorption coefficient is function of wavelength λ and differs depending on the crystallinity of the material and the absorption mechanism of the material (shown in figure 2.2). Direct bandgap materials have a higher absorption coefficient since the momentum of the light does not have to change to be absorbed, lower traveling distances are required to absorb all the incident light. The disadvantage to cope with, is the increased recombination speed since it electron- hole pairs fall back easier. Since silicon does not face this problem, the focus is set on silicon structures. The dependence on crystallinity is why for example nc-Si and a-Si are placed in tandem stack. a-Si has a higher absorption coefficient for the higher energetic wavelengths, while nc-Si does so for the lower energetic wavelengths. The thickness of the active layers in the cells lie in the order of 3 µm, which means the optical pathlength must be maximised implementing light management techniques and this is addressed in the following section [6].

2.2.3. Light management

As mentioned before, the optical pathlength of the light must be increased for thin-film technology but this is not the only purpose light management serves. It serves the purpose to minimize all types of optical losses including thermalization, non-absorption, reflection, parasitic absorption, not-complete absorption and surface shading. The techniques to minimise this are divided in 3 categories:

- Decreased spectral mismatch
- Decreased losses of non-active layers.
- Increased absorption in active layer

Decreased spectral mismatch

Light management plays a role in increasing the spectral utilisation, since it can affect the 2 fundamental losses reducing the performance: thermalization and non absorption. The active layer used in thin-films is characterized by a bandgap E_g, which defines the minimum energy that is required to create an electron-hole pair and push an electron from the valence band to the conduction band. If the energy from a part of the solar spectrum is lower than the required bandgap energy ($E_\lambda < E_g$), no electron-hole pair is formed and this part is not utilised. This effect is called ”non absorption”. If the energy is greater than the bandgap energy of the semiconductor ($E_\lambda > E_g$), an electron-hole pair is formed. Since the photons contain more energy than actually required by the layer, the electron gets pushed deep into the conduction band. Afterwards, this excess energy is released in the from of heat due to its higher metastable nature compared to an electron that is situated lower in the conduction band. This effect is called ”thermalization”.

For example, a c-Si absorbing layer loses almost 50% due to spectral mismatch, which is shown in figure 2.3.

Light management comes in at the aspect of multi-junction solar cells. Different materials with different bandgaps E_g are stacked on top of each other. Lower losses are obtained by stacking multiple layers on top of each other. In this way less energy is lost due to these phenomena. For example: stepping from a nc-Si (E_g around 1.2 eV) cell to a micromorph cell containing a-Si (E_g around 1.75 eV), the thermalization in nc-Si reduces since the amorphous layers on top contains a greater bandgap [6].

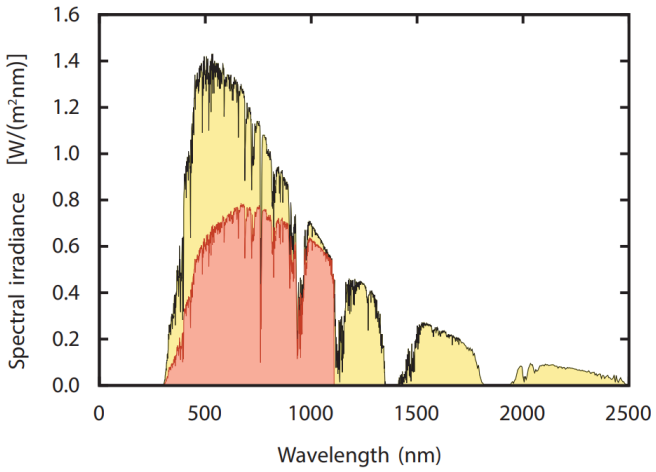

Figure 2.3: Thermalization and non absorption losses shown for a c-Si absorbing layer [6]

Decreased losses of non-active layers
Light management plays also a role in decreasing the losses in the non-active layers. This is performed by selecting non-active layers containing low absorption coefficients in the range the active layers absorb light, by implementing anti-reflection coatings (ARC) or by the texturing of surfaces. ARC uses an intermediate layer between the interface of 2 mediums, which results in a lower total reflectivity based on the Fresnel equations or constructive and destructive interference of light. Since this method lies outside the scope of this work, it is not further discussed [6].

Texturing a surface is a second way to decrease the total reflectivity of a surface for which the size of the features is important. The idea behind it, is that the light has a higher chance to penetrate the material and deviates from its original short optical path-length. Scattering effects are divided into 3 different categories: macroscopic scattering, Mie scattering and Rayleigh scattering. Textures are considered as macroscopic, if the scale of the surface feature are larger than the wavelength of the incident light (nd>λ). The changing amount of reflection and transmission are completely defined by the Fresnel- and Snell's equations (2.4,2.2,2.5) and also define what is called the "geometrical limit". These textures help to couple in the wavelengths reflected at the interface, this interaction is shown in 2.4 and decreases the total reflection of a surface. If compared to a flat surface, the amount of reflection is lower in every case. Second, structures with an increased inclination angle increases the amount of light in-coupling due to the fact that wavelengths with increased refracted angles still get a second chance to be transmitted [6].

For Mie- and Rayleigh scattering, the theory is not based on previously mentioned laws. For Rayleigh scattering, the particles must be much smaller the the incident wavelength, which implies there should not be a noticeable difference in the phase of an electric field around the feature. This quantifies itself in the following equation for a particle and interface interactions:

$$Particle : \frac{2\pi d}{\lambda} << 1 \tag{2.11}$$

$$Interface : nd << \lambda \tag{2.12}$$

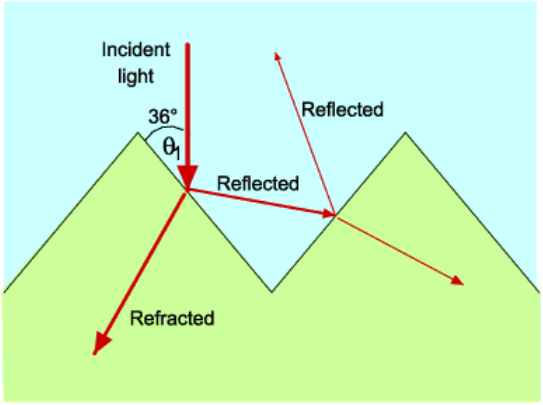

Figure 2.4: Example of the interaction of light with a macroscopic pyramid structures on a transparent layer

If this criterion is satisfied, the power radiated by the particle or interface is described by equation 2.13. The abbreviation for which this equation is obtained, lies outside the scope of the scope of this project, but the insights it gives are interesting.

$$\sigma_{scattering} = \frac{2\pi^5 d^6}{3\lambda^4}\left(\frac{n^2-1}{n^2+2}\right)^2 \tag{2.13}$$

The scattered power is dependent on the difference between refractive indexes of the 2 mediums. If the difference increases, the scattered power increases. This is the opposite to what Snell's law describes to minimize the reflection at the surface. The power differentiates in function of the angle with its maximum directed along to the propagation vector of the incident wave. The feature size is proportional to the particle size to the order 6, which means smaller particles have better scattering properties. It is also inversely proportional to to the incident wavelength, which implies high energetic wavelengths have better scattering properties [12].

For Mie scattering, the solution is generalised and also describes the scattering of an electromagnetic wave at an homogeneous particle/ interface with a different refractive index. Just as Rayleigh scattering, the phenomena can be described by the Maxwell's equation (see equation 2.1, which means it is not an independent theory. Solutions are obtained for a large range of feature sizes, such as for dust, rain drops etc. The differences with Rayleigh scattering are shown in figure 2.5. Its pattern is more directive and is scattered in smaller angles. This implies the lower energetic wavelengths (infrared) follows the Mie scattering properties easier than the higher energetic wavelengths of the AM1.5 spectrum (UV-light) that follows the Rayleigh pattern more easily [12]. If all 3 phenomena are considered in the design of the texturing of non-/ active layers, a complete understanding of the reduced reflection is obtained and optimized textures can be processed.

Increased absorption in active layer

After deciding upon the material used as active layers and a maximisation of energy reaching the active layer, as much light must be transformed into electron-hole pairs. This is performed by light trapping techniques that have a goal to keep as much energy trapped in the active layer, so it can be absorbed according to the Lambert-Beer's law 2.10 [6]. In general, there are 4 different techniques that can be combined to optimize the light trapping capability of the layer:

- Front surface light-in coupling: It is identical to the mechanism described in the previous subsection and tries to reduce the total reflection at the interface of the active layer.
- Intermediate reflectors: It is only used in tandem devices and gets placed between 2 active layers (for thin film in between the a-Si and nc-Si layer). By changing the thickness, the amount of light reflected and transmitted can be controlled, which relies on diffraction phenomena (constructive and destructive interference) that are not further discussed in this work (out of scope of this work).

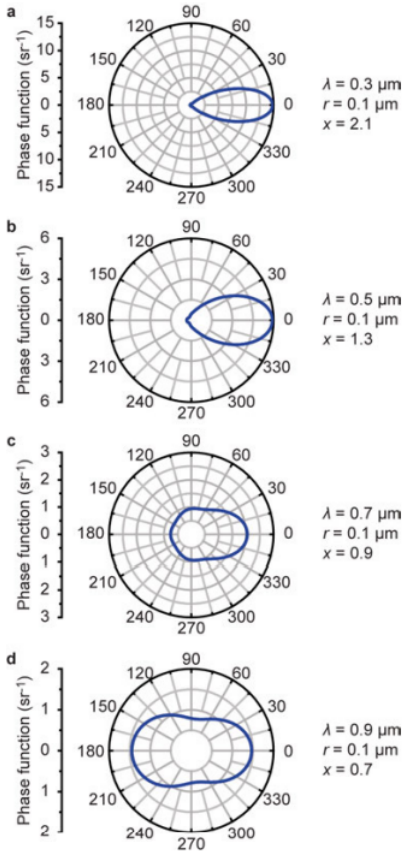

Figure 2.5: The difference in scattering pattern for a changing wavelength. Depending on the wavelength, the scattering patterns follows more a Rayleigh- or Mie scattering pattern [12]

- Back side reflection: It reflects light back into the cell so it can be absorbed again by the active layer. Since this lies outside the scope of this work too, it is not further discussed.
- Scattering at interfaces: It is identical to the mechanism described in the previous section and tries to increase the optical path length of the transmitted wavelengths so according to the Lambert-Beer law (see equation 2.10) a larger portion of the light is absorbed.

The last bullet-point describes scattering at an interface of a random texture because light phenomena such as light interference etc. do not occur. A second part of this work is to create periodic textures that have a high optical performance too. This results in the fact that interference effects also play a part in the optical behaviour, which is best explained by introducing the concept of light diffraction. Light can be represented as a wavefront that joins all points of the wave describing the same phase. When a parallel wavefront comes in contact with a partially blocked screen with narrow openings, this opening acts as a point source from which a secondary wave advances the wave front in the form of concentric circles. These secondary sources arrive at the receiver with different amplitude and phase which results in a temporal and spatial variation of amplitude and phase.This is understood as ”diffraction” [12].

In light trapping schematics, it is common knowledge that a maximum enhancement factor of $4n^2/sin^2(\theta)$ is achievable, where n represents the refractive index and θ represents half of the absorption cone. For a Lambertian scatterer, the optical response is isotropic and this angle is equal to 90°, which implies that the scattering intensity is independent of the angle. This results in a limited maximum enhancement of $4n^2$, which is also known as the ”Yablonovitch limit”/ ”bulk limit”. It must be noted that this limit holds for certain assumptions from which only the important ones for this work are discussed. First, there is assumed the film thickness of the cell is much larger than the wavelength. Second, there is assumed that the random roughness or grating of the texture is much greater than the wavelength. In this second assumption, periodic- and random textures reach an identical enhancement of the light trapping. Both assumptions ensure that interference- and diffraction effects are weak and the problem can be solved as a ray-tracing

problem. The proposed periodic textures have the purpose of introducing diffraction effect, which implies that this bulk limit is not applicable anymore and an increased enhancement for period gratings can be obtained that exceed the performance of random textures [13]. The enhancement factor is calculated according to the following formula:

$$F = \frac{A}{\alpha d} = \frac{2\pi\gamma_i M}{\alpha d \Delta\omega N} \tag{2.14}$$

In this equation, α represents the absorption coefficient. Maximising the enhancement factor is determined by the free space properties such as the number of plane wave channels accessible (N) and the layer itself for the number of resonances (M). For films that are a couple wavelengths thick, the number of resonances over a broad spectrum of wavelengths does not change much. This means the periodic textures affecting the number of channels in the free space must be maximally affected. For in-depth information about the calculations, the journal article itself can be read through. For example, for 2D gratings (such as HC-textures) the enhancement factor can be increased to $8n^2\pi/3^{1/2}$ [13]. This explains why an investigation into periodic textures is performed which can reach increased absorption values exceeding the one of random textures.

2.3. Physical and optical parametrisation

The objective of this work is to design high optical performant glass superstrates (texturing) on which high quality nc-Si can be grown. This implies the right parameters characterising the surface must be in place from a physical and optical point of view. Since glass superstrates are transparent, there are twice the amount of parameters that can be measured because both sides of the material interact with incident light. Transmittance measurements are generally not applicable for thick crystalline materials because they are highly opaque and transmittance values are negligible to non existent. For example, a textured c-Si substrate can be optically characterised only in reflectance because it is opaque. Second, there are a significant amount of parameters describing a surface (Sz= max height, Sa= arithmetical mean height, Std= texture direction, Sal= autocorrelation length etc.) and the same parameters can also be determined for the line roughness. Since the characterisation must be concise, only the parameters holding the most information are considered.

2.3.1. Physical parametrisation

In literature, the most used parameters are root-mean-square roughness (S_q), auto-correlation length (S_{al}) and aspect ratio (S_{tr}). Isabella et al. [14] and Guangtao et al. [15] both use these parameters to describe the surface. The parameters are described in the list underneath:

The root mean square roughness (S_q) calculates the root mean square of the height values (z(x)) over the entire sampling length (1- or 2 dimensional). It is preferred over the average roughness (S_a) because it is correlated to the optical quality of the described texture. The average profile height S_c is a similar parameter but it calculates the mean height of the entire profile instead of calculating the roughness compared to the reference line [16].

$$S_q = \sqrt{\frac{1}{l}\int_0^l z^2(x)\,dx\}} \tag{2.15}$$

The auto-correlation length (S_{al}) is described as the distance parallel to the surface of the auto-correlation function which has the fastest decay compared to a value s (lies in between 0-1 and is taken at 0.2 for smooth surfaces). The auto-correlation function relates the surface heights (z(x)) to an identical surface described by parameters (t_x,t_y). A high value correlates to a surface having textures with a low spatial frequency (lower values identify the opposite). It is a measure for the width of textures on a surface by which the texture is still statistically different from the original location [16].

$$S_{al} = min\sqrt{tx^2 + ty^2} \tag{2.16}$$

The texture aspect ratio (S_{tr}) is calculated as the height/ depth of the textures divided by the periodicity or width of the textures (similar to correlation length), based on the fact if the textures are periodic or random. In this work, S_{tr} is calculated based on S_c because it gives a better representation of the actual depth of

the creater but it is also possible to use S_q. Except from these 3 parameters used in previously mentioned papers, 2 extra parameters must be introduced to describe how peaked the surface profile is and how much the textured surface differs from a flat surface [16]. These 2 parameter are called: Kurtosis (S_{ku}) and Skewness (S_{sk}).

The Kurtosis (S_{ku}) is a measure to describe the sharpness of the height distribution and is calculated by considering the mean of the fourth power of the height values and the fourth power of the root mean square roughness (presented in equation 2.17). If the height distribution can be described by a Gaussian distribution, the value is equal to 3, while a peaked height distribution reaches values higher than 3. Second, the parameters also describes the spikiness of an area, such that low values (lower than 3) describe a smooth surface. The only disadvantage of this parameters is that it cannot differentiate peaks and valleys. A visual representation of this parameters is shown in figure 2.6 [17].

$$S_{ku} = \frac{1}{Sq^4} * \frac{1}{l} \int_0^l z^4(x)\, dx \tag{2.17}$$

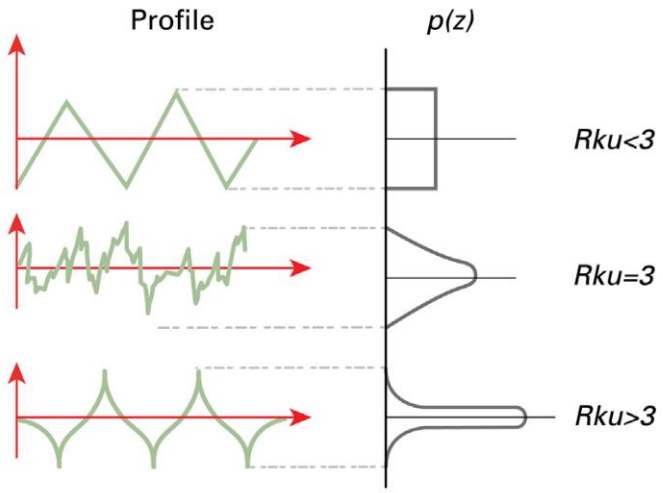

Figure 2.6: The physical interpretation of Rku [16]

The Skewness (S_{sk}) is a measure for the texture symmetry deviations between the part above and below the mean reference line. It is calculated as the ratio between the mean of the third order of the height values and the third order of the root mean square roughness. Since it only considers the third order of the profile, it cannot say anything about the spikiness of the profile (the kurtosis (R_{ku}) describes the spikiness) but its value is influenced by individual peaks and valleys. For negative values, the bulk material finds itself above the mean line, while for positive values it finds itself below the mean line. It is possible to interpret this value as a measure for the flatness of the surface and its deviation from ideal pyramidal texturing patterns with identical heights. A visual representation of this parameter is shown in figure 2.7 [16] [18].

$$S_{sk} = \frac{1}{Sq^3} * \frac{1}{l} \int_0^l z^3(x)\, dx \tag{2.18}$$

2.3.2. Optical parametrisation

In literature, different parameters are used to asses the optical quality of a surface such as Reflectance (R), Total transmission (T), Diffuse reflectance (R_D), Diffuse transmission (T_D), Haze and Angular Intensity Distribution (AID). The first 5 parameters are commonly used in literature and are therefore not discussed in-depth in this work [14].

First, T_D is defined as the amount of the incident light that gets transmitted in a diffuse way. Second, R_D is defined as the amount of light that gets reflected in a diffuse way. Third, Haze is a parameter that can be defined for Transmission and Reflectance. In this work, the parameter is only used for transmission and

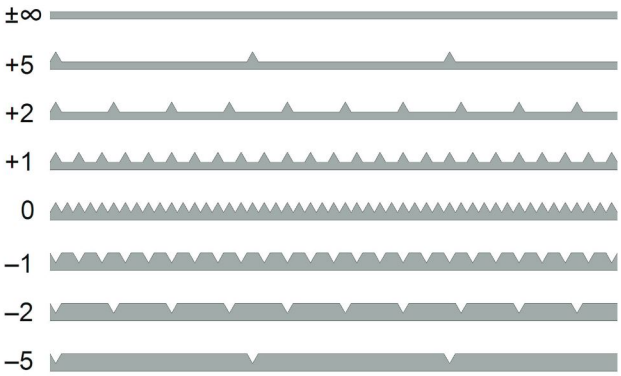

Figure 2.7: The physical interpretation of Rsk [18]

describes the amount of transmitted light that gets diffused and results always in higher values compared to T_D. The last parameter can be measured in 2 ways: Reflectance mode (AID_R) and Transmission mode (AID_T). In figure 5.2, a schematic is shown of the setup. Light gets radiated at an angle of 0° and the intensity can be measured over a range of angles [10-350°;1°]. Light intensities between 350° and 10° cannot be measured because the source itself is prohibiting it. Based upon the scattering properties light gets diffused in various angles. If angles in the 1st and 4th quadrant are measured, the AID is measured in Reflectance mode (AID_R), while quadrants 2 and 3 measured the AID in Transmission mode (AOD_T) [19].

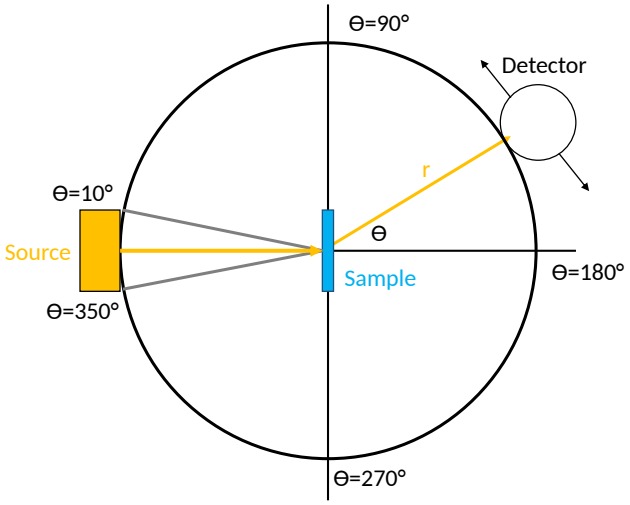

Figure 2.8: Representation of a measurement setup to measure AID in Transmission and Reflectance

Note: In this setup it is assumed that the scattering spectrum is identical/ symmetrical according to the altitude since the measurements are performed in a plane while scattering occurs in 3 dimensions. This assumption holds for random texturing because there is no preferred angle to scatter to. For periodic structures problems can occur because scattering profiles are not identical in function of the altitude (3rd dimension).

In this work, samples are processed to have textures on 1 side of the glass superstrate. This means

Table 2.1: AID can be measured for different relative positions between sample and detector because the sample is transparent. The detector can be placed in Transmission or Reflectance mode based on its quadrants and the sample can be placed with its flat or textured side facing the source.

Measurement mode	**Sample position facing source (Flat/ Textured)**	
Detector position (quadrants)	Flat	Textured
Reflectance position (1,4)	Reflectance-Flat (RF)	Reflectance-Textured (RT)
Transmission position (2,3)	Transmission-Flat (TF)	Transmission-Textured (TT)

sample and detector can be placed in 4 different modes described in table 2.1. Only measurement mode TF (marked in red) is useful because of the following reasons:

- Measurement mode RF is not measured because the interests lie towards how the sample scatters light and not so much on the reflectance of light.
- Measurement mode TT is not measured because it describes how light is transmitted if a textured surface is used as first interface in a solar cell. In this work, light falls in on a flat surface which makes measuring TT obsolete.
- Measurement mode RT describes how textures interact with light but as Zhou et al. **??** showed, the scattering of light is different for light seeing hills or craters. In this mode, the light sees the inverse structures which influences its scattering pattern (shown in figure 2.9). The diffuse part of the scattering profile is slightly different from 20° on (0.0001). Second, the specular component of the light is not included in RT (shown in figure 2.9) because the intensity of the light starts at 0.001.
- In this work, measurement mode TF is chosen as most suitable due to previously mentioned shortcomings of other measurement modes.

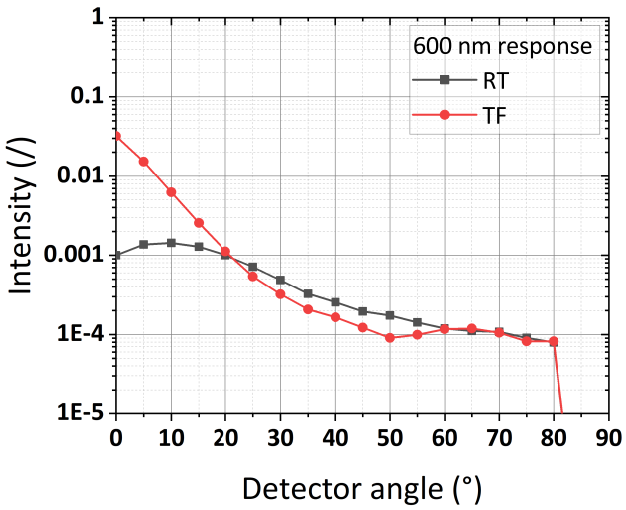

Figure 2.9: Difference in angular response between measurement modes RT and TF for an ITO sacrificial textured sample at processed 210W, 230°C for 7200s placed under an sample angle of 10° with a detector slit width of 1.6mm and measurement interval of 5°.

Optical measurement intervals

Next to the relative position between sample and detector, there rests still the aspect of measurement intervals and slith widths. Jäger et al. [19] describes the effects source and detector slits have on measurements. Increasing one of both increases the incident light intensity, which makes it easier to measure the scattering response. The disadvantage of increasing the source slit size, is the reduced spectral resolution. The disadvantage of increasing the detector slit size, is the reduced angular resolution and details in the scattering patterns fade. In the first instance, there must be opted for increased detector

slit size before changing the source slit because it is tougher to change it yourself and scattering peaks are broadened and show a more optimistic outlook than actually occurs in reality.

For this setup, the radius equals between 9-11 cm (depending if you include the size of the detector itself). This means that at measurement intervals of 1°, the detector opening (slit size) must be 1.57 cm 1.6 cm to measure the entire hemisphere.

$$radius * tan^{-1}(measurement_{interval}) = slit_{opening} \tag{2.19}$$

$$9cm * tan^{-1}(1°) = 1.57cm \tag{2.20}$$

In figure 2.9, the entire hemisphere is not measured because the slit width is not matched to the angular intervals, but this doesn't mean the measurement is performed wrong. There is considered between 5° intervals the optical response can be characterised by a linear interpolation between 2 points. The reason behind this measurement can be to increase measuring speed because it is slow (changing angle, setting up the different wavelengths again). To measure the entire hemisphere, the slit width must be increased to 6mm. Depending on what wants to be measured, 3 different approaches can be taken (shown in figure 2.10:

- Reduced slit width and reduced intervals: A detailed picture is given but measuring times increase significantly. The integration of the measured points over the hemisphere equals to T and T_D.
- Reduced slit width and increased intervals: The presented picture is less detailed and shows general trends better. It can still be interpreted as detailed if in between measuring points can be represented by a linear interpolation. Note, the integration of the measured points is not equal anymore to the T and T_D.
- Increased slit width and increased intervals: A less detailed picture is given but more general trends are shown. The integration of the measured points equals to T and T_D.

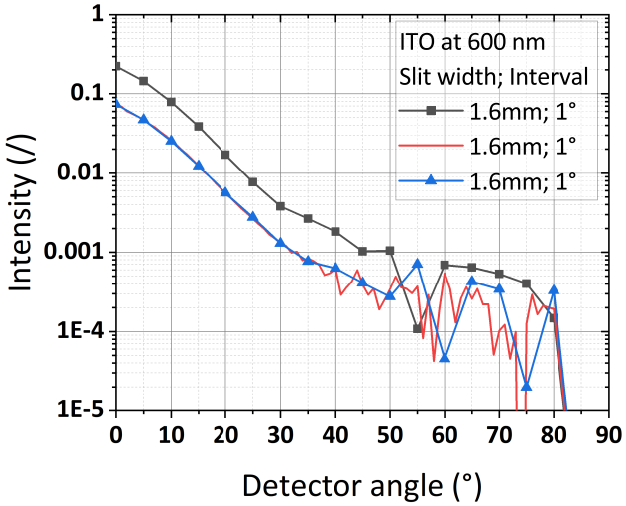

Figure 2.10: Different measurements while changing intervals and slith widths.

In case slit sizes are increased to 8mm overlapped measurements occur (shown in figure 2.11). The measured peaks of 6 mm are spread out over 2 measurements and indicate overlap. For this work, intervals and slit widths are kept small to give a detailed view to compare differences in response between different texturing methods accurately. Second, the data can still be translated to T and T_D.

Optical measurement interpretations

So far, there is determined what the relative position between source, sample and detector must be to represent actual light scattering properties inside a cell as accurately as possible. Second, the settings of source and detector slit openings are discussed to understand the measurement better. Last of all,

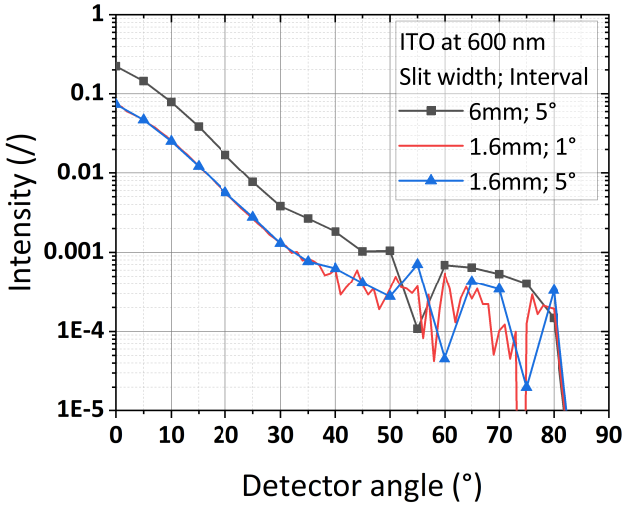

Figure 2.11: Difference between slit widths of 6 mm or 8 mm for slit openings of 1.6mm and intervals of 5°.

the interpretation of the measurement itself must be performed to understand how the measurement represents phenomena such as macroscopic-, mie- and rayleigh scattering.

As discussed, there are 2 type of features: nano-scale features and micro-scale features. Nano-scale features are described by scalar scattering theory that is wavelength-dependent and this part of T_D follows an exponential decay described by the following formula:

$$T_D = T[1 - exp[-(\frac{2\pi S_q|n_0 - n_1|}{\lambda})^\gamma]] \tag{2.21}$$

In this formula, n_0 and n_1 are the respective refractive indexes of the layers and γ represents an empirical value ranging from 1.5 to 3 depending on the height distribution of the created texture. Second, Micro-scale features are described by solving the Maxwell equations under Mie-assumptions and follows the following formula:

$$T_D = \frac{\pi a^2}{S_{al}^2} Q_{sca} \tag{2.22}$$

In this formula, πa^2 represents the cross-section of a spherical particle with radius ”a”. This cross-section represents an average size of crater created with the the texturing method (half of S_z of the surface texture). Q_{sca} represents the scattering efficiency of the texture and has a weak wavelength dependency [14]. Figure 2.12 shows the optical response for an AZO sacrificial textured superstrate. It shows light gets distributed in large angles from which a transition from the exponential decay (for small scattering angles) to a lambertian decay (for large scattering angles) occurs around 25 degrees. There must be noted, the measured AID represents a micro-textured surface and not an modulated surface texture (MST) which contains nano- and microtextures. This would imply there cannot be an exponential decay measured in the AID according to equation 2.21, but results from Isabella et al.[14] (AID of different textures were performend) show that microtextures also show this type of response and confirm these results. Nano-textures on the other hand, only show and exponential decay as expected.

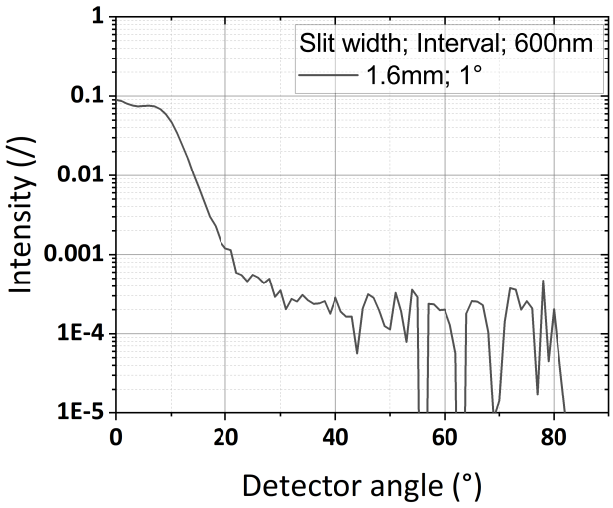

Figure 2.12: AID response showing an exponential decreasing part, after which a lambertian part of the scattering becomes dominant at an angle of θ_{exp} for an AZO-sacrificial textured superstrate processed at 400W, 400°C for 3600s

3

Methodology

3.1. Process flow

To obtain high optical performing textures that scatter light in high angles, a thought trough workflow is required. This work is divided in 4 different parts, which starts from an uncontrolled sacrificial texturing process or an unknown procedure to create the texture (honeycomb textures in this case) on glass superstrates. As a first step, a characterisation matrix (physical and optical) must be constructed to asses the quality of a texture and compare their performance. Since the starting point holds glass superstrates, the optical characterisation can be performed multiple ways (relative position of sample to a detector etc.). A well founded optical matrix must be constructed to concisely asses its performance. Second, there are multiple physical parameters that describe the surface but not all of them hold crucial information for this work. It means the second part of this first step must be to find out which roughness parameters to consider.

The second step, is to change the processing steps and different process parameters to understand its implications on the superstrate optically and physically. For random texturing, there has already been a lot of research performed the last decade. This means focus lies more on finding the right processing parameters instead of finding the required processing steps (and order) to fabricate them. For periodic texturing on glass superstrates the focus lies heavily on both aspects, since the periodic texturing on these superstrates is unknown territory. First, optical measurements are performed to asses how much light it scatters and in which angles it scatters light to. Second, physical measurements are performed which quantify the size of the craters ect. but also a qualitative inspection is performed to scan for defects in the created superstrate. After both measurements are analysed individually, measurements are combined to gain a deeper understanding of the optics resulting in these scattering phenomena and gain a better understanding of the process itself. The feedback loop indicates that different experiments are required to fully control the process and reach a highly scattering superstrate. The final result is a texture that heavily scatters light in high intensities over a large range of angles.

As a third step, nc-Si is grown on top of the optimised superstrates to asses the compatibility of optically optimal performing structures and nc-Si deposition (crystals start to grow from the superstrate on). If defects are detected which deteriorates the performance (in the complete cell), some process parameters must be changed in the previous step but since full control over the process is obtained, resulting textures can be adjusted. From this point on, the comparison between random and periodic textures is justified because different optical effects are dominant for the different textures (as is discussed in section 2.2.3.3). Afterwards, the electrical performance of a complete cell is tested and a similar approach as the third step is considered. The final result contains information for industry and further academic research. Based on the difference in performance, industry can research the actual implementation of these structures in commercial thin film technology and academic research can benefit from it in terms of breaking world record efficiencies.

Note: The thesis focuses solely on the optical aspect of the problem. Another thesis focuses specifically on the electrical side of the problem. The figures used in this thesis are related to that thesis and the sole purpose of showing a proof of concept that the textures affect the electrical performance.

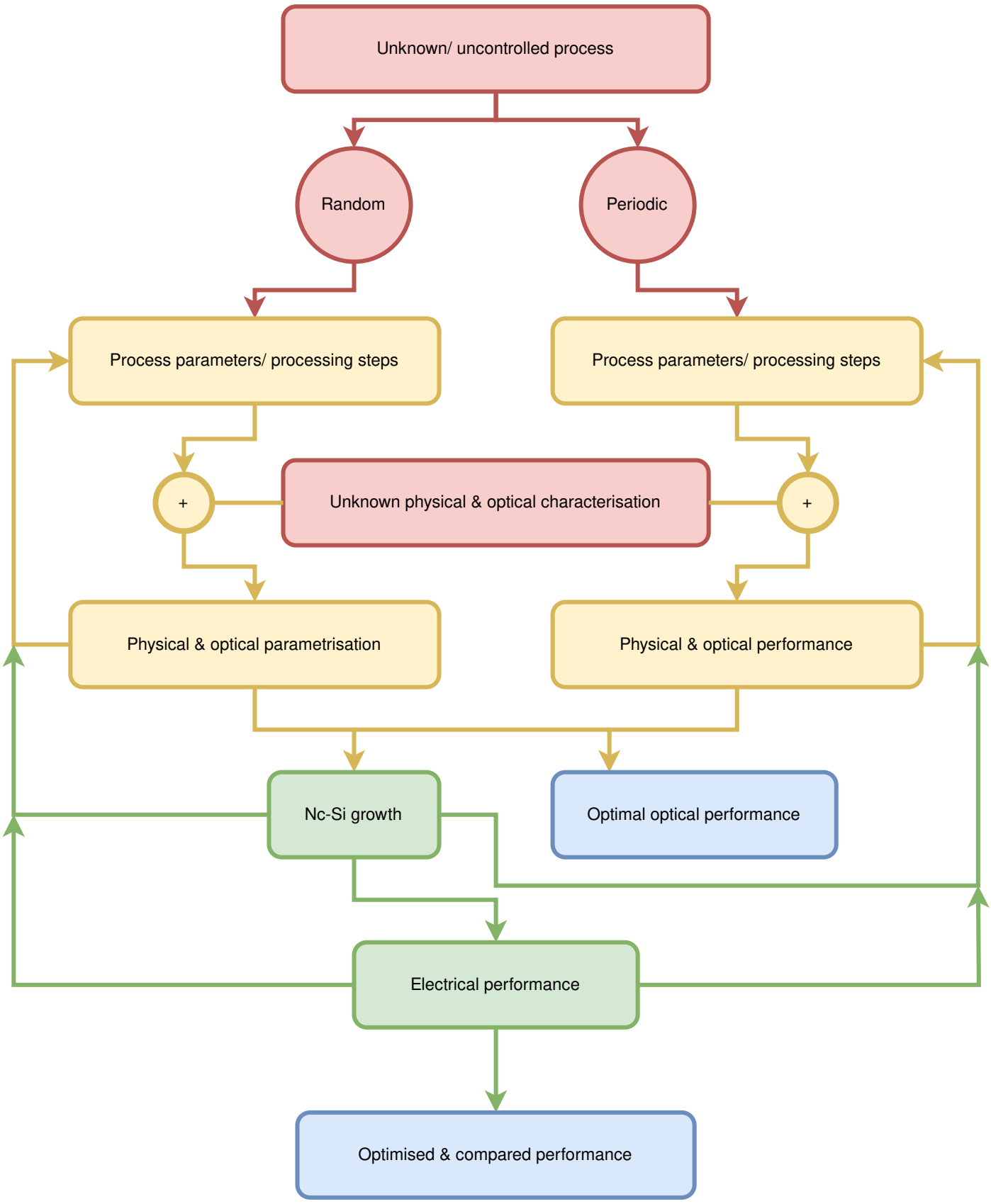

Figure 3.1: The overall methodology required to reach the objective of developing high optical performing textures on Corning Eagle XG superstrates

4

Sacrificial texturing

4.1. Introduction

This chapter describes 2 methods to create random textures that are most promising to obtain a high cell performance with according to Guangtao [20]. It is based on sacrificial texturing for which a deposition of a sacrificial layer is required. The deposition can done by a sputtering process, low pressure chemical vapour deposition ect. This layer acts as a mask for the etching procedure and is removed over time. Once the chemical solution reaches the superstrate, the etching of the glass substrate starts. After the sacrificial mask is consumed, a textured surface is left behind. This implies, the deposited layer highly affects the outcome of the texture. In the deposition step, the layer must be crystalline to ensure the formation of textures on the entire surface of the superstrate. The formed crystals are the reason why parts of the sacrificial layer are locally etched away faster than other parts. Crystal boundaries, different sizes of grains ect. lead to different etching rates, which causes the solution to reach the resulting layer at different time steps [8]. This procedure is optimised for Indium tin oxide (ITO) and Aluminum zinc oxide (AZO) sacrificial texturing.

4.1.1. Indium Tin Oxide sacrificial texturing

The commercial photovoltaic industry is dominated by c-Si technology which introduce light management by introducing a pyramidal texture. Since this work adresses thin-film technology, crack formation is often the result of growing the different layers on top of it. Second, depositions in this work are made on glass which is amorphous and makes it impossible to use traditional texturing methods that are focused on c-Si substrates to process cells on. De Vrijer et al. [8] researched the potential of different texturing approaches on crystalline silicon substrates for the purpose of creating high optical performing substrates while the electrical performance of the cell is not compromised. Although, the processing was not performed using ITO sacrificial texturing nor an amorphous substrate is used, insights stay relevant. The comparison between a sacrificial method and 2 alkine and acidic wet chemical etching methods is discussed.

1. An alkaline tetramethylammonium hydroxide (TMAH) solution is used to etch a pyramidal (111) surface (named T1).
2. An extra acidic poly-etching step containing HF:HNO3:H20 is used to smoothen the previously mentioned (111) surface (named T2).
3. The third approach grows a poly-silicon sacrificial layer. The texture is created after performing an acidic poly etching solution step containing [HF:HNO3:H2O] (named T3).

The characterisation of these processes was assessed with time as changing parameter. For T1, increasing etching time created pyramids with a maximum slope of 45 degrees and reflectivity kept decreasing with increasing processing time. The AID showed that increasing the processing time, broadens the peak and better scattering was the result. The reflectivity showed the reflectance decreases with increased etching time.

For T2, increasing the etching time creates less pyramidal textures and a more dominant crater structure where the roughness decreases and a mean slope of 30 remains. Due to the smoothing of the surface, an increased reflectivity intensity is observed with increased processing time and the AID showed the scattering intensity decreased too.

For T3, increasing etching times smoothens the surface and creates a flat-like texture. In this case, the AID and reflectivity intensity are mainly unaffected, which could be explained by the small features where perpendicular reflection is still dominant. The research concluded small and scattered pyramidal structures don't seem promising for further development (more dense texturing not possible due to cracks growth with <111> textures). The sacrificial texturing technique has wider reflection angles (influence optical path length) but they are less efficient than the etched <111> surface. However the texturing approach is not optimized and could be potentially increased/ characterized, which could increase their optical performance. The advantage is the lower risk of crack nc-Si growth compared to T2, T3, which makes it interesting. Similar effects occur for ITO-sacrificial texturing, which are used as comparison.

Tan et al.[21] researched the effect of micro-texturing on the front electrodes (amorphous layer) to increase the photocurrent density (I_{ph}) and the efficiency in the end. This was reached by creating micro-textures on Corning glass substrates (Eagle XG) using sacrificial texturing of ITO and the nano-textures of AZO-layer on top were created by applying wet etching, where this layer serves as the TCO. There was observed that 3 parameters change the light trapping capability of a layer: the feature size, shape and the aspect ratio. The thickness of the deposited ITO-layer is directional proportional to the feature size, in which texture size can be varied between nano-textures and micro-textures. If these textures in a single nc-Si:H cell are than compared to a cell with a flat glass superstrate and a non-processed nano-textured AZO layer (sharp textures), an increased efficiency of 3% is observed. The fill factor and V_{OC} are significantly increased without deteriorating the J_{sc}. This implies the textures of the nano-textured cell with a flat substrate are too sharp to grow crack free nc-Si on top of, which creates shunt paths for the absorbed light. This shunt path increases the recombination current of the cell, which leads to a lower J_{sc} and lowers the efficiency. To overcome this, smoothing these textures was performed and increased the efficiency of the cell is observed. Smoothing increases the crater correlation length, which lowers the aspect ratio and makes crack free growth of silicon possible. If the glass substrate itself gets textured, the performance of the cell increases even more (3% as mentioned before) due to the further lowering of the aspect ratio. This paper concluded, a maximum performance is obtained when the correlation length is similar to the thickness of the cell because the measured EQE is the highest for every wavelength.

To obtain the previous high quality textures, the sacrificial layer must have highly crystalline properties to be etched at a heterogeneous speed in function of the position on the surface. Tuna et al. [22] determined the parameter ranges for magnetron sputtering which are able to grown high quality layers. Analysing XRD patterns, deposition temperatures lower than 150°C resulted in amorphous layers. Crystallisation was detected between [150;300]°C in the <222> plane, which can be explained by the lowest energy plane of the body-centered thetragonal crystal structure has. The <111> plane is the most densely packed and therefore requires the least amount of energy. For temperatures around 300 degrees or higher, the <222> dominated plane starts to change towards a <400> grown plane. Second, planes like <440>,<211> also start appearing at higher temperatures. Higher deposition temperatures hold more energy, which makes the formation of higher energy containing planes possible. Similar changes for the crystal orientation are reported for increased sputtering power, where the <400> orientation is preferred. Another aspect is the effect of lack of oxygen during processing, which gives a change in preferred orientation (from <222> to <400>) at lower energetic process parameters. The layer thickness influence was also researched and was found to have an influence too because the layer has more time and space to develop crystal formations. Since these parameters influence the crystal structure, they influence the surface morphology of the final substrate too. The increased temperature and power also contributed to an increased grain size, while similar effects of oxygen deficiency and layer thickness are not mentioned. Grain size and crystal orientation both have an effect on the resistivity which can be measured with common measurement tools. Both parameters have an influence on the heterogeneity of local etching speeds and can explain the formation of obtained textures. In this chapter the goal is to reach optimized ITO texturing ourselves based on previously mentioned literature so an micro-texture is obtained and in future work an optimal MST texture can be obtained.

4.1.2. Aluminum Zinc Oxide sacrificial texturing

An alternative texturing method to the In2O3:Sn method, is the ZnO:Al sacrificial layer texturing method which makes use of the same principle. The grown layer is heterogeneous polycrystalline, which implies it has an inhomogeneous etching character. Guangtao et al.[15] has shown that with a HNO3/ HF etching solution a stable sacrificial texturing morphology is obtained. The relevant parameters influencing the

surface texture are sacrificial layer thickness, sputtering temperature and etching composition/ratio. Full control over the process has been obtained since the RMS roughness could be modified from 20 - 400 nm. These results and key parameters are confirmed by Guangtao [20] and further broadened to 500 nm. The RMS value decreased with increasing [HNO3:HF] concentration, since HNO3 is the main etchant of ZnO:Al while HF is this for glass. The increased HNO3 concentration results in a faster etching rate of the sacrificial layer that results in the craters formed in the superstrate to have less time until the sacrificial layer is consumed. For an increased RMS roughness, the relative HF concentration must be increased. Second, the RMS value is positively affected by the initial AZO film thickness which causes the RMS to increase when the film thickness is increased. Increasing film thickness causes increasing grain sizes in the film, which explains the increased RMS values. This effect can be reversed to a certain extend by increasing sputtering temperatures for depositing thicker films (deposition temperatures were changed from [50;400]°C). At high temperatures, the ZnO:Al sputtered layer is polycrystalline, while for low temperatures the layer is microcrystalline and reducing the temperatures even further creates amorphous layers. Highly crystalline structures are more uniformly etched compared to microcrystalline structures so lower RMS values are obtained. In case of amorphous layers, uniform etching is obtained which results in a lack of texturing. For the thinner films, this effect is negligible which make etching concentrations and film thickness the dominant parameters. Applying this method becomes highly interesting, when increased optical performance from flat substrates is obtained.

In addition to the mentioned parameters, Guangtao [20] also determined the quality of the film can be controlled by other sputtering variables like pressure and power density. Bose et al. [23] confirmed this increased scattering performance and increased the electrical performance at the same time (which implies crack free growth is obtained between the layers). It was performed by a 2 step wet etching process in which the first step focuses on the widening of the micro-cracks in the sacrificial layer [HNO3:HF] and the second step focuses on the glass substrate itself [HF:H2O]. The relation between etching times of step 1 and the surface texture was made and concluded that there exists an optimal etching times which gives the smoothest surface texture and high RMS roughness. Longer texturing times, increased the roughness but damaged the deposited p-layer due to previously mentioned effects (see section 4.1.1). Higher haze values are obtained and increase the efficiency (compared to flat glass substrate) until the point that the surface texture start damaging the p-layer. Although results were positive, there was still room for significant improvement in terms of texturing and haze since only 3 etching times were observed.

4.1.3. Modulated surface texturing

In previous subsections, 2 different texturing methods are explained. Both methods have their own range in which the roughness is controllable. This implies, they have a certain range in which the interaction with different wavelengths can be modified. Since in thin-film technology textures must maximise scattering the UV- and IR-region of the AM1.5 spectrum, textures sizes must be matched accordingly. For example, the Rayleigh scattering principle defines the size of the textures must be smaller than the incoming wavelength to create a symmetrical light-distributions scattering pattern ($n * D < 0.05 * \lambda$). Since, the UV-irradiation is defined from wavelengths below 380 nm and IR-irradiation from 780 nm onwards, textures including UV scattering must be at least 2 times smaller to obtain effective scattering in the high energy range. Different texture sizes must than coexist to maximise the optical interaction. One method is to create Modulated surface textures (MST) which is defined as the superposition of 2 textures on top of each other. Guangtao [20] researched different methods to create MST.

For micro-texturing, ITO sacrificial texturing was performed while for the nano-textures 3 different methods were considered: Aluminum induced texturing (AIT), a sputtered AZO layer (EAZO) and ZnO:Al induced texturing (ZIT) (or AZO sacrificial texturing). The procedure to for ITO sacrificial texturing can be found in chapter 4.2.1.

AIT is created by Alberle et al. [24] and textures in range the of 2-5 µm were obtained. It follows the mentioned procedure: Al is evaporated on the substrate after which it gets annealed. Than the material is exposed to a mixture of HNO3 and HF to remove the deposited layer and leave a textured glass surface behind. The annealing step in this procedure transforms the Al and Si_yO_x to Al2O3 and Si_x, which can be removed by the previously mentioned mixture. There was concluded, the dominant variables affecting texture sizes are deposited Al thickness, annealing temperature and annealing duration. Second, the relative [HNO3:HF] concentrations seem not to play a significant role in this perspective. Last, the textures are ideal to combine with thin film a-Si:H layers.

EAZO is created with the sputtering of AZO on the surface for a predetermined time to reach a certain thickness after which it is exposed to an HCl solution to create texture. The crystallinity and density of the layer gets determined by the superstrate temperature and affects the wet etching process afterwards. Since the etching solution etches the easiest through defects in the material, the crystallinity heavily influences the roughness of the substrate. The etching rate decreases with increased temperature since the density and crystallinity of the material increases at higher temperatures and less defects inside the material are observed through which the etching solution etches easier. At high temperatures (for example 300°C), the roughness decreases due to a more uniform etching behaviour. This was confirmed by Kluth et al. [25]. The maximum roughness in this work is obtained at a substrate temperature of 250°C. Second the normalized surface angle distribution (A_D) was observed, which reflects the steepness and its statistical variation of the surface. At temperatures around 250°C, the highest peak angles are obtained while having a broad tail distribution. This implies textures of 250°C have a better compatibility with nc-Si.

For ZIT, the procedure is described in 4.2.2 (introduction or methodology). The advantage this method has compared to the other texturing techniques is the lack of annealing step, low etching times, the sacrificial ZnO:Al only contains abundant elements and wide scattering angles. The superposition of the 3 structures on the ITO sacrificial texture structure results in different levels of roughness since the applied mechanism is different to create the MST structure. ZIT is the only method reaching lower levels of roughness compared to the IIT, due to the lower sacrificial thickness of the AZO layer originating from the craters created by the IIT step.

After texturing of the substrate, the nc-Si growth on the surface must be compatible and performed in complete control of the process step since a relation exists between the substrate texture and silicon growth. Python et al. [26] worked on the texturing of the TCO layer of a single-junction microcrystalline silicon cell. It describes an improved electrical performance is obtained if V-shaped (sharp) structures are replaced with U-shaped (smooth) structures independent from the material interaction or feature size. The distinction between valleys and peaks in the textures are made because sharp valley texture have a larger chance to create more defects compared to sharp peaks of the layer. Identical conclusions are drawn for micro- or nanotextures, although lateral texture dimensions between 300 nm and several microns seems to undergo the largest effects. Nanotextures also create cracks but do not propagate through the whole layer which reduces their influence on the electrical performance. Considering this, the density of cracks inside the nc-Si gets reduced, which lowers the recombination current occurring inside the layer. Guangtao [20] obtained a difference of $\delta J = 10^{-2} mA/cm²$ between U-shaped and V-shaped textures. This results in an increased V_{OC} and FF considering the following formulas:

$$V_{oc} = \frac{kT}{q} ln \frac{Jph}{Jo + 1} \tag{4.1}$$

$$FF = \frac{V_{mpp} Impp}{V_{oc} Isc} \tag{4.2}$$

Guangtao [20] researched nc-Si growth on top of the MST substrate for the different techniques (MST-AIT, MST-EAZO and MST-ZIT) for a 2 or 3 µm thick silicon layer. For the deposition of the layer, Plasma Enhanced Chemical Vapour Deposition (PECVD) is applied, which makes use of a gas that gets ionized and directed towards the substrate. Other deposition methods like Physical Vapor Deposition (PVD) or Chemical Vapor Deposition (CVD) are less suitable for thin film applications. Since, deposition temperatures are higher (600-800°C) compared to the PECVD technology (350°C), devices could potentially break and thermal stress is induced [27]. Second, better adhesion between layers is obtained which implies purified chemical reactions and lower electrical losses in the cell. For all 3 cells, a higher EQE response was obtained compared to only ITO sacrificial texturing. The 3 structures were compared to each other and the following observations were made:

- The MST-EAZO obtains the highest J_{sc} because it contains steep V-shaped craters and results in higher scattering properties.
- Although the previously mentioned texture has the highest J_{sc} value, MST-AIT and MST-ZIT have the highest $V_{oc} * FF$ product (for t_{nc-Si}=2µm [MST-AIT;MST-ZIT;MST-EAZO]=[0.383;0.407;0.378]). The cause lies in the increased defect density in the silicon of the MST-EAZO.

- If the thickness of the layer gets increased from 2 to 3 µm, the J_sc-value increases between 0.4 (MST-AIT) and 1.7 mA/cm² (MST-EAZO) (due to increased light absorptance) and the $V_{oc} * FF$ product decreases between -0.7% (MST-AIT) and 9.3% for (MST-EAZO). MST-EAZO results in the lowest efficiency because it suffers from increased crack density which gets worse with increased layer thickness. Defects appear in the beginning or during the deposition, which creates increased recombination locations or even shunt paths as the thickness increases.
- MST-ZIT is the most suitable to grow nc-Si:H since it has to highest efficiency for both thicknesses (10.4% - 10.5%), due to a low defect density. An increase of 13.9% is obtained for a 2 µm thick layer and 7.8% for a 3 µm thick layer compared to sole ITO sacrification texturing.

4.2. Methodology

4.2.1. Indium Tin Oxide experiments

The goal is to reach optimal texturing (scattering purposes) for the sacrificial texturing methods (ITO, AZO) while obtaining complete control of the process parameters, so the superposition of these methods gives an optimal result for MST. First, for both processes microtextures are created and compared to each other. Since complete control of the process is gained, it is possible to tune towards nanotextures as seen in literature. For the ITO, a preliminary study is performed based on the paper of Tan et al. **??** in which a layer [100 - 300 nm] of $In_2O_3 : Sn$ is sputtered on cleaned Corning glass (Eagle XG). As first experiment, Corning glass is considered as the starting material for texturing. Afterwards, the samples undergo a ultrasonic cleaning in acetone and isopropanol for 10 min each. For this research, deposition machine ”Zorro” sputters (magnetron sputtering) In2O3:Sn on the superstrate. Deviations from deposition parameters of Tan et al. **??** are made since results of this work were not reproducible. The depositions were made in a machine named ”Laskar” which can explain the problem. The deposition parameters are changed as following:

- Variable deposition temperature: [200-300°C:50°C]
- Variable deposition power: [135-245W:55W]
- Variable deposition time: [3600-7200s:1800s]

Afterwards, the superstrate is exposed to a wet etching step composed of an aqueous solution of hydrogen fluoride (HF) and hydrogen peroxide H_2O_2 with the following volume ratio: [H_2O:HF:H_2O_2=10:1:2] until the ITO layer is removed. Afterwards reflectance and transmittance measurements are performed using an R,T-setup ”Lambda 1050”.

After characterisation of the previous experiment, a second experiment is proposed varying only 2 parameters in between smaller boundaries for which deposition time is fixed at 7200s:

- Variable deposition temperature: [230-270°C:20°C]
- Variable deposition power: [170-210W:20W]

The chemical solution for this experiment is identical to the first one because higher concentrations lead to less uniform and moderate etching characteristics. The etching time cannot be specified since there is a dependency between time and number of samples etched in the same (this is described in 4.3.3.1). After etching, the samples undergo again a reflectance and transmittance measurement including an Angular Intensity Distribution measurement using ”Lambda 950”. Second, the roughness profiles and other physical parameters of the samples are measured underneath a confocal microscope ”Keyence VK-X250”.

After the characterisation of the previous experiment, a third experiment is proposed in which the deposition times for the samples containing uniform textures is performed. Deposition times are changed between [3000-7200s:1000s] for the following samples:

- Deposition power: 210W; Deposition temperature: 230°C
- Deposition power: 190W; Deposition temperature: 250°C
- Deposition power: 210W; Deposition temperature: 250°C

The chemical solution for this experiment is kept identical because uniform textures resulted from this concentration in the previous experiments. Identical to the previous experiment, the etching time cannot

be specified (this is described in 4.3.3.1). After etching, identical measures are undertaken to characterise the surface.

In a fourth experiment, the rotational speed of the sample during deposition is changed, which is kept constant for the previous experiments at 10 rpm. The deposition parameters are fixed at T=230°C, P= 210W, t= 7200s and the rotational speed is changed between [5-15rpm:5rpm]. The etching solution and characterisation methods are kept identical to previous experiments. After these experiments, a high optically performing sample (P=210W, T=230°C, t=7200s) undergoes further observation using spectral electron microscopy and atomic force microscopy.

4.2.2. Aluminum Zinc Oxide experiments

For Aluminum Zinc Oxide sacrificial texturing, only 2 experiments are performed because this already lead to visual uniform and high optical scattering textures. Second, already more knowledge exists in literature. For these experiments, Corning glass is again considered as suitable for these processes. Before the deposition, they undergo an ultrasonic cleaning of 10 min in acetone and isopropanol each. Afterwards, deposition machine "Amigo" sputters $Al_2O_5Zn_2$ on the superstrate and parameters are based on literature 4.1.2. As a first experiment, the deposition temperature and time are kept constant at 400°C and 3600s, while the deposition power is changed between [350-450W:50W]. Afterwards the superstrate is wet etched in a non diluted solution of [HNO_3:HF=8:1] until the layer is removed (3 min). The samples are optically characterised with a reflectance- transmittance measurement on "Lambda 1050", AID- measurements are performed to gain more depth knowledge about the scattering properties of the material on "Lambda 950". Second, a physical parametrisation is performed on the samples using confocal technology "Keyence VK-X250" and confirmed by SEM and AFM measurements.

In the second experiment, the influence of deposition time is researched by keeping the power and temperature constant at 400W and 400°C, while the time changes between [900s; 1800-5400s:1800s]. The etching solution is kept identical because the first experiments already gave uniform etching results, optical and physical parametrisation is also performed identical to the previous experiment.

4.3. Results: Indium Tin Oxide sacrificial texturing

4.3.1. Initial optimisation point

Since, the results from Tan et al. [21] could not be reproduced, an initial point towards optimisation must be found. A high optical- and electrical performant texture must be obtained, but to reach this, an optical optimisation must be performed. After this the tweaking of the electrical performance is made possible (as mentioned in 3). Visual inspection combined with diffuse transmittance (T_D) measurements state the initial point of research. In the power-temperature-time matrix (size <3x3x3>), superstrates with a great variety of uniformity are observed and only 20 out of 27 samples show any sign of textures. The difference in quality is shown in figure 4.1 and determines the quality aimed for in this work. An overview of their average diffuse transmissions is shown in table 4.1. One aspect that must be kept in mind is that the deposition time is not equal to one defined thickness, the combination of power and temperature affect the deposited thickness too. As general notion, the following parameters result in a defined thickness:

- Deposition power: 135W; Deposition temperature: 300°C; Deposition time: 2000s= 109.7nm
- Depostion pwer: 190W; Deposition temperature: 300°C; Deposition time: 1600s= 144.1nm

Table 4.1: Average diffuse transmission (T_D) values for ITO-sacrificial texturing: the red marked values diffuse in average over 70% of the incident light over a spectrum [300:1200] nm

		P (W)								
		135			190			245		
		time (s)			**time (s)**			**time (s)**		
		3600	5400	7200	3600	5400	7200	3600	5400	7200
T (°C)	200	/	/	/	/	43.1	26.7	37.7	18.9	44.3
	250	/	24.7	39.9	77.1	69.9	72.1	/	65.7	49.0
	300	45.8	66.5	38.0	5.4	/	/	28.8	33.0	39.6

Figure 4.1: Visual inspection of the samples where the sample on the left is highly non-uniform. The sample in the middle is processed at P=210W, T=230°C and t=7200s at 10rpm and describes an optimal sample. The sample on the right describes the best quality of ITO textures when a change towards 5rpm is made.

Due to the lack of datapoints (in terms of uniform textured superstrates) and large range (over 100°C), it is not clear to describe different trends. Therefore, only an average optimal point can be described. The optimal texturing point lies around a deposition power 190W and deposition temperature of 250°C because all values around it are significantly lower. Second, this point is chosen as optimum because the textures are uniform over the entire surface (which is not obtained for the other textures). For the deposition time of this parameter set, no conclusions are made because values lie close to each other and no clear trend is observed which is required to determine an optimal value. Since, the initial optimum is found a further optimisation is useful.

4.3.2. Optimal optical texturing

In previous section, the only thing that can be described is a course optical optimal point with a uniform structure and a diffusivity above 70%. Before a deeper analysis of a more precise optimal point is defined including exposing different trends, an analysis of the wavelength interaction must be made to understand the difference between high- and low quality scattering samples. Therefore 4 samples out of the second experiment are observed for analysis using T, T_D, Haze, confocal, SEM and AFM measurements in the range [300:1200]nm:

1. Deposition power: 170W; Deposition temperature: 230°C; Deposition time: 7200s
2. Deposition power: 210W; Deposition temperature: 230°C; Deposition time: 7200s
3. Deposition power: 170W; Deposition temperature: 270°C; Deposition time: 7200s
4. Non processed superstrate

First, the confocal measurements are considered. The 3 different height profiles are visualised by a colored height map. A dark blue color describes an increased depth while a brighter red color describes an increased peak. From figure 4.3 is observed, the left-bottom figure has a flat-like character since colors do not have a deep tone and are described by a white color, while the right-top one is described by strong colors and wide craters. The depth and width of craters seem to be correlated to each other for this process. To confirm the accuracy of the confocal measurements, SEM and AFM imaging is used. Results are shown in figure 4.28 and the presented peaks and craters in confocal measurements look very similar to SEM, AFM. No sudden drops/ jumps are measured for SEM, AFM which means this must not the case either for confocal measurements. Since differences between measurements are limited/non existent, the confocal technology is concluded to be accurate.

For total transmission (T) is observed that all processed wafers have an identical curvature in function of the wavelength that remains a constant from 1200 nm - 500 nm, increases till 375 nm and than drops to values lower than 70%. Between the different samples, only a small vertical shift downwards of 2% is measured for the 2nd sample, this can be explained by measurement inaccuracy or a slight increased reflectance. Second, an increased total transmittance is observed for 300nm and a peak in T is observed at 375nm for the textured superstrates. For the flat one, this bump is not observed and the decreasing trend for the transmittance starts to kick in due to the fact light in this region obtains enough energy to be absorbed by the bandgap of the material (see figure 4.5). This holds for textured- and flat samples because it is a material property. The reflectance stays unaffected and it is the transmittance that makes the trade-off with

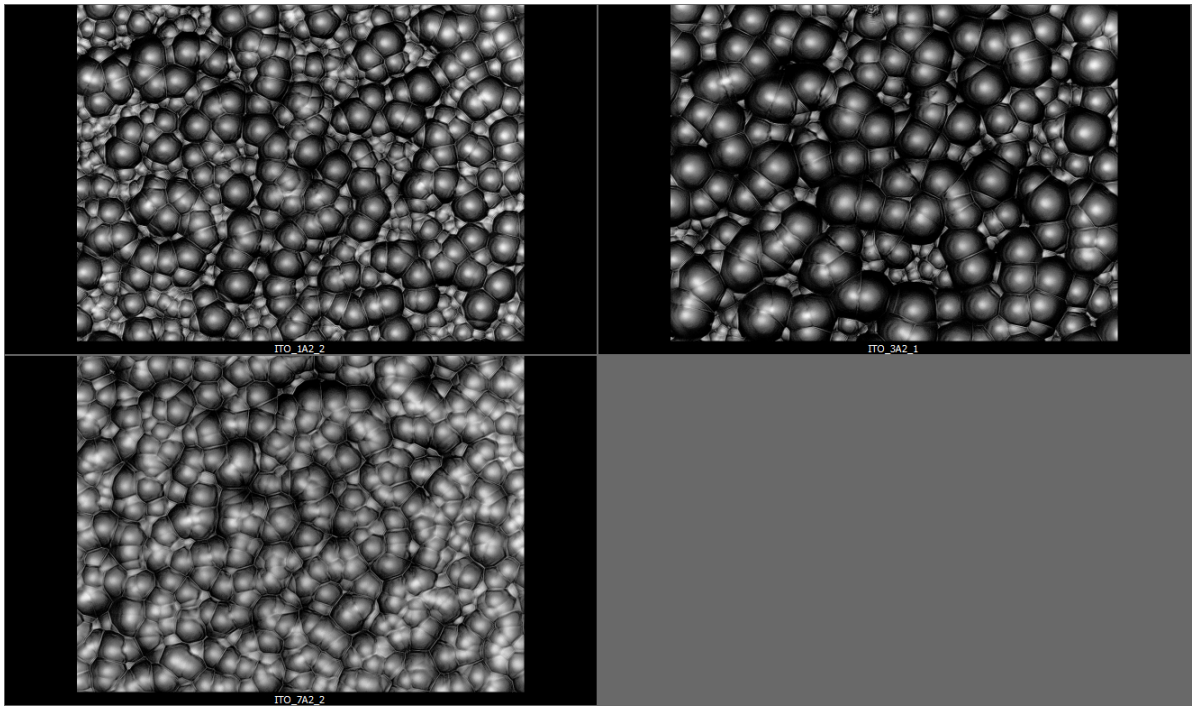

Figure 4.2: Confocal picture of ITO sacrificial texturing with different process parameters right-top: P=210W, T=230°C; left-top: P=170W, T=230°C; left-bottom: P=170W, T=270°C

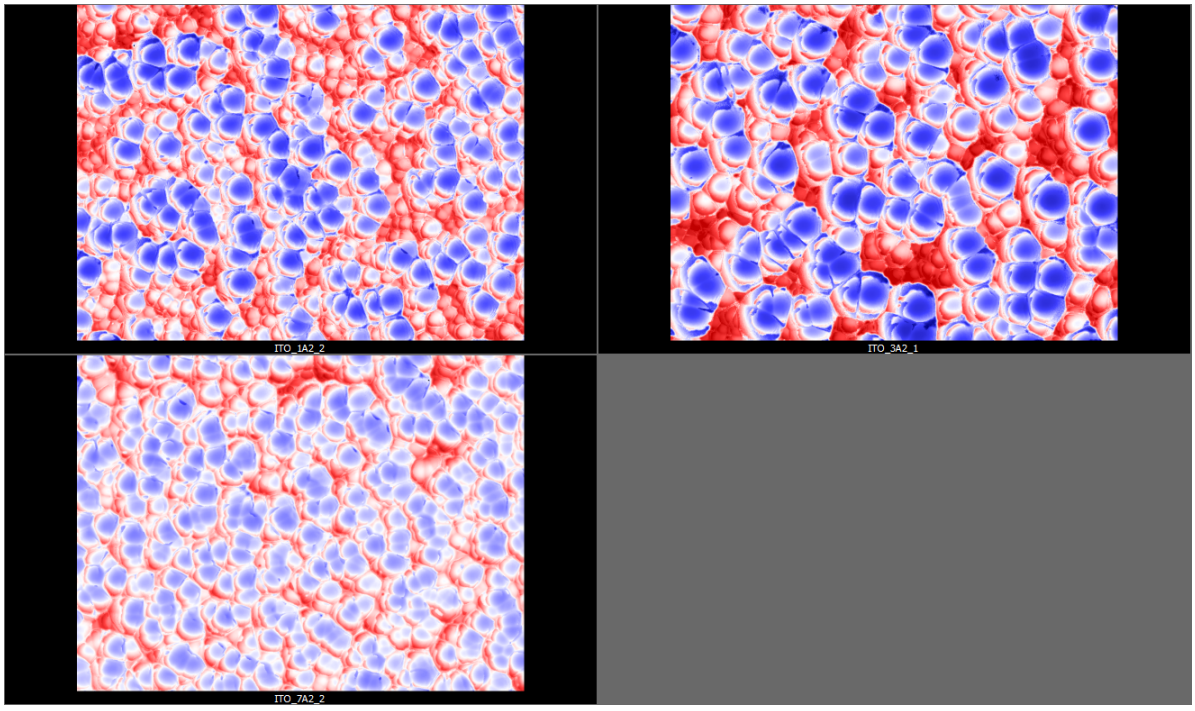

Figure 4.3: Confocal height measurements with range [-2.615:2.615]µm obtained with different process parameters right-top: P=210W, T=230°C; left-top: P=170W, T=230°C; left-bottom: P= 170W, T=270°C

increased absorptance. Comparing both types, the difference in T between flat- and textured superstrates increases from 500 nm (see figure 4.5). The morphological difference with a flat surface is observed in figure 4.3 and explains the increased T (between 5-8%). The increase in transmittance is related to a decrease in reflectance at the second interface (glass - air). A possible explanation could lie at wavelength interaction itself in which larger wavelengths are more transparent for similar texture sizes and smaller

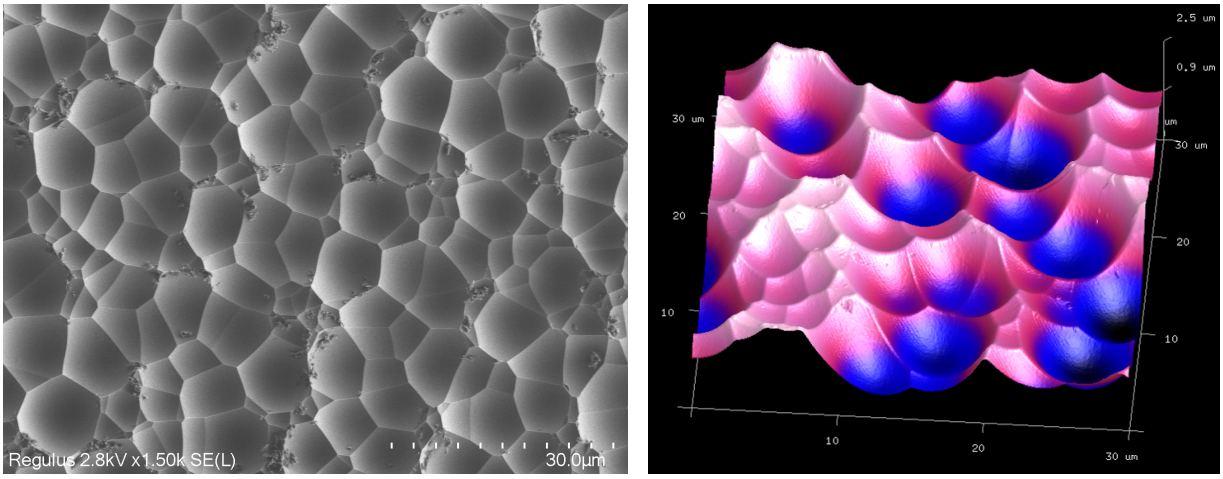

Figure 4.4: SEM image of ITO processed at P=210W, T=230°C and t=7200s. Particles shown on these images represent dust particles and represent wear of the sample because the image is first exposed to different optical characterisations. AFM figures show large micro-textures with a hemispherical characteristic similar to confocal measurments.

wavelengths are easier to subject to light in coupling. Since wavelengths around 300/400nm are around 4/3 times smaller to the maximum presented range of 1200 nm, the size of a texture plays a part considering absolute values but trends remain similar compared to the flat type.

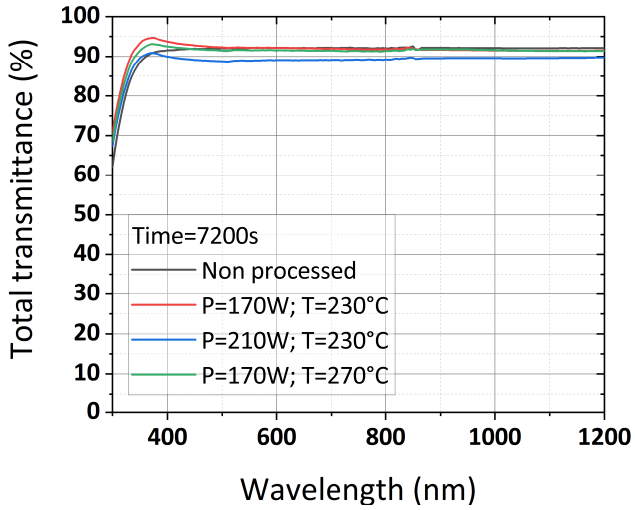

Figure 4.5: Total transmission of the defined 4 samples from the second experiment

For the total diffused light (T_D), table 4.2 and figure 4.6 are considered. The percentages define the part of the incident light that is diffused. The flat surface has negligible light scattering properties while the textured superstrates interact with the incident light. For all superstrates a wavelength dependent response is observed, which is explained similar to previous paragraph. Increased wavelengths are tougher to bend/ scatter, which means that independent of the craters sizes an increased trend in scattering performance with decreasing wavelength must be observed (shown in table 4.2). This observation holds until 375 nm, because all curves have a decreasing trend from that point on. At this point, the effect of absorption dominates the optical scattering because there is less light reaching the second surface to be scattered. Despite their similar trend, absolute responses differ which is correlated to the surface profile itself. Combining the confocal height profiles and optical measurements, an increased performance at increased wavelengths is observed for increased crater sizes which decreases the difference in performance compared to low wavelengths (375 nm). For these larger craters, the surface seems less flat-like and

macroscopic scattering/ Mie scattering becomes a possibility. Second, smaller wavelengths are easier to subject to macroscopic scattering/ Mie scattering. This is supported by table 4.2 because the performance at 1000 nm differs between 36.7% and 78.2% while at 400 nm it lies between 55.6% and 81.4%. The difference for 400 nm is smaller and implies smaller wavelengths already reach a stabilised scattering values for smaller textures. The paragraph than results in the conclusion that an optimised micro-texture is equal to a response independent from the wavelength (on the air-glass-air interface) because these textures serve the purpose to affect the longer wavelengths and also influence the lower wavelengths if possible (which is shown here). This does not imply that nano-textures are redundant because the texture sizes are too large for Rayleigh scattering which means inside a cell interference effects can occur.

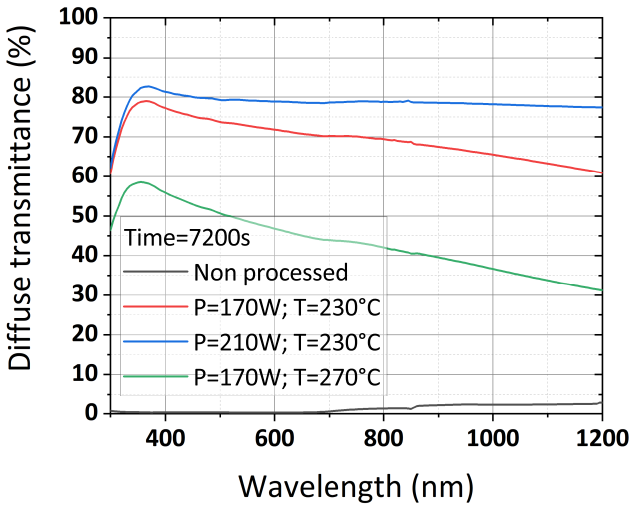

Figure 4.6: Diffuse transmission of the defined 4 samples from the second experiment

Table 4.2: Comparison of diffuse transmittance (T_D) at discrete wavelengths of textures processed at different process parameters. At low wavelengths a highly increased optical performance is observed compared to the other steps. Optimised micro-textures reach a stabilised response over the entire range.

	P (W)		
	170	210	170
	T (°C)		
Wavelength (nm)	230	230	270
1000	65.5%	78.2%	36.7%
800	69.5% (+6.1%)	78.8% (+0.8%)	42.1% (+14.7%)
600	71.8% (+3.3%)	78.9% (+0.1%)	46.8% (+11.1%)
400	77.2% (+7.5%)	81.4% (+3.2%)	55.6% (+18.8%)

Haze ($\frac{T_D}{T}$) is the third parameter describing the optical performance and describes the part of the diffuse light that is diffused. Since the total transmission values do not vary much (+-2%), Haze values have a similar order in their rank of optical properties and only a vertical shift upwards is observed (see figure 4.7). The only difference in curvature is the lack of the measured peak at 375 nm for T and T_D, which is explained by the definition of haze itself that excludes absorption effects. The conclusion for haze is identical to the diffuse transmission where micro-textures must reach a response independent from the wavelength.

Note: A more in-depth explanation how these optical parameters relate to the physical performance is provided in section 4.3.5.

In the previous paragraphs, knowledge is gathered about how light interacts with texturing from which the optimal response can be defined. For this, results of the second experiment are considered (see 4.2.1

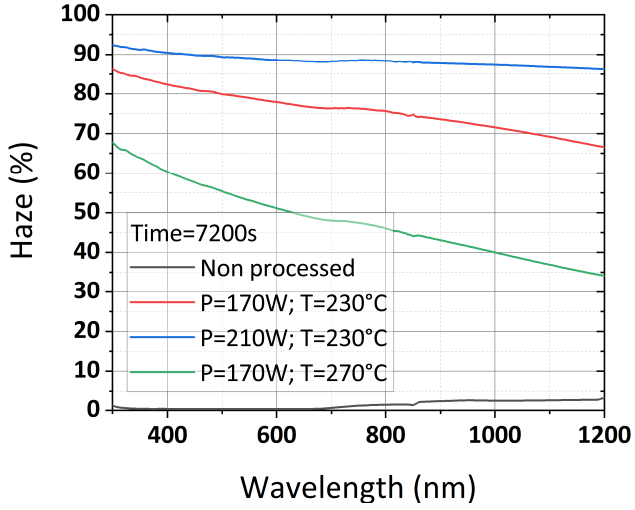

Figure 4.7: Haze values of the defined 4 samples from the second experiment

Table 4.3: Average T_D and haze-values of the second experiment varying deposition- temperature and power while keeping the deposition time at 7200s. The red number indicate the values obtained in the 3rd experiment for identical process parameters and show the variability of this combination of process parameters.

T_D/ Haze	**P (W)**		
T (°C)	170	190	210
230	69.5%/ 75.9%	75.7%/ 83.6%	78.6%/ 88.5%
250	36.7%/ 40.0%	34.8%/ 37.8% versus 78.5%/ 87.2%	79.7%/ 87.8%
270	43.7%/ 48.0%	42.3%/ 46.5%	47.8%/ 52.7%

and table 4.3) because samples are more uniformly textured compared to the first experiment. There must be noted, the first experiment sets the initial optimum which determines the starting point for a more in-depth optimisation study. The reason for using deposition times of 7200s is made after visual inspection, although a deposition of 3600s gives a higher diffusivity, the textures after 7200s is uniformly distributed over the surface. Second, the values marked in red in table 4.3 are included for the optimisation study but not chosen as optimum because the set of parameters give highly variable results which is undesirable. For the optimisation, T-, T_D- and haze values are considered. From T-values, there can only be decided that all samples have a transmittance of 90% or higher, which marks the samples as suitable transmitters. From T_D-values, 3 curves are described by an almost independent response in function of increasing wavelength. The highest diffusivity is produced by depositing ITO at T=250°C, P=210W, the second highest at T=230°C, P=210W and T=250°C, P=190W as lowest performing one. If these results are compared to haze values (see figure 4.7 and 4.6), the order remains similar except for the top 2 samples where the deposition at T=230°C, P=210W has the highest diffusivity. There is concluded process parameters of T=230°C, P=210W and t=7200s (and 10rpm) results in an optimum. It is unknown, if the obtained optimum is a global optimum because an optimisation study is performed at a small range starting from an initial optimum. Other ranges can be further researched an could potentially give even better results (deposition temperatures lower than 150°C are certainly amorphous and must not be investigated).

4.3.3. Optical parametrisation

In previous section the optimal process parameters are described but the influence of these process parameters is as important since it gives control and understanding over the process together with the literature. The sample processed at 250°C and 190W for 7200s gives unstable results, but for the parametrisation the uniform textured sample (red value in table 4.3) is included to correctly asses trends. This section describes the influence of 6 different process parameters: batch processing, temperature,

power, time, rotational speed and a-Si deposition.

Influence of single- versus batch processing
When processing samples, the processing time must always be minimized to work efficiently. In this case, samples must be processed in batches (as many samples as possible in 1 batch) and from these experiments an implicit effect is observed. The etching times increases if the number of samples undergo simultaneous etching. For 3 samples, etching times reach values of 16-21 min to dissolve the sacrificial layer under the condition that samples reach a uniform response 4.1, while for 7 samples, processing times can reach etching times between 25-30min. The wet etching speed provides an explanation, which describes a logarithmic response in function of time. The chemical reaction reaches an equilibrium after a couple minutes because it must stabilise first. This implies, if the number of samples increases it stabilises at a different point in time because the stabilised etching speed differs. Simplified, there is less HF and H_2O_2 inside the solution to affect the result which than requires more time to etch the ITO. For the diffusivity, it does not have an influence because control over the process is obtained for both and no differences in diffusivity is observed.

Influence of deposition temperature and deposition power
The influence of temperature and power are assessed with contour plots showing T_D, haze for discrete wavelengths [400-1000nm:200nm] shown in figure 4.8 and 4.9. These plots show similar trends for T_D and Haze, which is explained by the T-values mentioned in section 4.3.2. First, the influence of temperature is discussed after which the power is discussed. Last of all, the inter-dependency between temperature an power is discussed.

For changing temperature and a fixed power (vertical on contour plot), scattering properties (T_D, haze) increase with decreasing temperature or at least reach a stabilised value. All deposited ITO layers reached at least some form of crystallinity since all of them scatter light (which would not have been the case for amorphous layers) and values are conform with literature. A different temperature affects the balance between crystal growth and crystal initialisation, which causes the morphology to change (crystal orientation <222>). Second, a different temperature provide the difference between a poly-crystalline and microcrystalline layer. This than affects the scattering properties after etching. Lower temperatures seem to translate itself to increased scattering independent from the wavelength. To reach a desired optical performance that scatters light independent from its wavelength, a decreased temperature provides a solution.

For varying power and a fixed temperature (horizontal on contour plot), scattering properties increase with increasing power. The power determines the amount of energy the atom holds when bombarded onto the surface, which must affect the crystal growth (unlikely to affect the initialisation of crystals) and the scattering properties after etching. Higher power depositions seem to translate itself to increased scattering independent from the wavelength. Similar as previous paragraph, to obtain a scattering profile independent from the wavelength, an increased power provides a solution.

If both parameters are changed, an interdependency between both parameters is observed. This means an increased temperature can be compensated by an increased power to reach similar scattering properties. Since both parameters affect the crystal growth of the layer, this correlation is expected. A similar observation is made for reaching an independent relation of the wavelength (shown in figure 4.8).

Note: these trends cannot be extrapolated to the results of the first experiment since most results are unstable, which implies these trends hold until a certain boundary.

Influence of deposition time
Results of the third experiment are assessed to determine the influence of deposition time. It is observed that an entire Design of Experiments is not performed to asses its influence, which has 2 reasons behind it. Unstable/ poor performing samples are not functional to asses the influence of a parameter like deposition time with. Therefore, a previous high performing sample is required which shows trends most clear. Second, reaching results as efficient as possible is a main goal of an engineer and increasing the matrix of experiments with a factor 5 is not realistic. Literature mentioned in 4.1.1 and 4.1.2 is used to analyse and confirm results. Samples processed at P=210W, T=230°C and P=210W, T=250°C show highly different

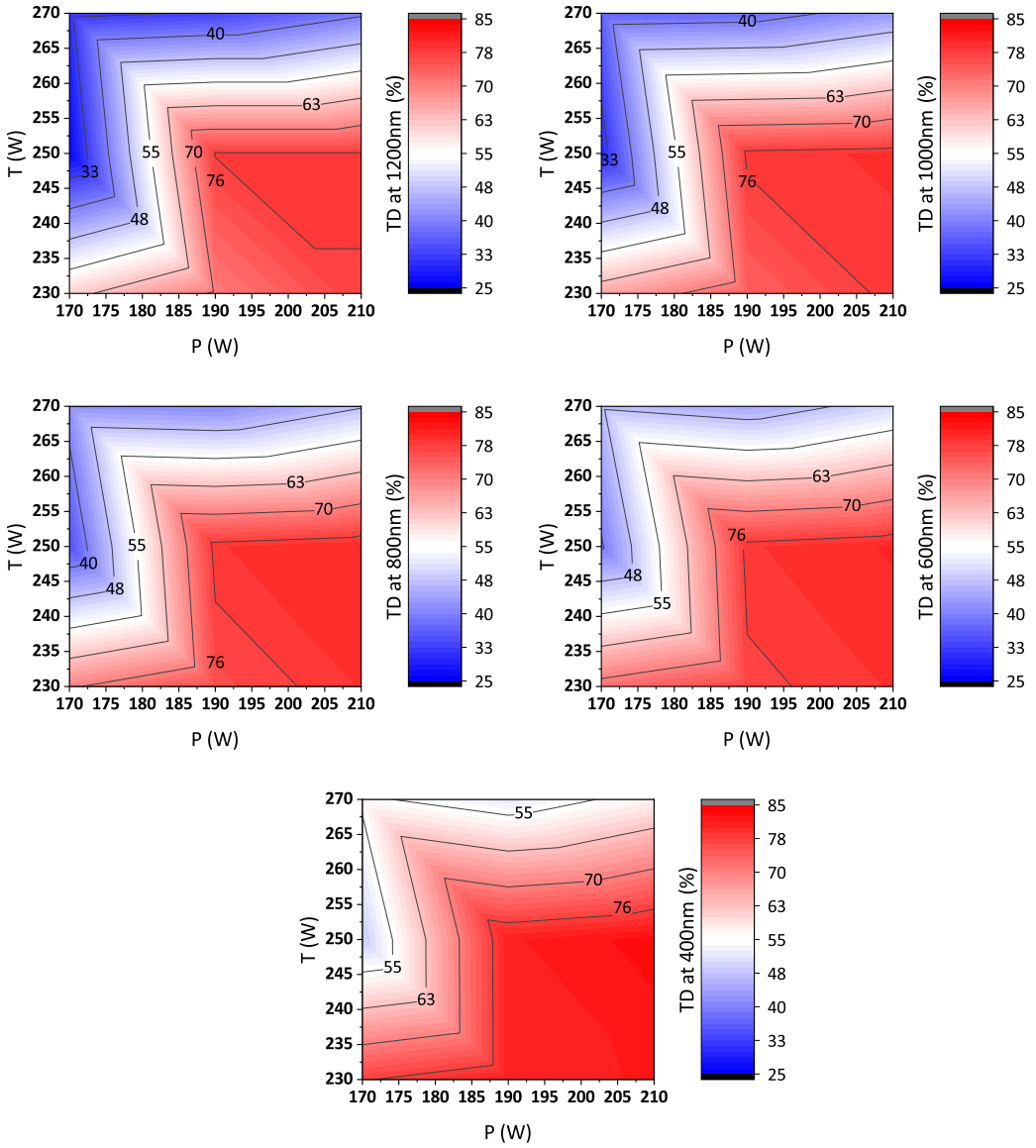

Figure 4.8: Contour plots describing T_D for discrete wavelengths [400-1000nm:200nm]

results for T_D and Haze shown in figure 4.10, 4.11. Multiple samples for each time step are made but differences in outcome occur (are as small as 1.65% up to 45.5% for T_D), for research purposes the highest performing sample is considered. Samples processed at 230°C have diffuse transmittance values not dropping below 60%, while samples processed at 250°C diffuse around 33% of the incident light in the IR-region. The wavelength where the lowest amount of light is diffused differs too, samples processed at 230°C have at 300nm their lowest performance while samples processed at 250°C show this at 1200nm depending on their processing time. For Haze, samples show a similar trend with values not dropping below 75% for diffuse transmittance at 230°C and minima of 36% are reached at 250°C. Last of all, processing at 230°C gives similar results over the entire time range for T_D and Haze.

To explain trends and observations made in previous paragraph, graphs are first observed individually and afterwards compared to each other. For 250°C a general trend is observed, if the processing time increases the optical performance increases. Processing times of 5000s and 6000s overlap for T_D but not for Haze where processing times of 5000s dominates the performance. The general increasing trend is explained by non uniform etching characteristics. If a crystalline or microcrystalline layer is deposited, non uniform spatial etching rates occur (see 4.1.2) and if the layer thickness increases due to increased

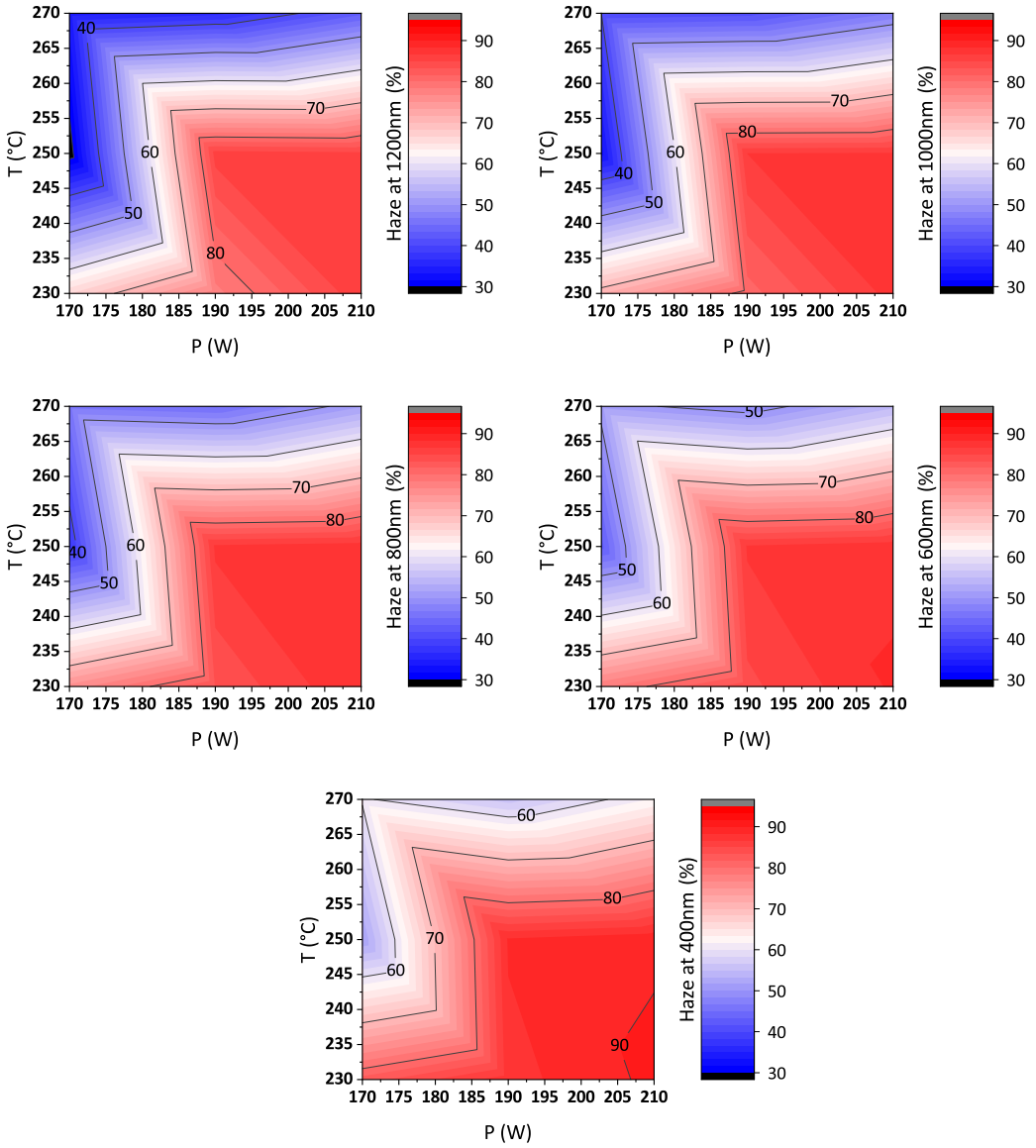

Figure 4.9: Contour plots describing haze for discrete wavelengths [400-1000nm:200nm]

deposition time, this phenomena becomes greater and explains the general trend. For deposition times of 5000s and 6000s, the trend is not followed because it is possible the maximum performance is reached. If this is reached (maximum can be identified by a horizontal response see **??**), it becomes a possibility identical results can be obtained for 5000s and 6000s (actually also including 7200s).

For 230°C, the previously mentioned trends are not observed. All curves lie close to each other (maximum 3% difference)/ overlap except the curve of 7200s which lies around 5-7% higher than the rest (at 1200nm where the differences in optical performance is the biggest). These graphs could lead to contradicting conclusions compared to previous paragraph but the fact that the temperature dropped 20°C must be considered too. Temperature determines the crystallinity (see **??**) and affects the end result too. For 250°C is stated, the maximum performance is possible to reach already at 5000s but for 230°C this maximum is already reached at 3000s. This can explain the difference in trends for the different temperatures.

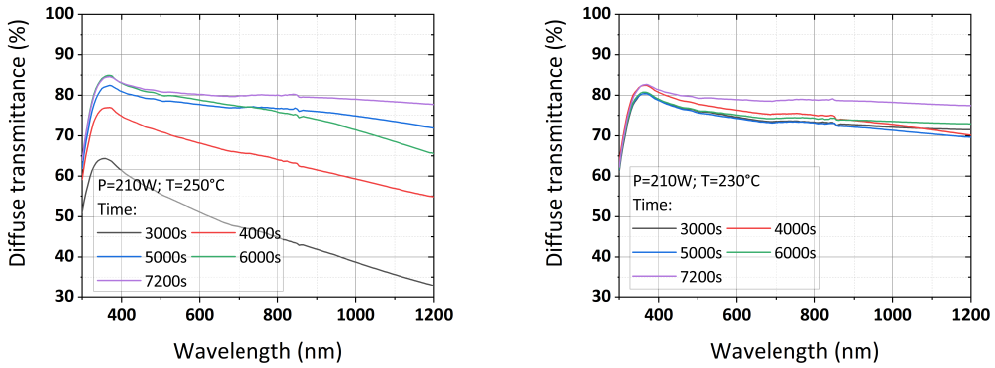

Figure 4.10: Diffuse transmittance of etched samples processed with different ITO sputtering deposition times

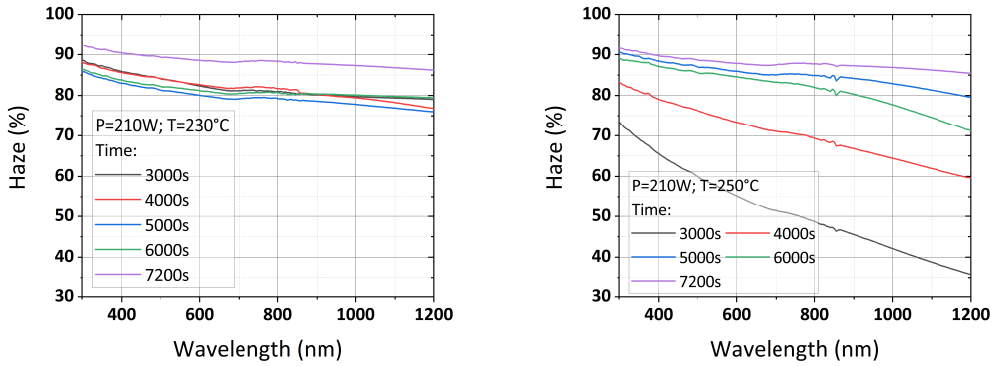

Figure 4.11: Haze of etched samples processed with different ITO sputtering deposition times

Influence of rotational speed

Results from the fourth experiment are assessed to determine this influence, in the work of Loef [28] an increased rotational speed increased the uniformity. Since depositions are performed with the same machine, it must have an identical influence but because 5 years have passed by, upgrades and changes are made to the machine and this parameter must be reassessed.

For scientific purposes, the best performing samples are shown (see figure 4.12) out of a batch of 4 samples per parameter set. These results show a lower performance compared to values from table 4.3 but their relative performance reveals the influence of the parameter. This figure shows the highest performance (T_D, Haze) is reached at 5 RPM but a morphological foundation is not the cause as identical process parameters are used (P, T, t). A difference in rotational speed influences the thickness variation of the sacrificial layer.

Ideally, a PECVD sputtering tool deposits a uniform layer on top of the superstrate but due to wear of the machine and the target, non uniformities in sputtering pattern occur. To overcome this, there are 2 options: finding a match between the non-uniform sputtering pattern and the sample or increasing the rotational speed until the non-uniformity disappears. The first option is desired because a stepper motor is responsible for the rotation and only handles limited increasing values. Samples at 10 or 15 RPM reached in this batch a significantly lower T_D and Haze compared to 5 RPM (around 15% at 1200 nm for both optical parameters). This means at 5 RPM a more uniform result is obtained since the other process parameters are identical (also confirmed by visual observations in figure 4.1, which gives an idea of uniformity differences). The match between sputtering pattern and rotational speed is found here and provides the value at which samples must be processed to obtain a visual uniform structure.

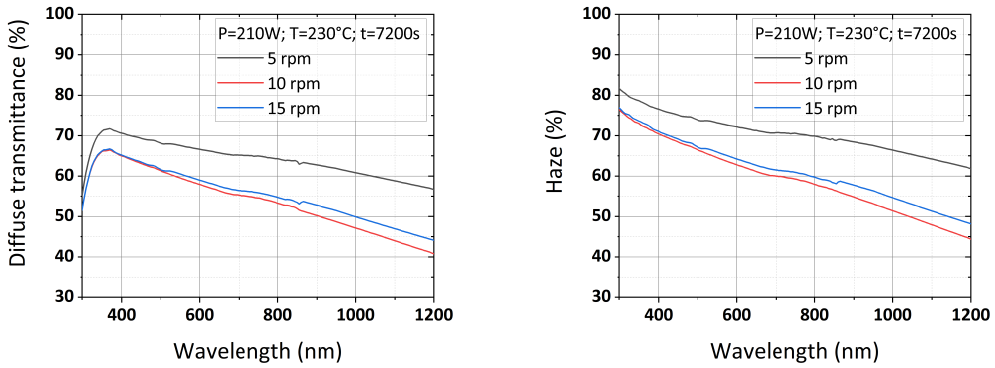

Figure 4.12: Line plots describing T_D, Haze for ITO sacrificial texturing at different processing rotational speeds [5-15rpm:5rpm] and identical process parameters of P=210W, T=230°C and t=7200s

Influence of a-Si deposition

Until now, the optical behaviour of textures is analysed under an air-glass-air interface. To asses the interaction of incident light with layers having a high refractive index, a layer of 30nm a-Si is deposited on top of the textured layer. This deepens the understanding of phenomena occurring in an actual solar cell.

The effect on T_D and Haze are shown in figure 4.13. T_D shows a decreasing trend in function of its wavelength, but does not show solely the difference in scattering performance because of the following reasons:

- T_D includes an increased R because a high refractive material is introduced. This is described in the following formula:

$$R = (\frac{n_1 - n_2}{n_1 + n_2})^2 \tag{4.3}$$

- T_D includes the absorption of light in a-Si in range between 300nm to 800nm for a-Si.
- Below 400nm, glass starts to absorb light and because heavy reflection occurs at the Si-air interface, a large amount of this reflected light gets transmitted again in the glass layer and gets another chance to be absorbed again.

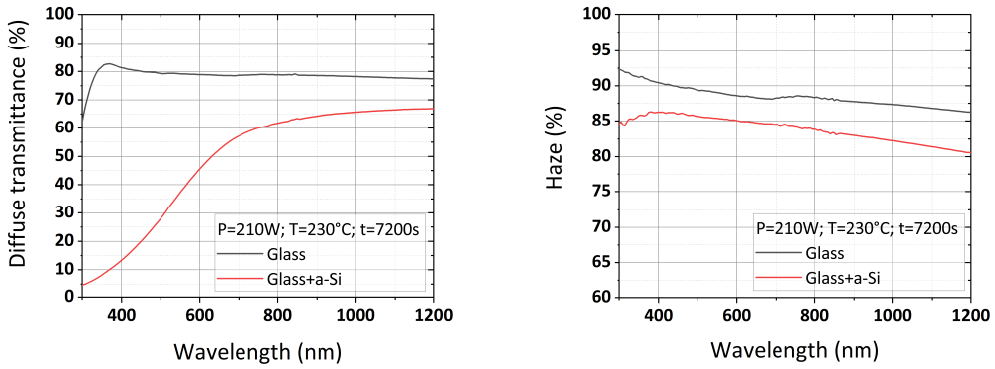

Figure 4.13: Effect of a-Si deposition on T_D and Haze of an ITO-sacrificial textured sample

To asses the scattering behaviour closer, Haze must be considered. For Haze, a decrease of around 3-8% is observed which has the following reasons:

- Between [300-800]nm, a-Si absorbs light which means that diffused light at for example 600nm undergoes heavier absorption compared to the specular component which contributes to the lower haze-values.
- At low wavelengths, haze-values follow a different trend compared to a air-glass-air interface. In principle do haze measurements exclude the effects of absorption as discussed in the definition of

the parameter, but from the previous point is this not always applicable. The heavy reflection at the Si-air interface where a part of this large amount of reflected light gets transmitted again in the glass layer heavily reduces light intensities. This could have influenced the diffuse component of the transmitted light.

- Above 800nm, a-Si absorbs no light anymore which means that the refractive index of a-Si is the only factor affecting the diffuse component of the transmitted light.

The observation is made that T_D and haze-values are affected by the absorption of the a-Si. This implies that the diffuse component of the light is influenced by the deposition of a certain layer on top of it. If there would have been a layer deposited on top with a lower bandgap, differences in T_D and Haze between different micro-textures can become bigger and give an extra confirmation which texture will perform the best inside an actual cell. Second, the deposition of an extra layer on top can provide an extra element to the characterisation of transparent superstrates.

Optically optimal performing parameter set

In previous section, the optical optimal parameter set is decided upon to create micro-textures. The 3 best processing parameter sets are again shown in figure 4.14. Since, processing samples at P=190W and 250°C gives highly variable results (see section) and does not give the highest response for T_D or Haze it was not considered as optimal. For T_D, samples processed at P=210W and T=250°C gives the best response while for haze, samples at P=210W and T=230°C gives the best response. Since haze values are most interesting, P=210W, T=230°C, t=7200s and 10 rpm was chosen as the most optimal parameter set. After the processing of samples at different RPM, 5rpm gives the best result (visual and optical) which means that the optimal shifts towards 5rpm.

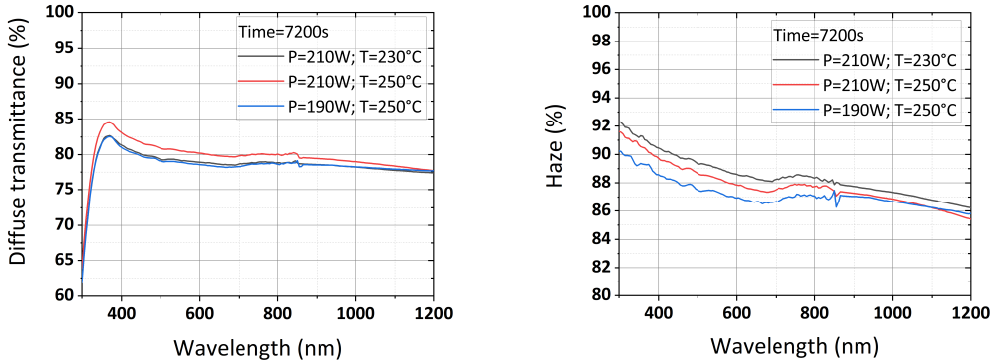

Figure 4.14: Samples processed with the highest optical responses for T_D and Haze under ITO-sacrificial texturing

4.3.4. Physical parametrisation

As mentioned in 2.3.1, there are 6 parameters chosen to characterise the surface (S_q, S_c, S_{al}, S_{tr}, S_{ku}, S_{sk}). In this section trends in function of deposition power, deposition temperature and deposition time are discussed. A physical assessment is as important as the optical one since different layers must be grown on top of the superstrate. Parameters describing height and width (S_q, S_c, S_{al}, S_{tr}) are discussed first and afterwards the parameters describing the curvature (S_{ku}, S_{sk}).

Influence of deposition temperature and deposition power

In previous section, the influence of these parameters to their optical performance is discussed. Now, the influence is tested to the physical parameters for which contour plots are created (shown in **??**) and therefore samples of the second experiment are utilised.

For the interplay between T and P, values of S_q, S_c, S_{al}, S_{tr} are observed first. For S_c and S_{al} the same type of correlation is observed because a maximum is found at the same parameter set (P=190W, T=250°C) (see figure 4.15. This is definitely a local maximum and can be a global maximum for this method because the first experiment resulted only in an initial optimum while most other parameter combinations lead to a

non uniform texture that implicitly translated itself in poor valley depths and widths. In the region towards 210W and 230°C or 250°C another peak can be the result and could prove an even higher peak that translates itself into an even higher peak. It must be noted that in the initial experiment P-values of 245W are tested and didn't prove to have increased texture sizes. Second, this peak indicates both parameters are correlated and finding the right combination is important to get the desired optical and electrical properties. In section 4.3.3, is already described that a correlation of these parameters can exist between the crystal growth and initialisation, which is confirmed by the physical measurements. At higher temperatures, the depth of the craters decreases from 250°C on. From this point the balance of crystal- growth, initialisation is affected which also results in a different crystallinity (amorphous versus microcrystalline versus crystalline). The effect on crystal initialisation is tough to measure but the crystal growth is measured since increased crystal sizes translate itself in increased S_c, S_{al}. From these measurements it is tough to conclude anything about the crystal size and crystallinity of the material since therefore are XRD measurements required, the sole conclusion that can be made is the crystal sizes and crystallinity are high enough to create high non-uniform local etching rates to create a uniform etched surface.

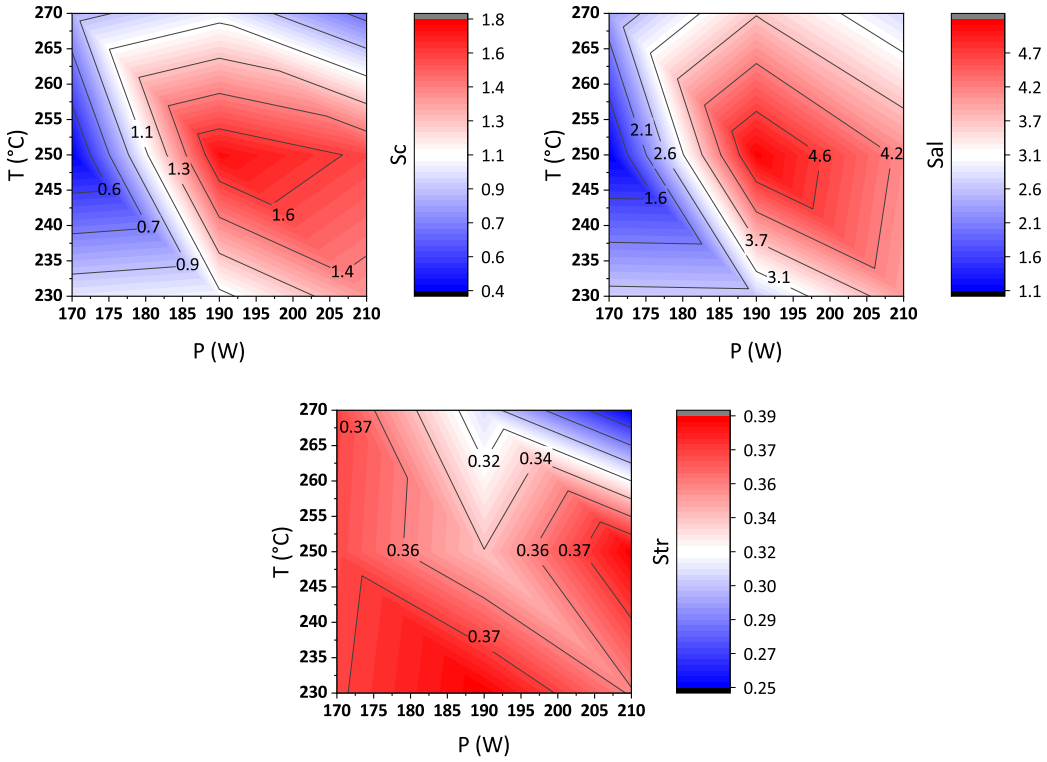

Figure 4.15: Influence of deposition power and temperature on S_c in µm, S_{al} in µm and S_{tr} for ITO-sacrificial texturing

If previous 2 parameters are combined, an influence on the aspect ratio is the outcome (see graph 4.15). The correlation is different to the previous parameters and increases with decreasing power and temperature. Second, there is only a difference of 15% observed, which indicates the height to width ratio has limited adjustability. For the determination of the optimal aspect ratio for electrical parameters, a more in depth study of nc-growth on random textures must be performed.

For S_{ku}, S_{sk} there is no clear trend observed (shown in figure 4.16), but there are regions which must not be considered to process solar cells on. For S_{ku}, around T=250°C and P=170°C high Kurtosis values are obtained which implies the surface has sharp peaked structures and could pose problems when growing other layers on top of it. Values beneath a Kurtosis of 3 are considered smooth in literature, which means that lower temperatures and higher power values give desirable results. If the etching hemispheres created beneath this sacrificial mask have increased overlap, the sharpness of the peaks are decreased

and lowers the Kurtosis. This parameter is not necessarily related to the process parameters but acts as a quality of the outcome. For S_{sk}, it is difficult to describe trends and no correlation between T and P is found. The only observation is that low values (must lie close to 0, see 2.3.1) are obtained around the region with increased crater size. This describes a surface profile with no flat parts and contributes to the definition of well defined textures.

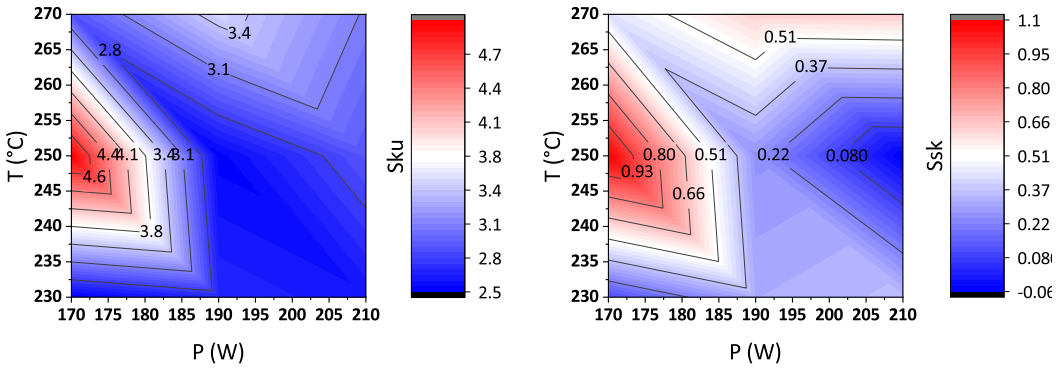

Figure 4.16: Influence of deposition power and temperature on S_{ku}, S_{sk} for ITO-sacrificial texturing

Influence of deposition time

The influence of the deposition time is combined with changing P or T individually (see figure 4.17. For S_c and S_{al}, a clear increasing trend with its deposition time is observed. The behaviour describing its optical performance given in section 4.3.3.3 is confirmed by these graphs. The effect of local non-uniform etching rates increases and leads towards greater crater sizes. Second, there is only a limited correlation between power and deposition time for S_c and S_{al} because the plot shows a vertical trend. For S_{tr}, trends for the deposition time are difficult to describe but P influences the aspect ratio around 0.1. It affects the grain sizes, which explains the aspect ratio difference afterwards.

For S_{ku}, S_{sk}, Kurtosis values show no clear trend/ correlation for both parameters, high deposition times above 6000-6500s obtain smooth surfaces. For Skewness, deposition times and power are heavily correlated in this window and obtaining less flat surface area is created by increasing the deposition power for the same amount of deposition times. This is interesting when thinking about growing nc-Si on top of it, where flat surfaces must be avoided due to crack forming phenomena.

The influence of deposition time is also combined with T, shown in figure B.1. The parameters previously unaffected by P are now correlated to T. The width of the craters S_{al} is related to T, increasing temperature lead generally to lower craters widths in this window but towards high deposition times (around 7000s) this effect becomes negligible. The aspect ratio S_{tr} shows similar trends as for P and are independent from the deposition time but lower aspect ratios are easier obtained for lower temperatures (although a bigger temperature range with stable performing samples must be created to verify this completely). This time the S_{ku} is the parameter affected and not S_{sk}, smooth surfaces are obtained at lower temperatures (at 230°C Kurtosis values lie all below 2.7) which makes it more beneficial to grow nc-Si on top of.

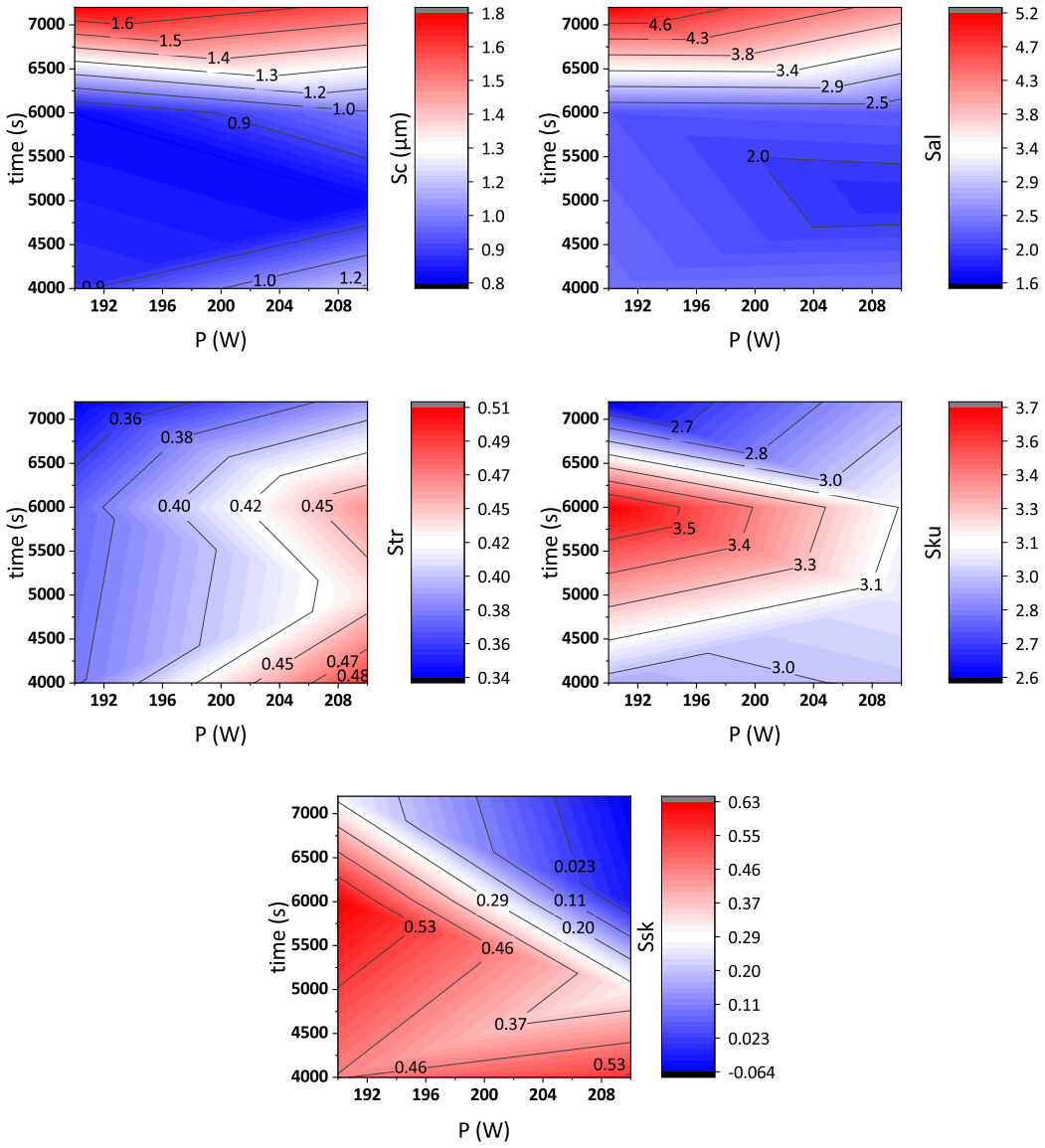

Figure 4.17: Contour plots describing the influence of deposition time and P for S_c, S_{al}, S_{tr}, S_{ku} and S_{sk} for ITO-sacrificial texturing

4.3.5. Correlation between optical- and physical parametrisation

Until now the process parameters are incorporated in the analysis of the physical and optical parameters, but since the physical profile determines the optical performance of sample, both parts must be correlated to each other. This section describes which physical parameters are dominant to cause a high diffusivity. In general, T_D is used as parameter to asses the correlation but for graphs showing prominent correlations with the physical parameters a comparison with Haze is also investigated.

Parameters S_q, S_c show a similar trend with T_D but for S_q the trend is most defined (see figures 4.18, 4.19). Both parameters are a measure for the crater depth but the way both are defined is different (see 2.3.1). At higher roughness values, the maximum T_D is reached and a saturation of the curve is obtained. This saturation is approximated by a sigmoid function and matches with the different data points. The fit is most defined for S_q since its R-square values are the highest and reach values above 0.7 (shown in table 4.4). For different wavelengths, absolute values of T_D in saturation are different and the point at which saturation starts at a roughness of 0.8µm and crater depth of 1.1 µm for 400nm and at a roughness of 0.9-1µm and crater depth of 1.4µm for 1000nm . Physical, the increased roughness means height deviations

from the reference plane increases which translates itself to increased crater depths. This increase gives higher wavelengths a better chance to be involved in macroscopic scattering or Mie-scattering because roughness values are in this case similar in size to the wavelengths of the IR-region. After this point, the maximum interaction with the light is reached no longer improves the results. Smaller wavelengths also find itself having an increased optical performance at increased roughnesses which is be explained by the increased surface area. Altough Mie-interactions are smaller due to increased profile heights, more surface area finds itself to be under an angle (deviation from flat surface) that deviates the path of the light upon incidence. Again this effect reaches a maximum interaction around 0.8µm because at that point the light is already heavily influenced by the texture.

Table 4.4: R-square values of a boltzman sigmoid fit to correlate S_q, S_c to T_D for ITO-sacrificial textured samples

	Sigmoid fit (R-Square)			
Physical parameter	400 nm	600 nm	800 nm	1000 nm
Sq	0.74	0.76	0.78	0.79
Sc	0.53	0.56	0.57	0.54

If Haze values are observed, identical trends are observed and only a vertical shift upwards occurs. Total transmission values lie all between 90-92% which causes no big shifts in trends to occur. To conclude, roughness measurements can predict the optical performance over the entire spectrum or the other way around.

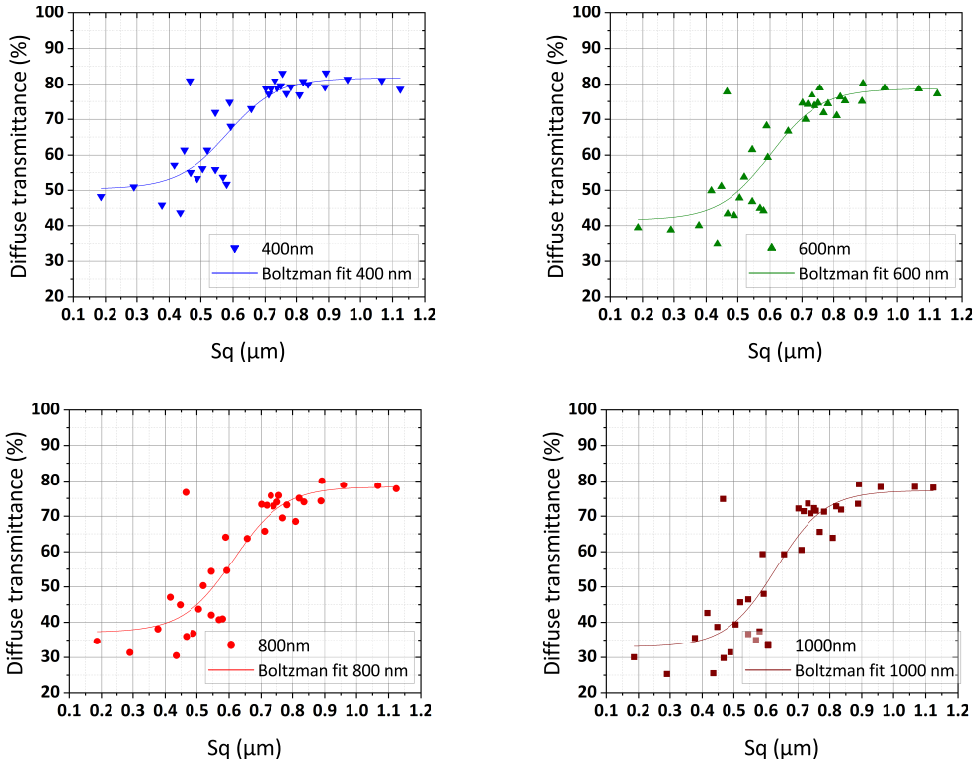

Figure 4.18: Scatter plot of the correlation between S_q and T_D for ITO-sacrificial texturing

Parameters S_{al} is a measure for the width of the craters and show also a trend with T_D (see figure 4.20). Their correlation is smaller because different fits reach maximum R-square values of 0.42 for 400 nm and 0.5 for 1000 nm with an exponential fit, other fits only reach lower values. A similar physical explanation is given as in previous paragraph. The increased width gives longer wavelengths a higher

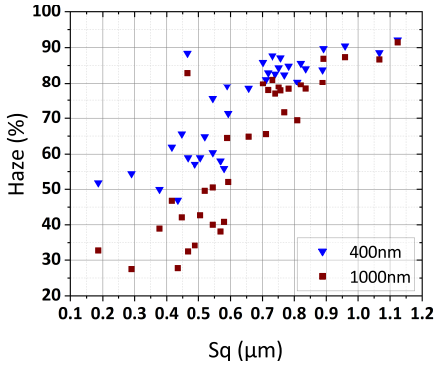

Figure 4.19: Scatter plot of the correlation between S_q and Haze for ITO-sacrificial texturing

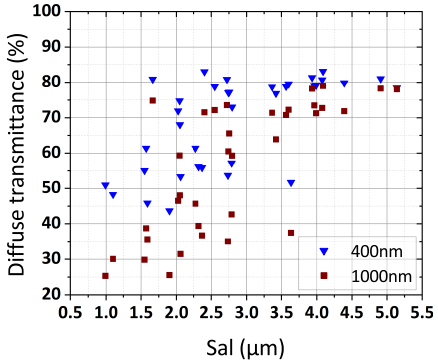

Figure 4.20: Scatter plot of the correlation between S_{al} and T_D for 400nm and 1000 nm for ITO-sacrificial texturing

chance to interact with it, which is seen as less flat so interactions like Mie-scattering or macroscopic scattering increases T_D. From R-squared values, the depth influences the light more compared to the width.

Parameter S_{tr} does not show a clear trend, which implies the ratio between depth and width does not accurately predict how well a sample performs (see figure 4.21). The only thing observed is the highest performing samples have aspect ratios between 0.3-0.4 (P=210W, T=230°C, t=7200s; P=210W, T=250°C, t=7200s; P=190W, T=250°C, t=7200s). The second best group of samples describe a aspect ration between 0.25-0.3 (P=210W, T=230°C, t=3000-6000s). Since samples with identical aspect ratio also exist, showing low absolute values and low relative values, other parameters must also be measured to be conclusive.

Since S_{tr} is not correlated to T_D, this gives suspicion the width and depth of the crater are correlated to each other. The correlation between S_q, S_c and S_{al} is shown in figure 4.22 and shows the following R-values for a linear fit:

- S_q = 0.84
- S_c = 0.77

As predicted, these parameters are correlated to each other which means that not any type of structure is able to be obtained. This observation is critical for the electrical performance and performing simulations. For example, if the nc-Si growth on top of this layer creates cracks in a nc-Si layer and a lower depth is required for the same width of the crater, different process parameters will not solve this. To create a highly different depth- width ratio, other sacrificial layers must be used because their linear trend has a different slope. For simulations, there must be noted not every type of structure can be created in practice

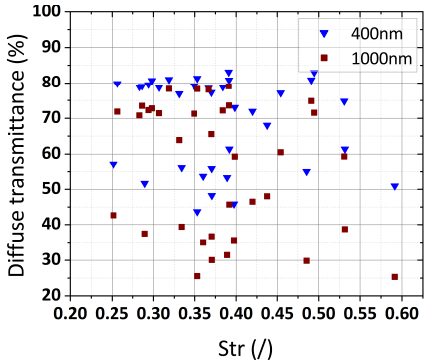

Figure 4.21: Scatter plot of the correlation between S_{tr} and T_D for 400nm and 1000nm for ITO-sacrificial texturing

and these type of slopes must be considered beforehand.

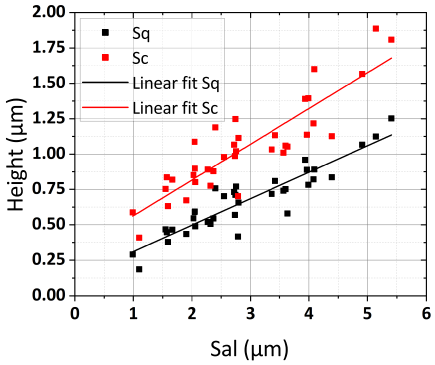

Figure 4.22: Scatter plot of the correlation between S_q, S_c and S_{al} for ITO-sacrificial texturing

Parameters S_{ku}, S_{sk} show no trend correlated to their optical performance and are therefore shown in figure B.2, B.3. These parameters are not correlated to optical performance but do not invalidate their importance because they are chosen as parameter to relate it to the electrical performance/ obtain a good electrical performance. The samples with the highest T_D (as mentioned for S_{tr}) seem to have the following values:

- S_{ku} = [2.5;3]
- S_{sk} = [-0.2;0.4]

To conclude, the parameters S_q and S_c are the parameters that determine the optical response of the texture. S_{tr} and S_{al} have less of an influence but both parameters are again correlated to the crater depth which makes them important too.

4.3.6. Angular intensity distribution analysis

The macroscopic scattering properties of these textures are already discussed via the T_D and this parameter confirms the textures are able to bend/ scatter the light almost independent from the entire spectrum if the layer is deposited under P=190-210W, T=230-250°C and t=7200s. The question that remains is if the textures scatter light in broad angles and how the textures interact with light exactly. This is performed by adjusting the sample angle, measuring the AID under different wavelengths and depositing a layer with a high refractive index on top of it (30nm a-Si). This in-depth knowledge gives us predictions, which type of textures provides us with the highest efficiencies if crack-free nc-Si can be grown on top of it.

One of the optical optimal textures (P=210W, T=230°C and t=7200s) is chosen to asses the AID with and the response at 600nm is shown in figure 4.23. It is clearly shown that the exponential decrease is

dominant until around 40 degrees after which Lambertian scattering becomes the dominant effect and stays above 1e-4. This indicates light is scattered heavily over 40 degrees and low intensities of light are scattered over larger angles.

If the angle of the sample is increased by 10 degrees, the intensity of the light perpendicular to the sample decreases. This is explained by the fact that light is bend over 10 degrees and some light goes straight through the sample. If both curves from figure 4.23 are compared to each other, a shift of 10 degrees to the left occurs, which means Lambertian scattering becomes dominant around 30 degrees. Second, Lambertian scattering intensities lie slightly lower which could also be explained by the initial lower intensities of the light. There is concluded, the angle of incidence does not have a significant influence on the scattering properties because the shift to the left seems to be the only effect it has on the AID.

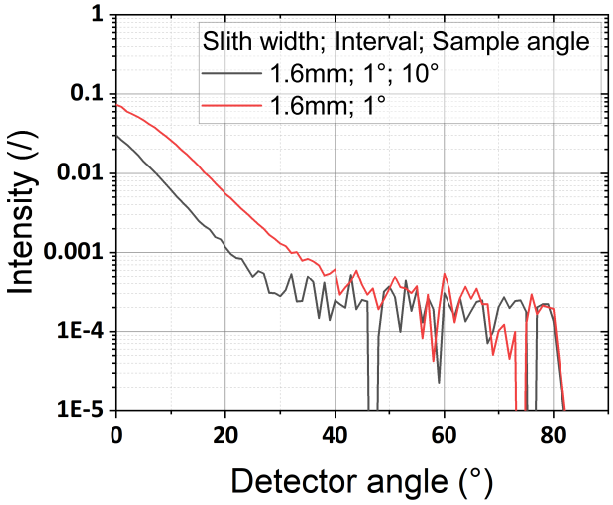

Figure 4.23: AID for ITO-sacrificial superstrate deposited under P=210W, T=230°C and t=7200s under 2 different angles 10° apart for 600nm

The effect for different wavelengths is shown for 4 different wavelengths in figure 4.24. The response of 600 and 800nm shows a similar response, while the response of 400, 900 nm has a highly volatile response. This volatility is not created by the surface itself but by the detector sensitivity and light spectrum observed by Jäger et al. [19]:

- The beam energy of the source depends on the wavelength and reaches low values around 370nm and also between 800 and 900 nm.
- The detector has a low sensitivity for wavelengths lower than 400 nm and between 800 and 900 nm.

These observations explain the volatility of the measurements because a low beam energy results in small deviations in measured intensities creating highly different outcomes. Second, a low sensitivity of the detector results in differences in intensities being difficult to detect or it does not respond to the incident light. The measurement for 400nm gives too high intensities from 25° on, which can be caused by the previous mentioned effects. The Lambertian response must give a lower intensity because micro-textures scatter less in broader angles for lower wavelengths. The volatility for 900 nm can also be explained by the previously mentioned effects. The exponential decrease is not observed, while a certain Lambertian response is observed. The Lambertian response is possibly too exagerated but it confirms the fact just as 800nm does, that higher wavelengths reach higher intensities at greater angles. Including previous statements, different trends/ observations are made:

- For increasing wavelengths, the exponential decay shows a vertical shift upwards, while the curvature stays identical. For example, from 600nm to 800nm, a vertical shift of 0.01-0.02 occurs. It shows that ITO microtextures scatter more light in the smaller angles at higher wavelengths. The exponential decay at 400nm also confirms this trend.

- For increasing wavelengths, the Lambertian decay shows a vertical shift upwards. The shift is more significant because from 600nm to 800nm, the intensity increases with a factor 10. It shows that ITO microtextures scatter significantly more light in higher angles for increasing wavelengths.
- Due to the difference in increased performance for exponential- and lambertian decay, the shift in dominant effect occurs around 5-10° earlier between 600nm and 800nm.

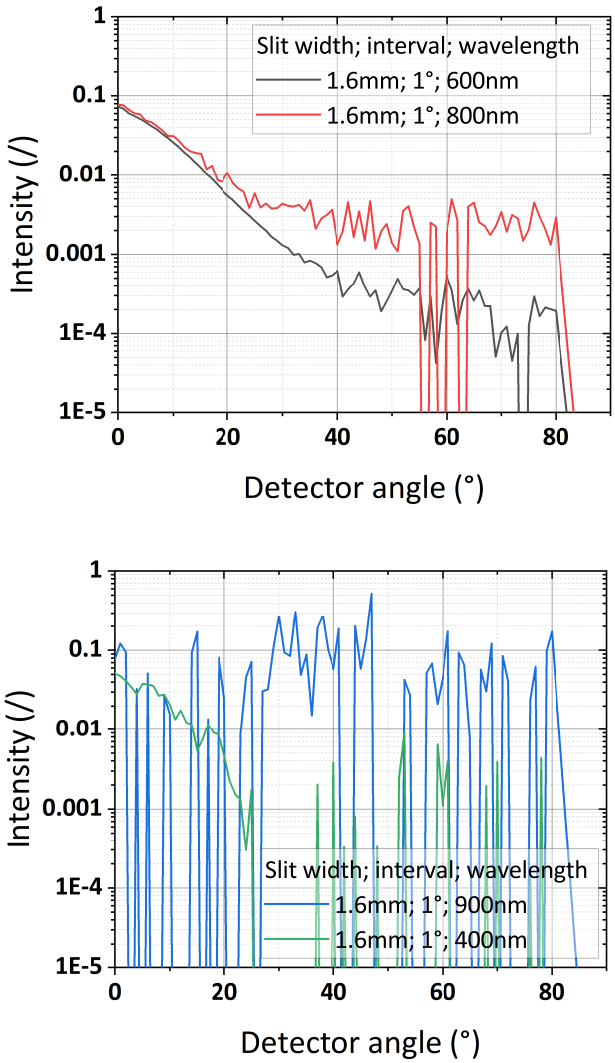

Figure 4.24: AID for ITO-sacrificial superstrate deposited under P=210W, T=230°C and t=7200s under 4 different wavelengths

These observations lead to the conclusion that the created sample is an effective scatterer, but because an air-glass-air interface is implemented, questions can be raised about their applicability towards solar cell applications. Therefore, an identical analysis is performed including a deposition of 30nm a-Si. In figure 4.25, the results are shown that include this a-Si layer. Before trends are discussed, the volatility for 400nm and 900nm is discussed. For 400nm, the exponential- nor Lambertian decay is visible which indicates the noise of the measurement is so large that the measurement data is lost. In this region, a-Si heavily absorbs light which causes the transmitted light intensities to be lower. For 900nm, the exponential decrease is not measured but there is suspicion the Lambertian decay is measured although it can be exaggerated. From previous statements, the following trends/observations are made:

- For 600nm, the initial intensity (specular component) decreases but this is the result of an increased reflectivity at the glass-aSi and aSi-air interface.

- For 600nm despite the lower specular component, the rate of exponential decay is lower and results again in an intersection of the 2 different effects around 40 degrees.
- Even including the a-Si layer, the Lambertian decay stays present and causes light to be scattered in wide angles. The Lambertian decay lies slightly higher compared to the air-glass-air interface (600nm for example).
- Similar to the air-glass-air interface, increased overall intensities are measured for increased wavelengths which indicates that adding high refractive layers does not compromise the efficiency of the scatterers.
- If both experiments are compared independent from the wavelength (excluding 400nm), the Lambertian decay always shows an increased response including the a-Si interface.

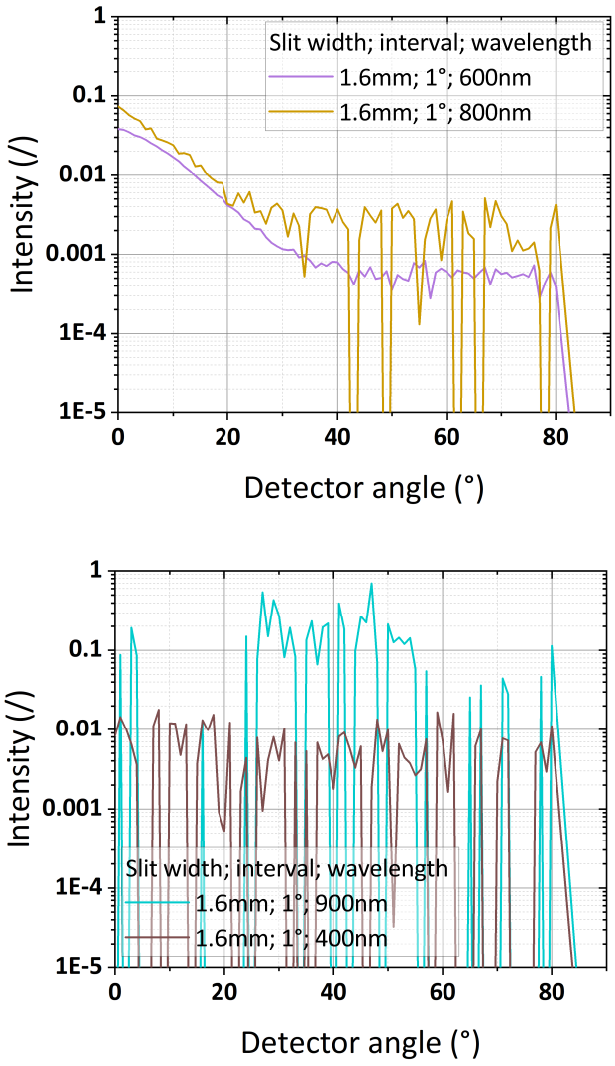

Figure 4.25: AID for ITO-sacrificial superstrate deposited under P=210W, T=230°C and t=7200s, including a 30nm thin layer of a-Si for 4 different wavelengths

This section states that light heavily scatters in high angles for high wavelengths but also affects lower wavelengths although intensities at higher angles are lower. This holds independent from the layers deposited on top of it. Compared to literature [14] and [28] an improved performance is obtained. This can result in cells having an improved EQE and efficiency afterwards.

4.4. Results: Aluminum Zinc Oxide sacrificial texturing

Similar to the goal of ITO sacrificial texturing, high optical scattering must be obtained while not deteriorating the electrical performance of the final cell. Since the process develops micro-textures, the main focus lies on boosting the high wavelength response (IR-region) which can be compared to the ITO sacrificial textures. The only way to reach this is by a complete understanding of the process and finding the right combination set, that creates craters able to affect this. If complete control is obtained, it is also possible to create nano-textures to end up with an MST texture as described by Guangtao [20].

First, the influence of deposition power and the deposition time is discussed that provides this work with an optimal parameter set. Second, a physical parametrisation is performed to get a deeper understanding of the process. Afterwards, there is determined what physical aspect of the textures causes the light to be scattered. Last of al, there is determined where the texture scatters light towards.

4.4.1. Optimal optical texturing

Before the optimal process parameters are discussed, there must be discussed if the physical outlook and optical response are similar to section 4.3.2 to completely understand the process. Therefore, 2 samples processed with different parameters are discussed:

- Deposition power: 400W; Deposition temperature: 400°C; Deposition time: 900s
- Deposition power: 400W; Deposition temperature: 400°C; Deposition time: 3600s

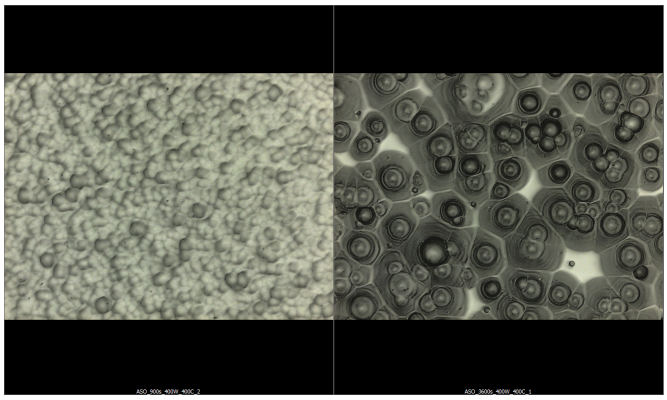

Figure 4.26: Confocal picture of AZO sacrificial texturing with 2 different process parameters: left: P=400W, T=400°C and t=900s and right: P=400W, T=400°C and t=3600s

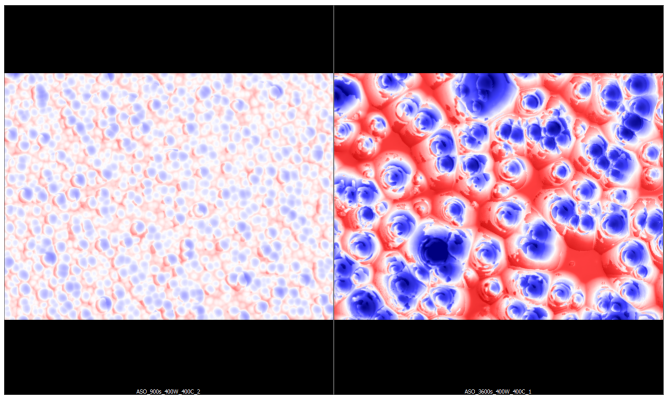

Figure 4.27: Confocal height measurement of AZO sacrificial texturing [-2,253:2,253]µm with 2 different process parameters: left: P=400W, T=400°C and t=900s and right: P=400W, T=400°C and t=3600s

First, the confocal measurements are considered (shown in figures 4.26, 4.27)). From the height measurements, blue areas indicate zones lying below the reference lines and define the craters of the texture while red areas lie above the reference lines and define the peaks of the texture. The left measurement shows

only slight coloring which indicates the superstrate is flat-like and only shows an indication of nano-textures, which is not the result that is striven for. The measurement on the right shows well defined coloring which indicates wide and deep craters are created. The width and height of the craters seem to be correlated to each other. To confirm the confocal measurements, they are again compared to SEM- and AFM imaging. SEM gives an identical outlook compared to the confocal measurements and crater widths are identical in size. For the AFM, craters depths are similar and here the difference in crater shape with ITO sacrificial textures becomes clear. From these measurements is concluded that the confocal measurements are a valid tool to asses the textures with.

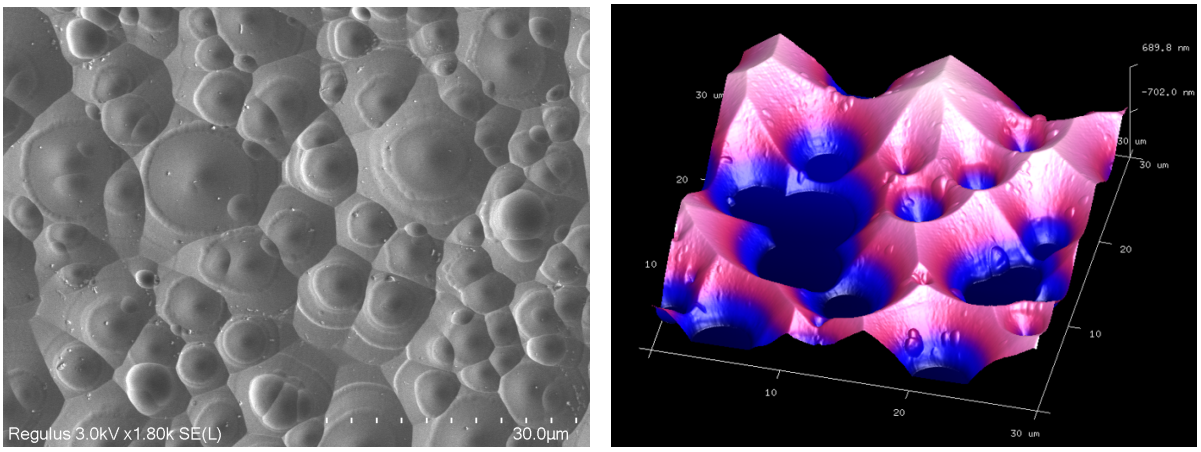

Figure 4.28: SEM image of AZO sacrificial texture processed at P=400W, T=400°C and t=3600s. Particles shown on these images represent dust particles and represent wear of the sample because the image is first exposed to different optical characterisations. AFM figures show large micro-textures with non-hemispherical characteristics.

Second, the expected optical performance (T,T_D and Haze) must be described to understand the interaction in function of different wavelengths better and they are shown in figure 4.29. For T, both curves follow a high transmittance (˜91%) that is comparable to non textured glass superstrates of 91.5%. Around 370nm, a peak is observed that does not exist for the non textured superstrates. This is explained by the decreased reflectance at the textured interface and is already explained in section 4.3.2. The decrease of T around 370nm and other light interactions that occur is also already explained in the same section. For T_D, results are similar to section 4.3.2 and can be explained accordingly. Although the outlook of the craters differs from ITO sacrificial texturing, the optical response is similar. Longer wavelengths still require bigger craters to affect it, the decrease after 370nm is caused by the absorption of the light... For Haze, the outlook of the measurements are very similar to section 4.3.2. Since T shows no variation, results are similar to T_D while simultaneously taking the absorption out of the equation. Although results are similar (T, T_D and Haze), it does not imply the wavelength interaction with light is identical and the physical outlook of the crater does not have an influence. Aspects that can differ between these texturing methods are the angles where the textures scatters light towards and their respective maximum optical response.

In section 4.3.3.1, the influence of implementing batch processing is determined to be important. For AZO texturing, this is not important because high concentrations are used for the etching process. Stable results are obtained independent on the number of samples processed. In general, higher concentrations of chemicals increase the etching rates, which reduces the control over the process. This can potentially destabilise the process but for this process it is not the case. Since the concentrations in the bath are already high [HNO3:HF=8:1], increasing the number of samples processed simultaneously does not affect the end result or processing time significantly.

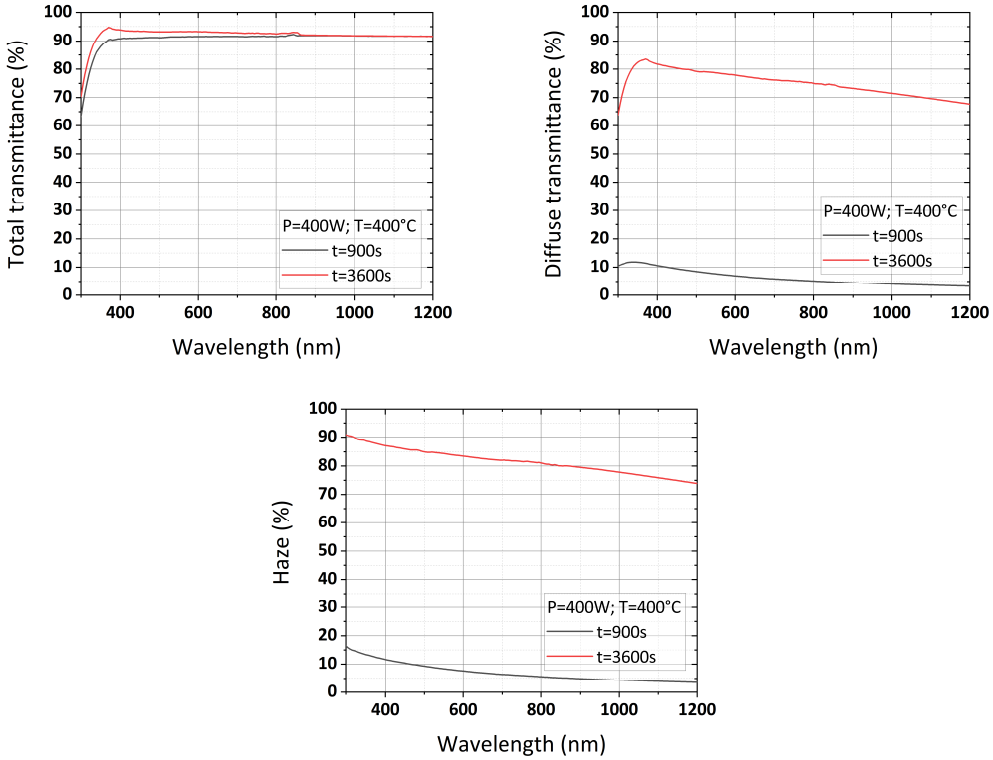

Figure 4.29: Total transmittance, diffuse transmittance and Haze of the defined 2 samples from the second experiment for AZO sacrificial texturing

Influence of deposition power

To asses the influence of the deposition power, line plots shows the influence on T_D and Haze in figure 4.30. These results show processing samples at 400W is the most optimal because T_D (between [300-1200]nm responses of 84% to 68%), Haze (between [300-1200]nm responses of 74% to 91%) show the highest overall response, which implies that at least a local optimum is found. As mentioned in 4.3.3.2, the crystal growth can be affected by this parameter. Increasing P, leads towards increased crystal growth, increases the roughness and that leads to an increased T_D. For 450W, this explanation does fit the results. The boundary of this effect of increased power is reached because for a fixed T a balance needs to exist considering P. If P is further increased, the effect of increasing RMS does not hold anymore. For ITO sacrificial texturing a similar result occurs when values of the first experiment are considered.

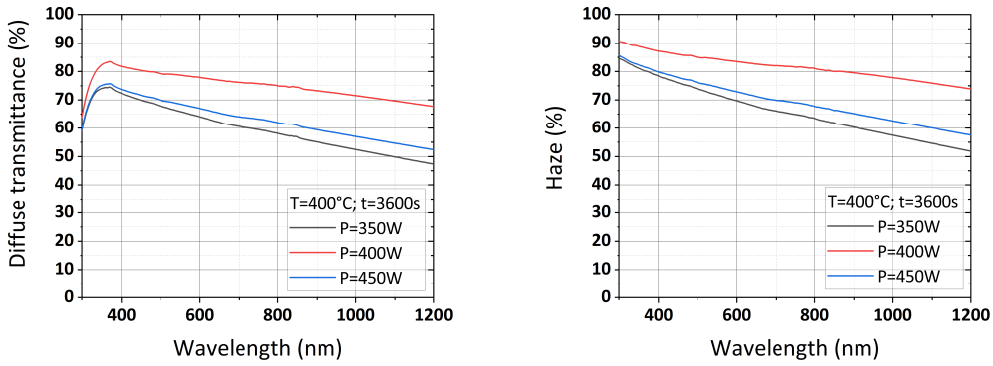

Figure 4.30: Line plot describing T_D, Haze of AZO sacrificial textured substrates between [300-1200nm:5nm] for changing P between [350-450W:50W]

Influence of deposition time
For the deposition time, line graphs shown in 4.31 show an increasing trend in function of deposition time. Large differences in scattering properties occur, T_D reaches values lower than 5% at 1200nm for t=900s, while 68% is reached for 1200nm for t=3600s. Since the sample with t=5400s did not result in textures, it is not shown. From these graphs is observed, a maximum performance occurs at 3600s, where performance is identical to the optimal sample of section 4.4.1.1 (identical process parameters). The reasoning behind it lies at the non uniform local etching rates which has an increased influence on the outcome. The grains have an increased chance to grow further during deposition and during the etching process, chemicals require more time to remove the complete layer. From both sections can be concluded that using processing parameters P=400W, T=400°C and t=3600s has the best scattering properties. According to this reasoning, a processing time of 5400s must give an increased optical performance but this parameters also has its limitations. First, if the thickness keeps increasing, it becomes a possibility the glass surface is already completely textured while the sacrificial layer is not removed yet which can pose a problem for the texturing. Second, reaching uniform textures over the surface is always a matter of balancing different processing parameters. If the time aspect is disregarded, saturation of the textures or non-uniformity's can develop.

Similar to section 4.3.1, the deposition thickness is not equal to one defined thickness. As general notion, the following parameters result in a defined thickness: Deposition power: 400W, Deposition temperature: 400°C, Deposition time: 3600s results in a thickness of 817nm and Deposition power: 300W, Deposition temperature: 400°C, Deposition time: 3600s results in a thickness of 593.1nm

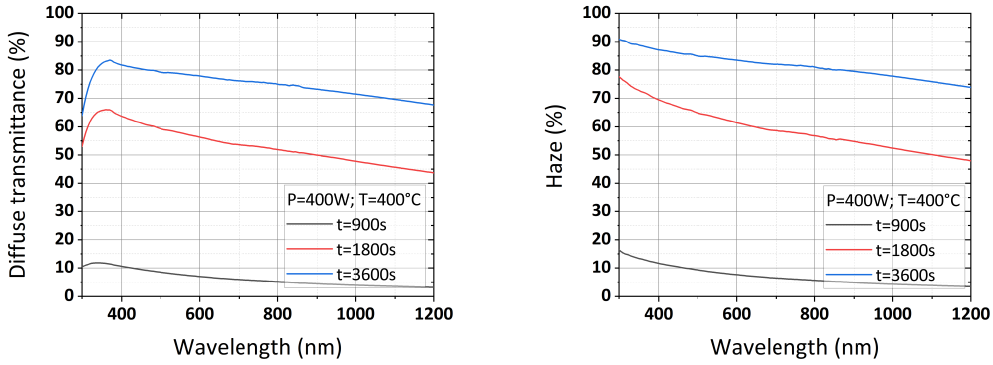

Figure 4.31: Line plot describing T_D, Haze of AZO sacrificial textured substrates between [300-1200nm:5nm] for changing t between [900s; 1800-5400s:1800s]

Influence of a-Si deposition
For AZO-sacrificial texturing a similar approach is taken to section 4.3.3.5 to represent light interactions in a solar cell better. Results are shown in figure 4.32 and it shows a similar interaction. For T_D, the only difference is that a maximum occurs around 950nm. For Haze, the difference in performance is very similar and also lies around 2-9%. Since, interactions are similar there is referred for further explanation to 4.3.3.5.

Optically optimal performing parameter set
In the previous sections, the effect of power and time are discussed to gain control over the process and reach an optical optimal texture. From the performed experiments, changing P and t resulted in the following optimal parameters set: P= 400W, T= 400°C and t= 3600s. It must be noted, the parameter of T is not changed in this worked because adjusting P and t-values already resulted in uniform textured superstrates. In future work, T can be adjusted to boost the optical performance even more according to literature Guangtao [20].

4.4.2. Correlation between optical- and physical parametrisation

In section 4.3.4, the physical parametrisation and the correlation to their optical performances is discussed in depth. Due to the limited amount of samples produced for this topic, conclusions and correlations that can be made are limited and further research must be performed to reach the same level of in-depth insights as for ITO sacrificial texturing. There must also be stated that literature about AZO sacrificial

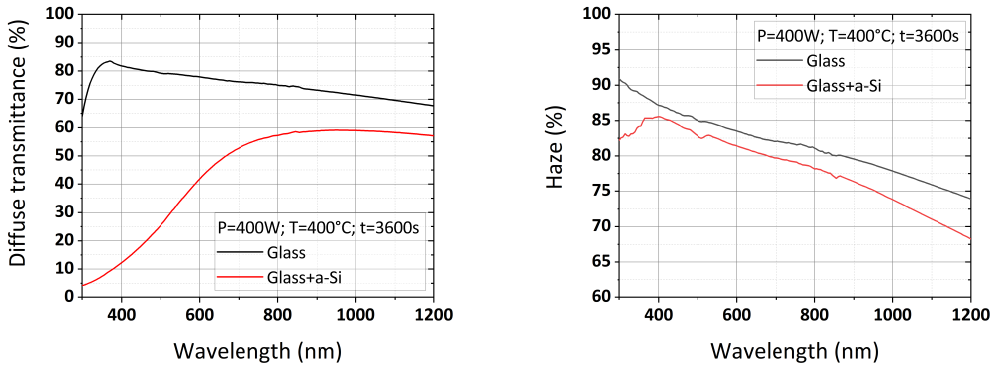

Figure 4.32: Effect of a-Si deposition on T_D and Haze of an AZO-sacrificial textured sample

texturing is more abundant compared to ITO sacrificial texturing Nevertheless, both texturing methods have similarities in processing steps and outcome which makes parameters and reasoning behind occuring effects (roughness, crater width..) similar. The physical parametrisation is not discussed because of the limited amount of datapoints it has, compared to ITO sacrificial texturing. For example, in section 4.3.4 a clear interplay between T and P exists for S_q, S_c, S_{al}, S_{tr}, which exists of 9 datapoints compared to 3 datapoints obtained for AZO sacrificial texturing.

For AZO-sacrificial texturing, only the parameter S_q shows a trend (other parameters have too little samples to expose trends with) and is shown in figure 4.33. S_c in this case does not show a trend, which means that the definition of the crater depth in terms of S_q defines the surface better. A linear trend is observed and a maximum T_D of 71% at 1000nm and 81.8% at 400nm is generated for a roughness of 0.8 µm. Since S_{al} shows no trend, the depth of the craters is the influencing factor for creating macroscopic scattering/ Mie scattering. Low energetic wavelengths are similar in size compared to the crater depths which explains their high optical response. Higher energetic wavelengths also are positively influenced by this increased crater size, which is explained by an increased inclined surface area, which causes a straight light ray to deviate from its straight path length. According to this trend, increasing the roughness keeps increasing the optical performance. This is not realistic and saturation must starts to form around a certain depth/ roughness as seen in figure 4.18.

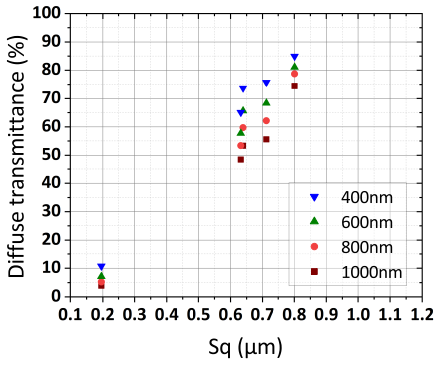

Figure 4.33: Scatter plot of the correlation between S_q and T_D for AZO-sacrificial texturing

Since no correlation exists between S_{tr} and T_D, an indication is given depth and width are related to each other again. Figure 4.34 shows a linear trend exists between these parameters since R-square values are high for S_q and S_c:

- S_q = 0.78
- S_c = 0.95

Despite the few datapoints, the trends confirms that not every type of crater can be created and this correlation can be defined as a texturing/ material property. This becomes important again whenever

nc-Si is grown on top of this structure because the focal point and crater size (depth and width) determine how easy defects in the structure initiates/ develops. Second, the type of processing methods must be considered in the simulations of GenPro4 or other types of optical simulation models because not any type of profile is realistic to simulate.

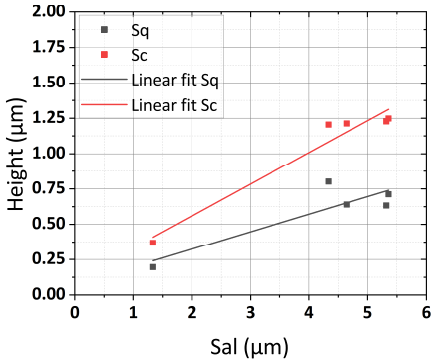

Figure 4.34: Scatter plot of the correlation between S_q, S_c and S_{al} for AZO-sacrificial texturing

4.4.3. Angular intensity distribution analysis

Similar to section 4.3.6, the macroscopic properties (T_D, Haze) already show that low energetic wavelengths are able to be effectively scattered and the high energetic wavelengths too, although effects causing this are different. The optical optimal performing sample (see section 4.4.1.4) is chosen for further analysis. The effect of a different sample angle, different wavelengths and a 30nm deposition of a-Si are assessed. Since this sample is the best one created, it is useful to compare both samples to each other in the next section 4.5.

If the response of 600nm is observed in figure 4.35, a steep exponential decay is observed that intersects with the Lambertian decay at around 30 degrees. Afterwards, the Lambertian decay stays the dominant effect and stays above intensities of 1e-4. This means high intensities of light are scattered in angles up to 30° and low intensities are scattered from that point on.

Similar to section 4.3.6, the sample angle is increased by 10° which reduces the intensity of the light perpendicular to the sample (shown in figure 4.35). The initial intensity of the light is equal to the intensity at 10° if the sample angle is not shifted. This means the Lambertian decay becomes dominant around 20 degrees. Second, the Lambertian decay lies slightly lower than if the sample is not turned. In general, the turning of the samples does not have a significant impact on the optical behaviour of the sample and there is only information lost about the exponential decay if the samples angle is changed.

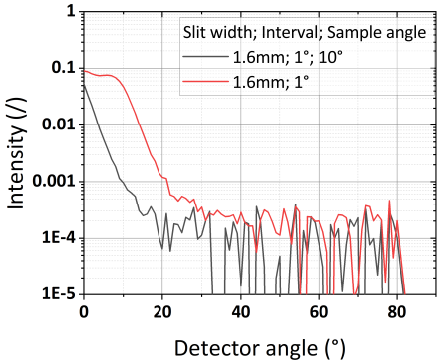

Figure 4.35: AID for AZO-sacrificial superstrate deposited under P=400W, T=400°C and t=7200s under 2 different angles 10° apart for 600nm

In figure 4.36, the effect of using 4 different wavelengths is shown. Similar to section 4.3.6, wavelengths

600nm and 800nm show a clear response, while 400nm and 900nm show high levels of volatility. The reasons behind it are identical to what is described in the ITO-section and are not discussed in-depth again. For these wavelengths, the following observations are made:

- Going from 600nm to 800nm, the exponential decay shows a vertical shift upwards of around 0.01 but the rate of decay is identical. More light is scattered at smaller angles for increased wavelengths which means that it becomes a more efficient scatterer.
- For the Lambertian decay, the intensity increases with a factor 10 from 600nm to 800nm that causes the intersection with the exponential decay to occur at 20-25°. The AZO-microtextures become more efficient at higher angles for increased wavelengths.
- Due to the difference in vertical shift for higher wavelengths, the intersection between lambertian- and exponential decay occurs at a different angle. This determines the scattering efficiency.

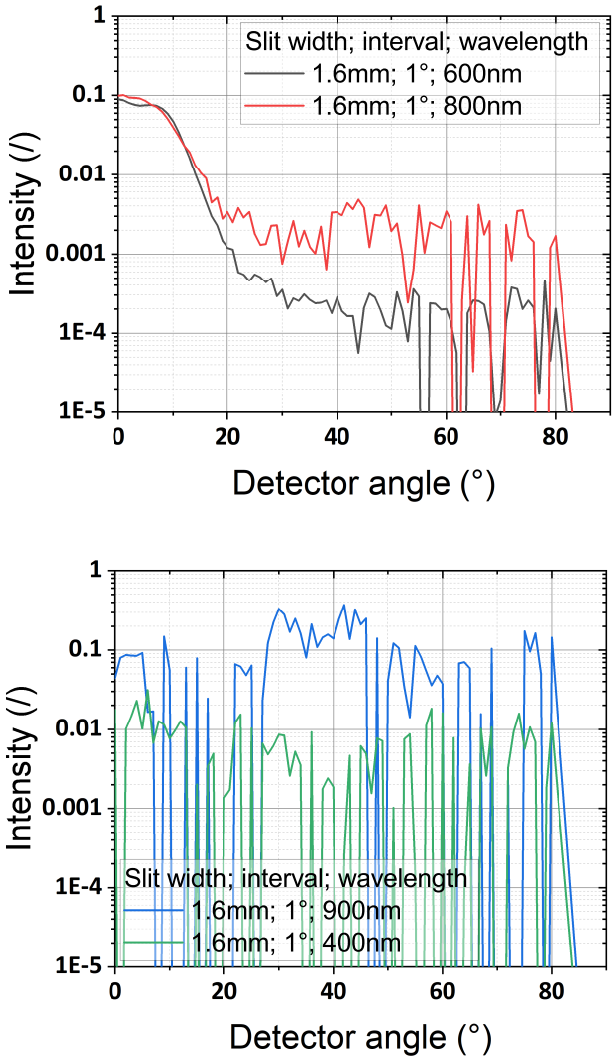

Figure 4.36: AID for AZO-sacrificial superstrate deposited under P=400W, T=400°C and t=7200s under 4 different wavelengths

The AZO-sacrificial texturing causes the exponential decay to have a fast decrease, which results in an intersection at low angles with the Lambertian decay. This optical behaviour is not as efficient because more light is scattered in lower angles and a more efficient approach would have to be an exponential decay that has a lower rate of decay. Similar to section 4.3.6, an identical analysis is performed under a deposition of 30nm of a-Si. Observations under 400nm and 900nm are similar due to identical reasoning. For these measurements shown in figure 4.37, the following observations are made:

- For 600nm, the initial intensity decreases due to increased reflectivity at the low-high refractive interface. Despite the lower intensity, the rate of decay goes down and causes the intersection to occur at identical angle.
- There is a slight increase of 0.0002 (at 600nm) for the Lambertian decay which indicates an improved optical behaviour is created at higher angles. This behaviour is also confirmed by comparing measurements from 800nm to 900nm, although more noise is measured for 900nm. There must be noted this increase is small considering the macroscopic T_D/ Haze measurement.
- The outlook of the graph remains similar for the range of wavelengths which indicates that high refractive index values don't compromise the optical efficiency of the texture.

To conclude, AZO-sacrifical textures is an effective scatterer but is characterised by a steep exponential decay which can result in a lower performance for wavelengths like 600nm-800nm. At higher wavelengths, the Lambertian intensities increase which makes this effect less significant.

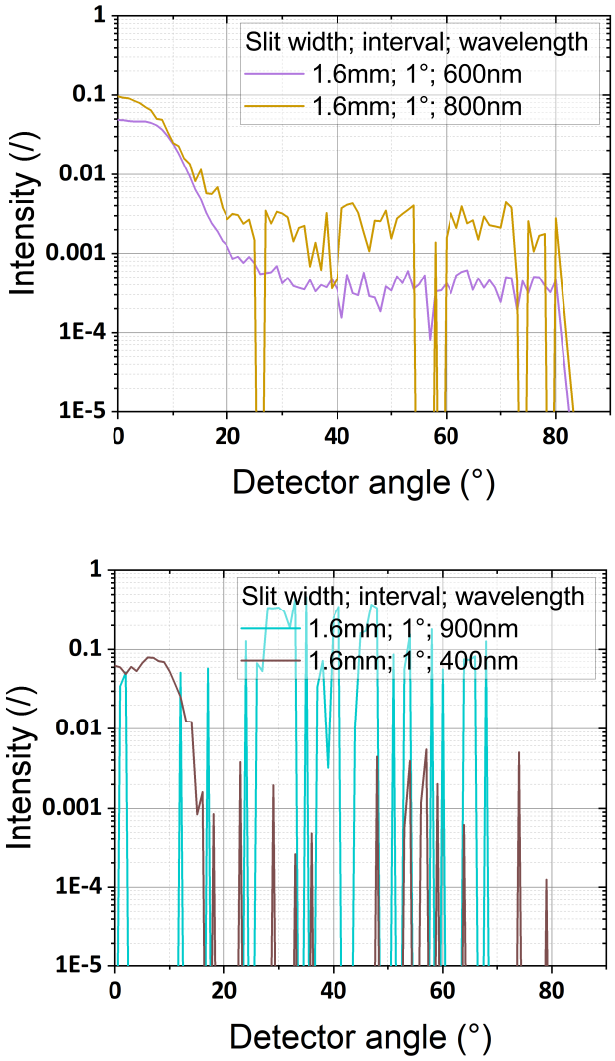

Figure 4.37: AID for AZO-sacrificial superstrate deposited under P=400W, T=400°C and t=7200s, including a 30nm thin layer of a-Si for 4 different wavelengths

4.5. Results: Comparison ITO- and AZO sacrificial texturing

4.5.1. Optical comparison

Until now ITO- and AZO-sacrificial textures are separately assessed in their performance. In this section, a comparison is made to asses and explain their differences in optical- and electrical performance. First, the best samples for ITO- and AZO- sacrificial texturing are compared for T_D and Haze. This behaviour is explained by their physical characterisation and their individual correlation to the optical behaviour again. Second, the differences in AID are shown to indicate the difference in angular intensity. This than results in a conclusion which sample will be superior in thin film technology.

For T_D and Haze, a comparison is shown in figure 4.38. All ITO- processed samples show a superior performance for T_D from 500nm on and for haze it is superior independent from the wavelength. Since, micro-textures have the purpose of increasing the optical path-length of high wavelengths and avoiding interference effects to occur inside a cell, the air-glass-air interface must reach high diffusivity values in this region. ITO shows at 800nm already an improved optical response of 5% for T_D and 7% for Haze and at 1200nm an increase of 10% for T_D and 15% for Haze. The physical properties of both textures provides an explanation because the S_c and S_q of ITO- textures are higher for an identical S_{al} (shown in figure 4.39). It is already discussed in section 4.3.5 that S_q is the main parameter determining the diffusivity. Second, an indication is given that saturation in figure 4.33 occurs at lower T_D-values than for ITO-sacrificial texturing. Increased crater widths are required to crate larger depths but since this cannot go on for an indefinite amount, which will than end up at lower T_D values.

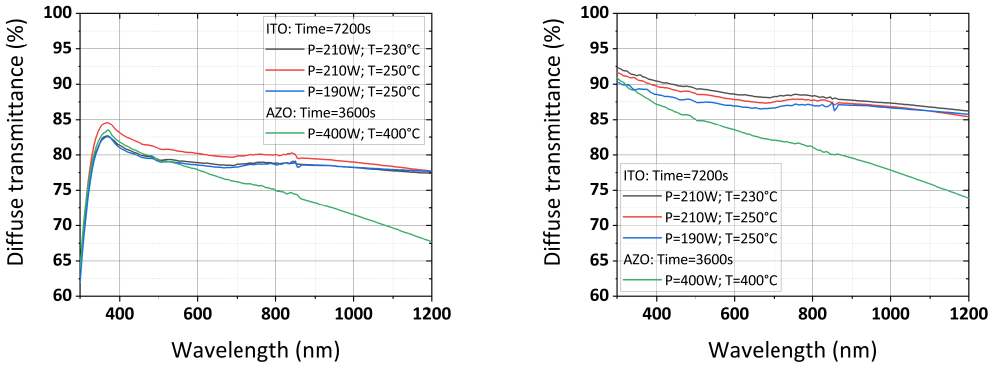

Figure 4.38: Samples processed with the highest optical response for T_D and Haze for both texturing methods

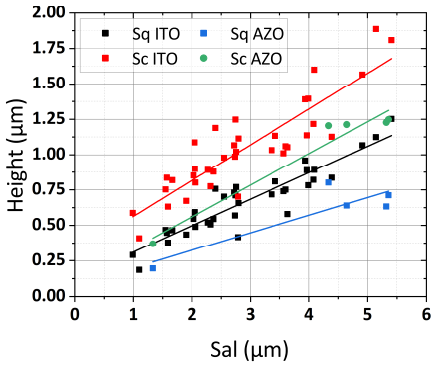

Figure 4.39: Scatter plot of the correlation between S_q, S_c and Sal for both texturing methods

For AID, a comparison is shown in figure 4.40. It shows that the scattering profile is correlated to the created texture. As long as the noise of the measurement is smaller than the measurement values itself, the measurement is valid. Between both textures the following observations are made for an air-glass-air interface:

- The spectral component of AZO at 0° is 0.02 higher and increases up to 0.03-0.04 between 5-10°. Since light intensities at low angles must be as low as possible (to increase it at higher angles), this is a classified as a disadvantageous property for a texture.
- The exponential decay of ITO has a smaller rate of decrease than AZO textures, which is caused by the the steeper crater sides that cause light to be easily bend into higher angles.
- The difference in exponential decay causes the ITO texture to become more efficient from 10-15° on, which is what is expected of a high optical performing sample.
- The Lambertian decay for both sample is quite low due to the low wavelength at which the wavelength does not perform optimal. If the wavelength get increased towards 800nm (see figure 4.40), the difference in Lambertian response becomes greater between both textures. ITO texture scatter slightly better here.

With the inclusion of a 30nm a-Si layer, observations are fairly similar but the shift at which ITO becomes dominant shifts 1° to the left. This means ITO becomes more efficient at lower angles with the stacking of different layers. This comparison leads to the conclusion that ITO-sacrificial texturing will give the highest efficiency under the assumption that both stacks are kept identical.

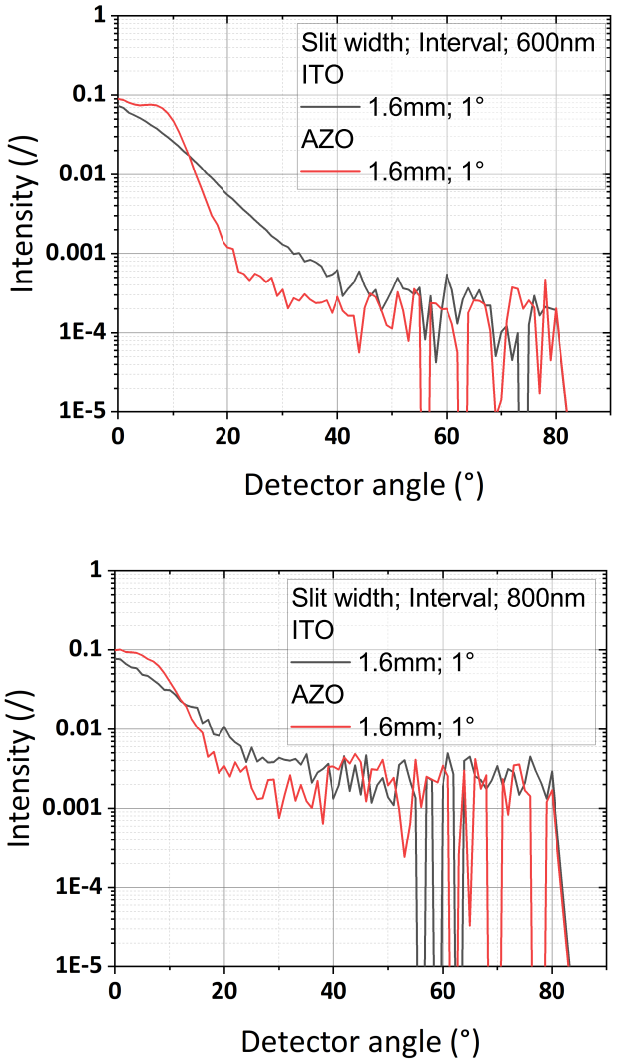

Figure 4.40: AID at 600nm and 800nm for both methods under a deposition of P=210W, T=230°C and t=7200s for ITO and P=400W, T=400°C and t=3600s for AZO

4.5.2. Electrical cell performance

In previous section is observed that ITO must give a better electrical performance. The thesis of Mehdi focuses on the optimisation of the intrinsic silicon layers focusing on nc-Si, a-Si and micromorph stacks, which involves extensive cell processing. Some of his results are shown in this thesis to prove the effectiveness of the textures. In this section, the shown cells have the following properties:

- Nc-Si cells are made with a stack shown in figure 4.41. In this case, ITO is used as Transparent conductive oxide (TCO). This layer has the function to collect the energy carriers, which means it needs a low resitivity and high carrier mobility (the complete discussion of this layer lies outside the scope of this work). These samples are shown in figure 4.42
- To improve the effectiveness of the TCO, instead of an ITO layer, a bi-layer is used which exists out of IOH and i-ZnO. The implementation of both materials result in a lower resistivity and higher carrier mobility compared to an ITO layer (shown in figure 4.43).
- There are also micromorph stacks made which use an MST texture that combines sacrificial micro- and nano-textures (shown in figure 4.44). These cells make use of 2 cells stacked on top of each other, existing out of a-Si and nc-Si. a-Si is always put on top because it has the highest bandgap which causes energy absorption to be more efficient.

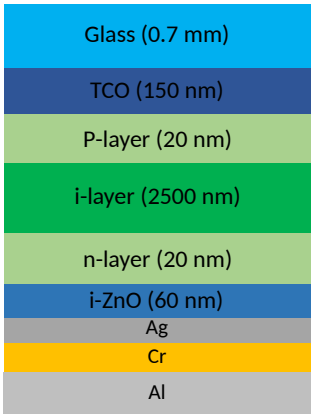

Figure 4.41: Schematic showing the solar cell stack for a single junction nc-Si cell that involves ITO being used as transparent conductive oxide (TCO).

Since the focus of this work is to asses the performance of the created textures, only the EQE's (external quantum efficiency determines the amount of free electrons that are created and collected by the external contacts) of the cells and J_ph are discussed. Although JV-curves are important, they are extensively discussed in Mehdi's thesis and left out in this case. For nc-Si technology in figure 4.42 is observed that a higher current is created for the ITO-texture and the same layer stack. It increases from 20.2 mA/cm² to 21.4 mA/cm², which indicates that ITO scatters more light in higher angles (from optical measurements this is already observed). The IR-region for ITO has a vertical shift upwards of around 1-2% in this case from 700nm on. Nevertheless, the efficiency of the cell is slightly lower (-0.06%) due to the slightly lower fill factor but this can be the result of many other factors during the deposition. Second, the difference in efficiency is small that this can almost be classified as measurement error.

At lower wavelengths, big interference patterns are showing in the R-measurements, which translates itself in dents in the EQE curve (at 500nm). This is something that cannot be solved by micro-textures because

they do not cause Mie-scattering. They only cause macroscopic scattering but this does not prevent interference from occurring. This indicates nano-textures are required to further boost the performance.

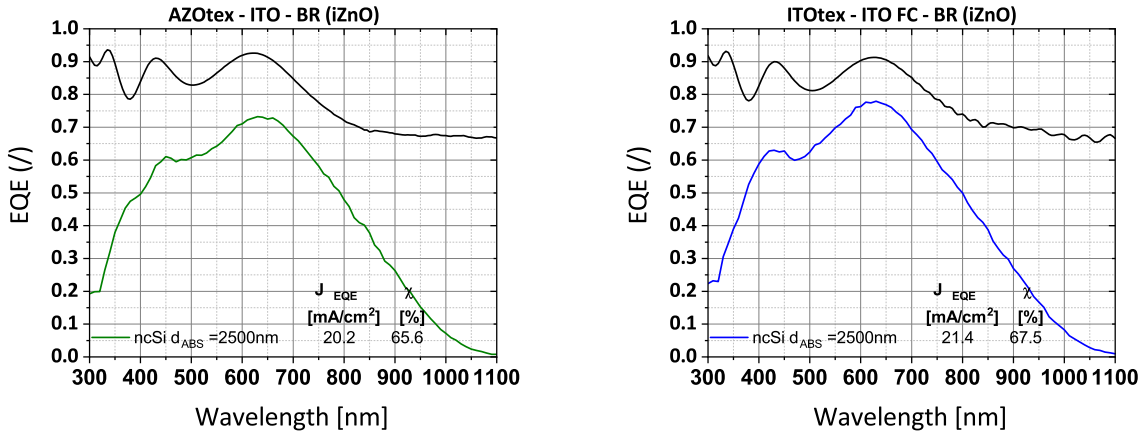

Figure 4.42: Nc-Si cells made on top of glass textured superstrates with AZO sacrificial textures on the left and MST sacrificial textures on the right. The black lines represents the reflected light from the cell, which indicate if interference effects occur. The EQE is represented by the colored lines. d_{abs} indicates the thickness of the absorber layer, χindicates the crystallinity of the nc-Si layer.

If a bi-layer is introduced for a nc-Si cell, a better combination of resistivity and carrier density is obtained. This means the electrical losses decrease which boosts the electrical performance, which is observed in figure 4.43. This figure shows the difference between ITO and AZO texture good because the EQE of the ITO sacrificial textured surface shows no signs of interference (contrary to the response of AZO sacrificial texture). Second, the response of ITO is always better than AZO from 700nm on. This confirms ITO has a superior response compared to HC textured superstrates. The superiority is also shown in J_{eqe} (22.6 mA/cm² versus 23.3 mA/cm²).

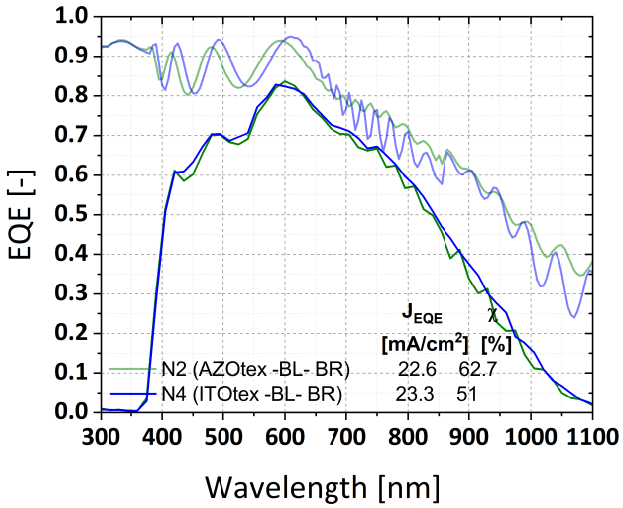

Figure 4.43: Difference between nc-Si cells using a bi-layer this time. BL indicates the use of a bi-layer existing out of IOH and i-ZnO. The reflectance of the sample is represented by the transparent line while the solid line represents EQE

In previous paragraphs is mentioned that nano-textures are required to reduce the interference effects for the lower wavelengths. In literature is known that this can be performed by texturing the TCO layer itself or creating textures on the glass superstrate itself. The effect on adding nano-textures straight on the micro-textures is shown for micromorph solar cells (a-Si, nc-Si) in figure 4.44. The reflection fringes

of the MST texture between 300-500nm do not reach 0.8, while AZO textures does. This indicates the nano-textures positively affected the interference fringes but they are not small enough yet to completely remove them. In the thesis of Mehdi is shown that by implementing nano-textures on the TCO layer, these fringes are completely removed.

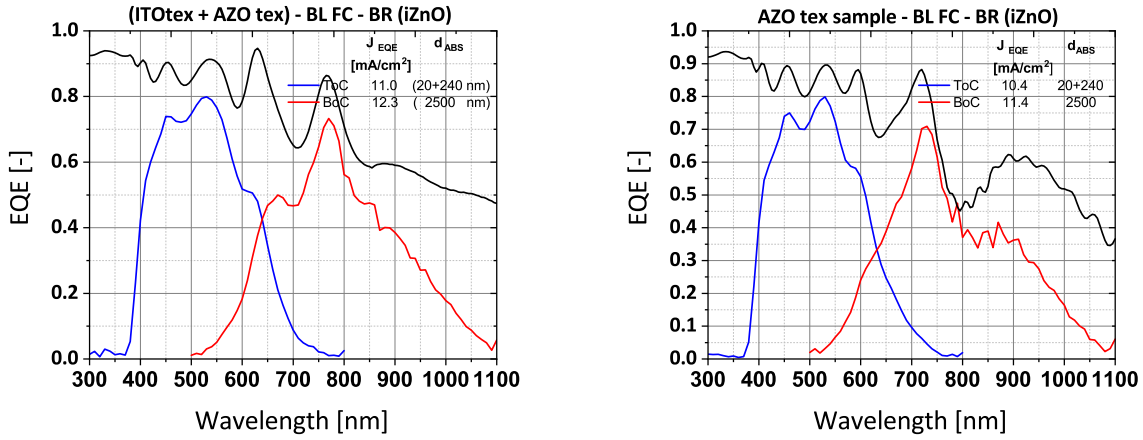

Figure 4.44: Micromorph/ tandem cells made on top of glass textured superstrates with an micro-texture using AZO (left) and ITO (right), a nano-texture using AZO (right) is implemented. ToC and BoC indicate the performance of the top- and bottom cell. The black line represents the reflectance of the cell while the colored lines represent the EQE of a-Si and nc-Si.

4.6. Conclusion

In this chapter, ITO- and AZO- sacrificial texturing properties (process-, optical- and physical properties) are discussed and compared to each other. Although for a local optimum less experiments are required for AZO-textures, the optical performance for ITO- textures optically outperforms AZO. This implies that AZO- textures are easier to process and to control but ITO- textures require a better understanding of the process/ concepts that results in a superior performance. A superior performance translates itself in a diffusivity that is independent from the wavelength and an AID with a slow exponential decay and high Lambertian response. In these AID measurements is proven that higher wavelengths are scattered more in higher angles which is desirable for micro-textures. The exponential- and Lambertian- decay are shifted vertically upwards for which the Lambertian component is more heavily affected.

Control over the optical properties is gained in the different experiments because the process parameters affect the physical parameters. Concepts like crystallinity, crystal initialisation and crystal growth cause the physical outlook of the sample in the end to differ.

The concept of ”crater size” determines the diffusivity of the texture must be replaced with crater-depth or roughness because this is observed to determine the scattering behaviour. Increasing the roughness results in increasing the scattering performance which can be described by a Boltzman sigmoid function. This implies that creating deeper craters do not create increased scattering after saturation which is the reason that this point in similar texturing approaches must be found before next steps are undertaken.

After the introduction of a-Si on top of the textured superstrate, indications are given that the characterisation of transparent superstrates can be expanded. Depositing different layers on top of the superstrate can be an extra elemenent in determining how light is scattered on a lower level and which type of method turns out to be superior.

After inspection of the electrical parameters, the created ITO textures perform superior AZO. Less interference occurs and higher currents are obtained. The performed optical analysis predicts ITO textures has superior scattering properties, which is conform the electrical measurements. Based on R,T and AID good predictions can be made which type of texture performs best in an actual cell.

Although finding the right process parameters is difficult, the required processing steps are limited and no expensive equipment is required to create these textures. This means for industrial application, this must be further researched.

4.7. Recommendations

This work mainly focused on the optimisation of micro-textures but as seen in the electrical performances, further optimisation of the nano-textures is still possible. Therefore, MST structures must be researched more in-depth remove optical fringes at higher energetic wavelengths. This can be performed with the implementation of creating on the TCO or creating a nano-texture on the glass itself. For the first option, the TCO affects the optical characterisation and this must be considered.

Random texturing can be optically further optimised by applying a 2 step etching process as Bose et al. [23] proved. The electrical performance was also increased because less cracks occured after processing.

Another texturing method that can be researched is Intrinsic Zinc Oxide sacrificial texturing. These results are not mentioned in this report but can be an addition to the comparison of the different sacrificial texturing methods.

5

Honeycomb texturing

5.1. Introduction

In previous chapter, the optical and nc-Si growth characterization of random textures is performed. In this chapter a similar approach is taken to characterise the honeycomb structures. The current stabilised efficiency records for single-, micromorph and triple junction silicon thin film cell efficiencies are 10.2, 12.7 and 14%. All of them implement periodic structures in their layers to optimize their optical and electrical performance.

The first aspect that must be addressed, is the method of processing honeycomb structures. A possibility is to create them via photolithography following consecutive wet etching steps. Sai et al. [29] processed these honeycomb on a silicon wafer. At the TU Delft, de Vrijer et al. [30] was able to recreate them and processed them according to the following steps:

1. A SiO_2 layer is grown on top of the Si-wafer with a wet oxidation process. The purpose of the SiO_2 is to stop the silicon wafer from oxidising in the following steps. Instead of using a wet process, a dry oxidation process could also have been opted for which would increased the density of the thermally grown oxide (higher quality). Since the oxide is only a temporary layer, this increase in quality has a negligible effect on the quality of the final texture.
2. A positive photoresist (PR) is spin coated onto the material and undergoes an annealing step/ soft-bake. The photoresist (like SPR3012) has a chemical composition that reacts with UV-light which changes its chemical composition. The difference between negative and positive photoresist is how it reacts with the developer fluid after exposure. The annealing step removes excessive PR solvent and partially hardens the layer.

   To ensure the PR layer sticks hexamethyldisilazane (HMDS) is spin- coated onto the substrate beforehand. It reacts with Si and makes the surface hydrophobic instead of hydrophilic, which ensures no liquid can creep between the 2 layers.
3. An UV-exposure step is introduced to change the chemical composition of the PR. Between the exposed PR and the source, a mask is introduced to implement selectivity on which areas are exposed to the UV-light.
4. A developer coating is spinned onto the substrate to create the required pattern. If a positive PR is applied (which is an approach adopted by de Vrijer et al. [30]), the regions exposed to the source are dissolved. If negative PR is applied, the regions not exposed to the source are dissolved. Another difference, is their sensitivity to chemicals (like wet etching processes). Afterwards an annealing step/ hard-bake is applied, to completely solidify the PR and make the layer more resistant to future processing steps (like wet etching, plasma related processes...).
5. Since the pattern in the PR should be transferred to the SiO_2, a buffered hydrogen fluoride (BHF) etching step is introduced. The used BHF exists out of 7 parts NH_4F (40%) and 1 part HF (49%). The HF dissolves the SiO_2 while minimally affecting the PR. Afterwards, the PR is removed with acetone after being rinsed with deionised water to remove the weak acid. The change from BHF to concentrated HF (47% in water) is discouraged since the etching rates of glass are too high (uncontrolled process) and the risk of peeling of the PR-layer is high. BHF in this case provides more controllable etching and further control can be obtained by changing the concentration of the BHF

itself. The use of HF is not impossible since Park et al. [31] used a diluted 0.5% HF etching bath in combination with a PR-layer and succesfully created HC-structures without the peeling effect of the layer. A dilution of the highly concentrated HF solution reduces the chance of peeling effects and could still result in a stable processing method.

6. A poly-etch solution etches into the Si-wafer, in which the etching time is crucial. It determines whether the final hexagonal structures are created, therefore the etching holes must start to overlap each other (since the hole pattern is made in such a way). If the etching time is too low, a large part of the surface remains flat and only holes are etched in the surface. If the etching time is too high, the etching holes highly overlap which reduces the roughness of the surface (optical performance in terms of light in coupling) and the properties go once more towards the one of a flat surface.
7. The SiO_2 serves no purpose for the future solar cells so it is removed by a second HF etching step.

As mentioned in section 2.1.1, there are differences between processing crystalline or amorphous materials. Therefore the process flow of Park et al. [31] is different but the main idea stays identical. Steps 1,5,6 and 7 from previous paragraph are removed because they concern the intermediate SiO_2 layer, which becomes redundant in this case. An alkine aluminosilicate glass substrate is in fact already an oxidised material (since it consists mainly of SiO_2, described in section 2.1.1) , oxidation problems are not applicable to this substrate. The applied method directly transfers the pattern of the PR into the glass superstrate and creates the honeycombs consecutively.

A lot of research has already been performed on HC-textures on silicon substrates by Vrijer et al. [30] , Eisenhauer et al. [32] and Sai et al. [33]. The papers mapped important parameters/ characteristics that must be considered to process high quality HC and high efficiency solar cells. Since the chosen substrate is Si instead of Corning glass, results could differ but Park et al. [31] confirmed that characteristics are transferable. Sai et al. [33] determined that the grown nc-Si thickness cracks depending on the periodicity of the HC texture. An optimum cell thickness exists for every periodicity and higher absorption is obtained for thicker nc-Si layers. If the cell thickness is similar to a thickness 0.5 µm thicker than the periodicity of the cell, the highest short current density (J_{sc}) is obtained. Second, the aspect ratio must be moderate and lie between 0.2-0.25 for the previous observation to be valid. After this point the focal point of the textures is reached and defects in the grown layer start to form, which deteriorates the performance of the cell. An extra recombination gateway is created, which cannot be externally collected. This was confirmed by measuring the EQE for cells with p=1.5-3 µm and layer thickness (t_i)= 1-3 µm.

For t_i=1 µm, the HC with p=3 µm has a lower EQE response for the whole AM1.5 spectrum. For t_i=3 µm, the EQE is lower for decreased periodicities and for 2 different reasons: increased optical loss and increased carrier collection loss. For thicker layers grown on top of a textured surface, the top surface evolves towards a more flat like surface which decreases its optical performance. If the periodicity increases, the threshold thickness at which this phenomena starts playing a dominant role increases. The origin of this carrier collection loss could be explained by non uniform coverage of the p-layer and defects occurring in the so called ”focal point” of the structure. The optical characterisation of the structure is not performed in this work. From EQE measurements is observed that interference patterns at higher wavelengths are not always occuring due to to little texturing but also due to a bad match with the grown layer thickness. This must be kept in mind when analysing future EQE’s.

Eisenhauer et al. [32] created HC at the back-side of a liquid phase crystallization silicon solar cell. Although, LPC silicon cells were produced, the characteristics are similar to the previous ones. Vrijer et al. [30] was also able to confirm previously mentioned characteristics. It was only possible to grow defect free nc-Si for a grating with p=3 µm, although Sai et al. was able to grow defect free nc-Si for lower periodicities. A silicon substrate was used which implies the light in coupling aspects are defined in terms of R and diffuse reflectivity (R_D). For the optical characterisation, an increased etching time created higher R-values because the features are smoothened and light in-coupling becomes less efficient (compared to the steep features obtained when etching hemispheres just overlap each other). The features have a periodic nature that results in interference effects observed in the AID spectrum. The peaks of constructive interference shift to higher angles with increasing wavelength. Nevertheless, the highest amount of light still reflects normal to the surface because of the flat areas on the bottom of the HC.

Park et al. [31] created a HC-textured glass surface. It showed texturing the surface minimally affected the total transmittance and stayed above 90% for every wavelength (300-1000nm). The Haze-values lied on

average around 40% which defines 40% of the light deviates from its specular path. The periodic texturing approach of the front surface is a proven methodology since the efficiency increased from 8.71% on a flat superstrate to 9.22% on a honeycomb type of structure and a final efficiency of 10.75% introducing a double texture and after the balancing of J_{sc} and FF was performed.

In the previous paragraphs is described that optical and electrical parameters contradict each other and must be optimised accordingly. Zhou et al. [34] modeled different concave and convex shapes deviating from their pyramidal shape (conventional angles of 54.74°). It quantifies the relation between front surface texturing, optical- and electrical properties for PERC solar cells (incorporating c-Si layers). The parameter of the concavity is not considered in the previous papers. To include this, the super-ellipse equation was incorporated and differences in shapes are created by a numerical change of the empirical parameter. It should be noticed, that textures in this case situates themselves at the air interface. Results showed the curved pyramid-like structures obtain a higher J_{sc}-values up to 0.8%, if the deviation from the conventional pyramidal structures is limited. The increase could be explained by the increase of illumination area (which increases the light trapping properties) compared to the standard pyramid. The effect of the type of curvature is not symmetrical and its increased performance differs accordingly.

Applying these textures only makes sense if they reach a higher performance than conventional random micro-texturing. de Vrijer et al. [30] processed a tandem n-i-p a-Si/ nc-Si wafers with a sacrificial-layer texturing method (creating random textures) and a honeycomb texturing method. The honeycombs although having a higher J_{sc} (of 23 mA/cm²) than the random structures under performed since there was an interference fringe found between 600-800nm that caused the EQE to drop. The cause here was the flat surface area on the bottom of the periodic grating, which represented a flat-alike surface again. The J_{sc} of sacrificial random textures were worse since in the EQE-values for large wavelengths (>700 nm) represented a flat surface since the roughness profiles of the structures were not large enough. For the efficiency, the honeycombs reached higher efficiencies (0.5%) but they suffered from stress induced effects because of the steepness and periodicity of the honeycombs. This caused the honeycombs not to reach their full potential but already showed their superiority by reaching an efficiency of around 10.3%.

The previously mentioned parameters and characteristics are considered while creating the microtextures in this work. Since, the most reports work with n-i-p structures, results are compared to the current p-i-n devices.

5.2. Methodology

To create periodic textures on glass wafers procedures are developed based on the literature described in section 5.1. A flowchart of HC processing on silicon- and glass wafers are shown in figure 5.1. As superstrate, a Corning glass 4 inch wafer (thickness equals 0.7mm) is used to process. First, the wafers undergo 10 minutes of ultrasonic cleaning in an acetone- and isopropyl bath.

In the machine ”EVG 120 Coater-Developer”, the wafers receive a coating that acts as etching mask afterwards. Before, the coating is applied, an adhesive increasing material is put on top. The wafer is vapor primed with Bis(trimethylsilyl)amine (HMDS) with a hotplate at 130°C. The heater is turned on and HMDS is deposited for 50s using N2 as a carrier gas. After, the wafer is cooled down on a cooling plate during 20s. As coating, SPR3012 or SPR3027 are used. SPR3027 is only used to asses the photoresist (PR) and the thickness of the PR on the texture.

For SPR3012 with a layer thickness of 1.4µm, a volume of 2600 µl is dispensed at 1000 µl/s on a spinning wafer at 600 rpm. After, an acceleration of 2500 rpm/s is introduced until the wafer reaches a rotational speed of 3450 rpm and this speeds is kept for 30s. The backside of the wafer is rinsed afterwards with PGMEA for 2 seconds at a rotational speed of 1700 rpm. To end, the rotational speeds increases up to 2500 rpm with 2500 rpm/s to remove the PGMEA.

For a thickness of 2.1µm, a volume of 3000µl is dispensed at 750 µl/s on a spinning wafer at 600 rpm. Than, an acceleration of 1000 rpm/s is introduced to reach a speed of 1575 rpm and this speeds is kept for 30s. The backside rinse is identical to the previous paragraph but performed at 1500 rpm.

For SPR3027 with a layer thickness of 3.1µm, a volume of 3500 µl is spinned at a rate of 1100 µl/s on a spinning wafer at 700 rpm. After, an acceleration of 800 rpm/s is introduced until it reaches a speed of 2840 rpm and this speeds is kept for 30s. The backside is rinsed identical to the method mentioned in previous paragraph.

To end the coating step, a softbake is introduced at 95°C during 90s to remove solvents remaining in the coating and is performed similar for both types of PR.

Afterwards the machine ”ASML PAS 5500/80 waferstepper” is used to perform a photolithography step. Therefore a mask is introduced with a periodicity of 3µm and a hole diameter of 1µm. The irradiation power is set as following:

- 140 mJ for a layer thickness of 1.4µm
- 315 mJ for a layer thickness of 2.1µm
- 400 mJ for a layer thickness of 3.1µm

Last of all, a developing step is performed on the machine ”EVG 120 Coater-Developer”. This can be performed in 2 ways: single puddle or dubble puddle. For the single puddle deposition, the wafer is heated on a hotplate at 115°C during 135 seconds. Afterwards, the wafer is cooled for 60s on a cooling plate. For the deposition, the wafer speed is set at 1100 rpm at an acceleration of 2500 rpm/s. MF-322 is dispensed for 2 seconds after which the speed is reduced to 7 rpm with 5000 rpm/s. Than the speed is further reduced to 5 rpm with a acceleration of 100 rpm/s and this speed is kept for 57s. After, the speed increases to 1000 rpm with an acceleration of 2500 rpm/s after which deionized rinses the wafer for 8s. A second rinse is performed while the speed is reduced to 600 rpm at an acceleration of 2500 rpm/s. To finish the process, the wafer increases its speed to 3000 rpm at 3000 rpm/s for 12s. To finish, the wafer is baked for 135s at 100°C. The difference with double puddle deposition, is after the deionised rinsing another MF-322 dispension is done for 26s.

Before etching the samples are put inside a Triton X-100 bath ([C14H22O(C2H4O)n:H2O=1:5000]) for 1 minute to reduce the surface tension on the sample. Afterwards, the sample is etched in an BHF bath for a predetermined amount of time. To remove the PR on top, it is placed inside an acetone bath at room temperature for 1 minute. To remove all organic particles, the wafer is put in a plasma cleaner ”Tepla Plasma 300” during 15 minutes.

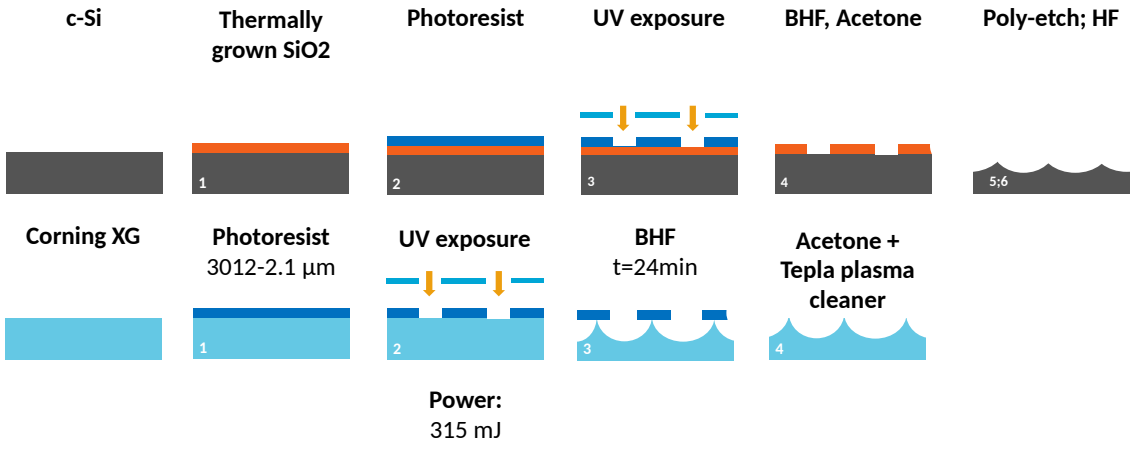

Figure 5.1: Flowchart showing how HC textures are obtained on the glass superstrates in this work and how it is processed according to literature mentioned in section 5.1.

5.3. Results: Honeycomb texturing

The result section is structured in a different way compared to the previous chapter. First, the assessment of the texture is discussed because the periodicity affects the analysis of the surface. Second, a proof of concept is shown to confirm the process flow actually creates a periodic structure. Literature states a S_{tr} between [0.2-0.25] results in the highest efficiencies, which gives this work already a target. This is the reason why the physical parametrisation is performed first. Afterwards, the optimal optical response of these periodic structures is discussed after which the correlation is made between the optical- and physical aspect.

5.3.1. Assessment of periodic textures

In this section, periodic structures are assessed which means a reoccurring pattern is created which must be included in the assessment of the structure. The created honeycombs have a 60°-symmetry, which means a rotation of the pattern with 60° gives an identical result. This implies that the entire structure can be described by 2 axes with a 30° difference between them (shown in figure 5.3):

- Both axes are named for convenience
- G-axis (green axis): It is the axis representing the center to center distance equal to the periodicity of the structure.
- R-axis (red axis): It is the axis representing the peak to valley distance.

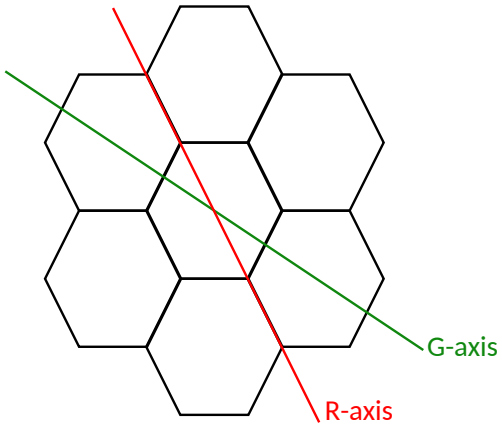

Figure 5.2: Principle how HC texture are assessed including 2 axes rotated 30° from each other, showing G- and R-axis

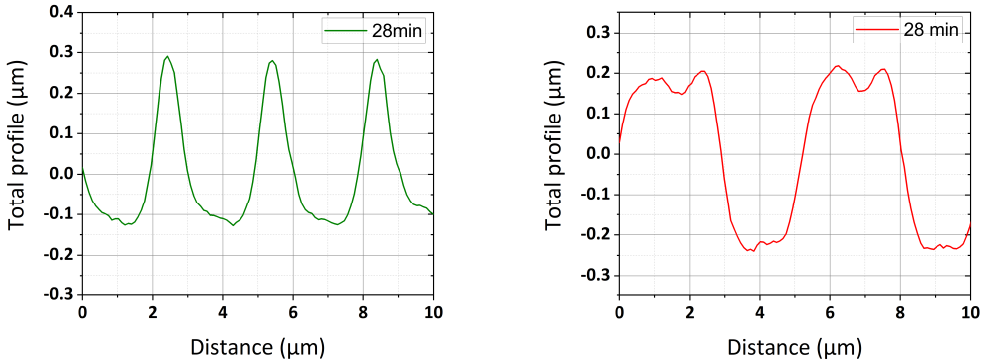

Figure 5.3: Representation of HC texture according to 2 axes with wafer processed at 3012-1.2µm during 28min for a single wafer

Physical parameters like S_q, S_c, S_{tr}, S_{ku} and S_{sk} are described for both of these axes which is required to describe the entire surface. From previous chapter 4 is concluded that the depth of the crater is dominant in determining the scattering behaviour. For HC-textures, this conceptually implies the height difference

(highest peaks) between the G- and R-axis must be as large as possible. The etching process creates hemispheres at the punched holes in the PR and all of them grow at the same rate. At some point, these hemispheres start to overlap which occurs first at the G-axis and it is also at this point the honeycomb is created. Increasing the etching time increases the overlap while the peaks of the honeycombs remain unaffected (R-axis), which means that the height difference between both axes is maximum. If the etching time is further increased, peaks of the HC get etched which results in a flattening of the surface and a decrease in optical performance. Both axes are required to completely describe the surface (sharpness...) and to find the optimal etching time so optical scattering is maximised.

5.3.2. Proof of concept

To show the process flow creates Honeycomb textures (HC), an etching time of 24min is chosen based on previous work [31]. This results in the confocal measurements shown in figure 5.4. These measurements show that the periodic structure is indeed formed. In the height measurements peaks occur in the left bottom corner of every HC, the question is if these are limitation of the measurement tool or they actually occur. Therefore AFM measurements and SEM images are made (shown in figure 5.5), which shows these type of peaks are non-existent. The confocal measurements can still be used for analysis because the software ”Multifile analyser” is able to filter out these peaks without interfering with the accuracy of the measurement. From these measurements, the profile can be extracted (shown in figure 5.6) which shows the significance of defining 2-axes. Accurate measurements are performed because the periodicity is accurately shown and no excessive jumps are made in the profile.

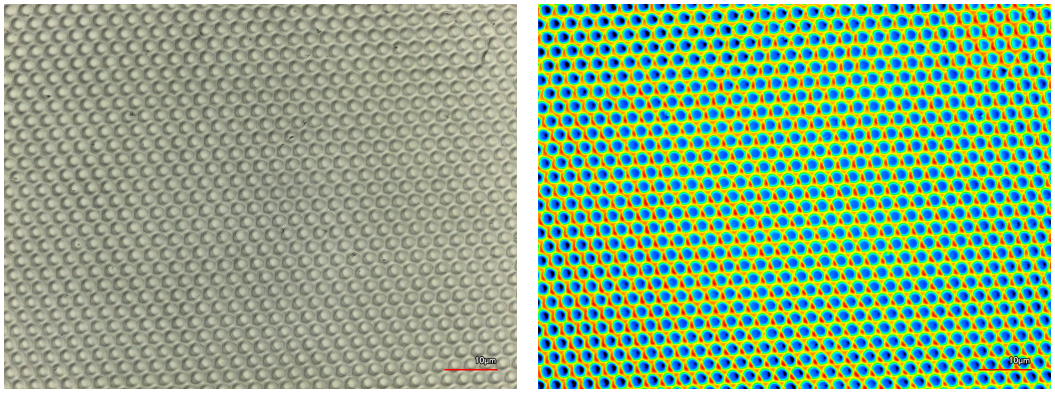

Figure 5.4: Confocal picture of HC texture going through a straight etch of 24min and confocal height measurement with a height range of [-0.379;0.454]µm. A larger defect is observed in the right top corner where an elevated plateau is measured.

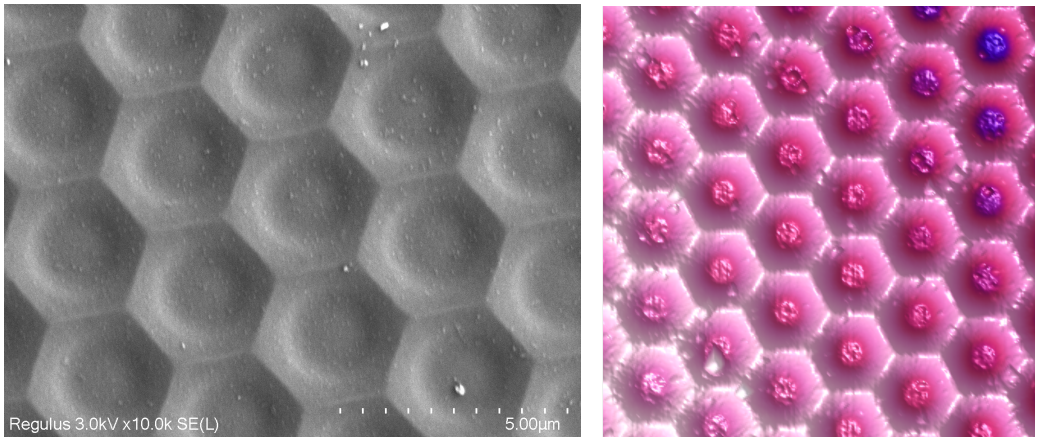

Figure 5.5: AFM and SEM measurement of HC texture going through a straight etch of 24min

Confocal measurements show the individual honeycombs are created and show to be defect free, while the entire structure has some large defects. Observing SEM- and AFM imaging, the individual HC are also

created but small defects occur, large defects are again observed as previously mentioned (shown in figure). The small defects look like particles have a size between 10-100nm and a possible solution to avoid them, is discussed in section **??**. The large defects (size around 10µm) are not part of the processing steps but are part of the industrial processing of these 4 inch glass wafers. The honeycombs are perfectly formed on these large defects which indicate they were already there before the processing started. A solution can be to acquire higher quality superstrates, if it would affect the performance of the solar cell (for example shunts). It is predicted that these defects will not have a significant impact because they do not occur often on the surface.

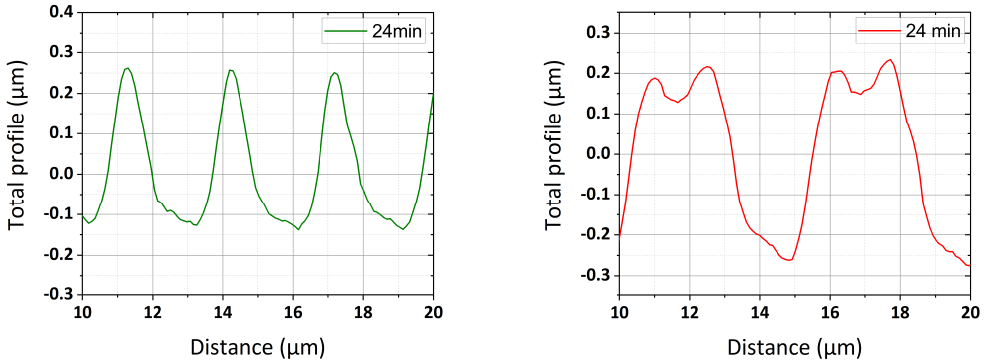

Figure 5.6: Profile according to G- and R-axis for HC going through a straight etch of 24min

Apart from the confirmation that HC-textures are created, the optical response of these textures must be discussed before the influence of different process parameters can be discussed in section 5.3.4, which is performed for 2 wafers. For T, the response is similar to a flat air-glass-air interface which can be explained by the visual inspection of the sample shown in figure 5.7. The sample looks identical to a flat superstrate except from the shown diffraction patterns.

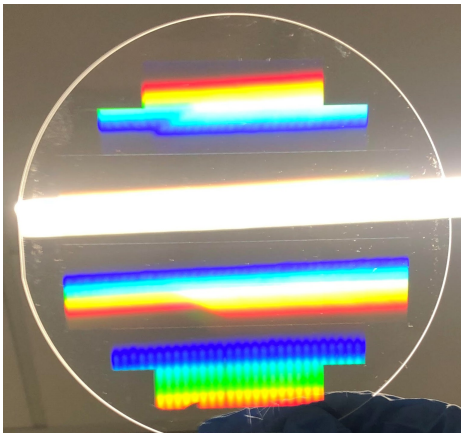

Figure 5.7: Visual inspection of a HC texture after 24min of etching

For T_D, the response is presented in figure 5.8 and shows overall low values in function of the wavelength. The figure shows 2 wafers processed both at 24min but using another thickness of PR. Between 300-1200nm only between 5-30% of the incident light is scattered for 2.1µm and 20% is not even reached for 1.4µm. This would imply only a limited amount of light is scattered. If this would be compared to the random textures, periodic textures would not even be considered as valuable scatterers which is contradictory to literature. It can be explained by the difference in light interaction for random or periodic textures, whereas periodic textures base themselves on diffraction and random textures on Mie scattering/ Macroscopic scattering. This implies both types of textures cannot be compared this way and a comparison is only possible between actual cells. The decrease from 370nm to 300nm is again explained by the absorption of the light by the glass superstrate. From both curves is concluded that a better optical response is characterised by a vertical shift upwards where smaller wavelengths are more easily affected by the

textures. This is caused by the increased diffraction intensities of the light.

For Haze, the response is presented in figure 5.8 and shows a vertical shift upwards due to the total transmittance not being equal to 100%. This means that observations and conclusions are identical as for T_D, but it gives a more accurate representation of how the transmitted light is influenced.

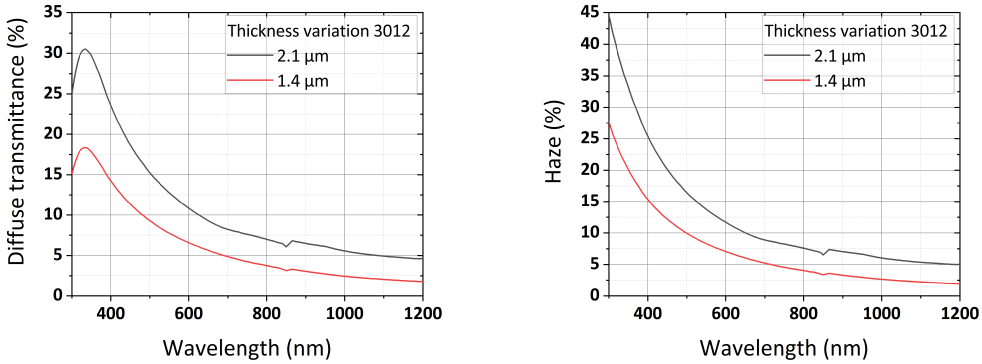

Figure 5.8: Diffuse transmission and Haze of HC-texture going through a straight etch of 24min

5.3.3. Physical parametrisation

Since a periodic texture is created, the width of the crater is constant which implies the parameter S_{al} describing the width of the craters for random texturing is replaced with the periodicity P. Second, in literature is already stated that S_{tr} is an important parameter creating compatibility with the deposited layers. de Vrijer et al. [30], showed that a flat surface is created at the center of the created HC on c-Si wafers, which results in higher stresses in the deposited layers and earlier crack formations. This means that S_{sk} is also an parameters that must be considered.

Table 5.1: Overview of the influence of different parameters on the outcome of the HC for S_{tr} and S_{sk}. The reference sample is processed singularly, etched straight for 24 min and using PR type 3012 - 2.1µm.

	Str		Ssk	
Type for t=24min	G-axis	R-axis	G-axis	R-axis
Reference sample	**0.133**	**0.18**	**0.69**	**-0.27**
Batch processing	0.108 (-19%)	0.131 (-27%)	0.54 (-22%)	-0.39 (+44%)
Discrete etching	0.095 (-29%)	0.123 (-32%)	0.589 (-15%)	-0.301 (+11%)
Soap dipping	0.088 (-34%)	0.113 (-37%)	0.58 (-16%)	-0.362 (+34%)
PR type 3012 - 1.4µm	0.12 (-10%)	0.142 (-21%)	0.35 (-49%)	-0.49 (+81%)
PR type 3027 - 3.1µm	0.096 (-28%)	0.123 (-32%)	0.68 (-1%)	-0.34 (+26%)

Influence of single- versus batch processing

To asses the influence of batch processing, bar plots are shown in figure 5.9. Samples processed in a batch, are processed with 7 wafers at the same time and from the figure is seen there is a significant impact. Table 5.1 shows the decrease in S_{tr}, which leads to the conclusion that every single wafer must be processed independent. If the number of wafers is increased in a single bath, the etching rate for each wafers starts to differ, the point of stabilisation during etching starts to differ and the ”amount of chemicals” available per wafer decreases. All of these influences take part in affecting the end result.

For S_{sk}, table 5.1 shows for the G-axis the value lies closer to 0 and the R-axis lies further from 0. The R-axis would suggest that the flat surface area is increased which is disadvantageous considering electrical properties and scattering of light. The G-axis suggests the opposite but the parameter does not take the height into account nor the wall thickness. These 2 aspects and the definition of the parameter probably results in a distorted picture.

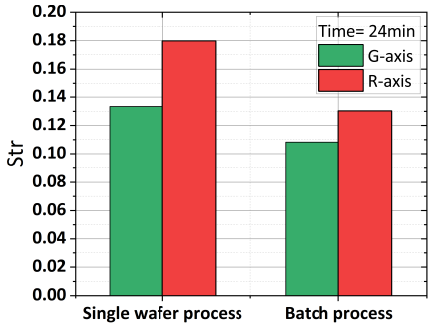

Figure 5.9: Influence of single- versus batch processing going through a straight etch of 24min

Influence of discrete etching versus straight etching
During etching, BHF not only affects glass but also the PR, which means if it is etched too long or if concentrations of HF are too high, the PR peels off and starts to flatten the surface again, which is the reason the concept of ”discrete etching” is introduced. Discrete etching removes the chemicals after 4 min by dipping it in water after which it is put in again in the concentration until 24min of etching is reached. The results on S_tr are visualized in figure 5.10 and quantified in table 5.1. It is observed it only had a negative impact on the depth of the craters, also in terms of S_{sk}. Craters only seem to have a greater flat surface area. From this can be concluded that rinsing it in water only had a negative impact and increased the effect of flattening which is trying to be avoided (heavily peeling off of the PR).

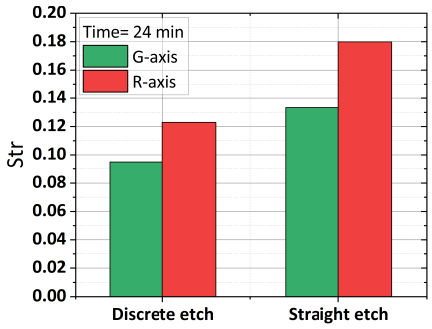

Figure 5.10: Influence of discrete etching compared straight etching for 24min

Influence of soap dipping
Before etching occurs, the wafer is put in a Triton X-100 solution to reduce the surface tension of the surface. This results in chemicals finding its way easier into the holes to start the reaction. For straight etching, this only occurs at the start of the process but when introducing discrete etching, this can also be performed after every dipping step. The results are visualised in figure 5.11 and quantified in table 5.1. The result is negatively affected by performing this extra step compared to not implementing this step. In fact, this setting performs the worst of all the different settings for the S_{tr} for both axes. The peeling effect mentioned in previous paragraph is worsened by putting it in more different baths. Using this methods must be avoided for actual processing, not removing the wafer from the etching bath is the best solution.

Influence of PR thickness and type
During the etching process, the PR thickness and hole size must remain intact to give the deepest crater possible (highest diffusivity). This means the layer must resist the 24 min of etching and the hole sizes must remain as small as possible. This is tested by changing the thickness from 2.1µm to 1.4µm and changing the PR from 3012 to 3027. The results are visualised in figure 5.12 and quantified in table 5.1. Decreasing the thickness, decreases the depth of the crater because the size of the holes opens up more

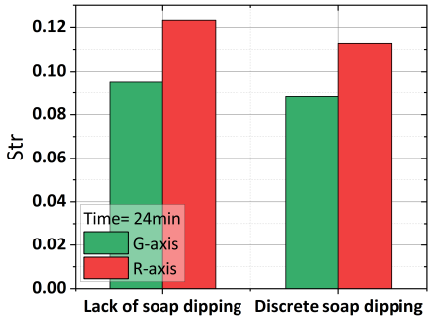

Figure 5.11: Influence of soap dipping for discrete etching steps of 4 min for a total etching time of 24min

quickly which broadens the contact area between the chemical and the superstrate and creates ”broader etching hemispheres”. This is also confirmed by the S_{sk} which describes the broadening of this etching hemisphere (observing S_{sk} of the R-axis). Due to the limitations of possible recipes, it is only possible to increase the thickness of the PR to 3.1µm, while also changing the type of PR to 3027. The lower observed response can be caused by the increased thickness or the type of PR, it is unknown which factor contributes to this result. It can be the increased thickness getting too thick so the chemical hardly reaches the superstrate so the refreshment rate of the chemical is too low, the PR is not well hardened yet and an extra hardening step must be introduced or 3027 is simply a bad match for creating these textures. Using the reference of 3012 - 2.1 µm creates the best result.

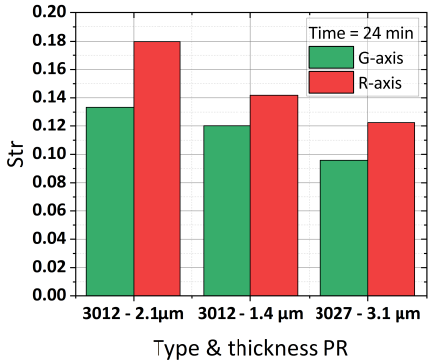

Figure 5.12: Influence of different PR thickness and type during a straight etch of 24min

Influence of stirring

The idea behind using a stirrer is to increase etching speeds and create deeper craters. The identical procedure is kept, using PR 3012 - 2.1µm and etching it in BHF for 24min straight, only now a stirrer is introduced. An AFM measurement of this sample is shown in figure 5.13 and shows the remains of a HC-texture. The different parameters are unable to be accurately measured according to these 2 axes, but it gives a good indication of how better HC in the future can be created. The increase in refreshing rate destabilised the etching process which resulted in a surface with a lot of defects and a flat-like surface. This means that HC structures with less defects can be created by lowering the concentration of the BHF (towards 8:1, 9:1 etc.) so more control over the process is obtained. It is also possible that this can increase the depth of the craters but a shift in optimal texturing time will also be the result. The use of BHF is described here because it matches well with the chemical properties of PR because the risk of peeling off is minimised. Implementing a HF solution is also possible but concentration must remain small (1%) otherwise peeling off will occur.

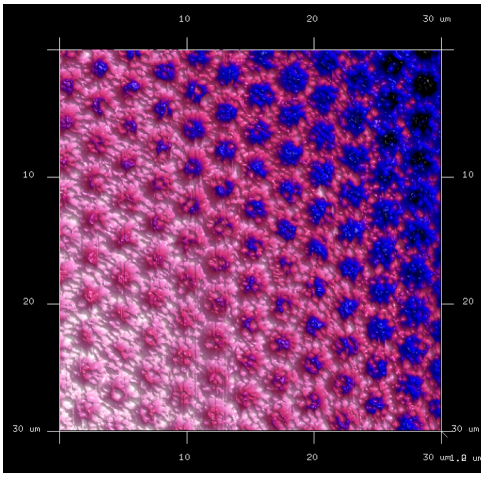

Figure 5.13: AFM measurement of HC texture going through a straight etch of 24min including a stirrer

Influence of etching time

Until now 24 min of etching is used to asses the influences of previously mentioned parameters, but a precise optimal point is not further researched until now. The optimal etching time is researched in a time frame between [18-30min:2min]. During this experiment, wafers are processed in batch but as previously mentioned in section 5.3.3.1, this negatively affects the results because the crater depth is decreased. This means these results only give an indication about the optimal texturing point and in future work, some interesting time steps must be reassessed to get a better idea about the trends in absolute values. The trend for the respective aspect ratios are shown in figure 5.14 and result in the following observations:

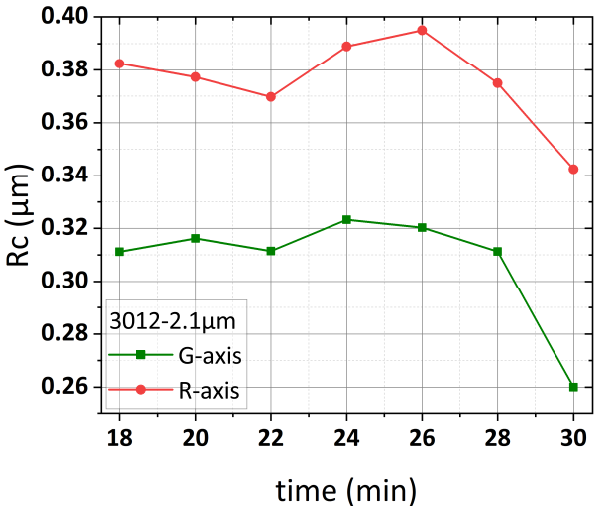

Figure 5.14: Influence of etching time in a batch process while performing a straight etch

- After 26 min, the etching hemispheres start to overlap so much that it starts to etch the peaks of the HC. This is a sign of overetching which results in poorer diffusivity because a more flat-like surface is obtained.
- Etching times around 24 min are indeed optimal for the combination with BHF, only 26 min performs better than 24 min. At 26 min the height along the R-axis still increases, while the height along the G-axis decreases. This trend only occurs at 26 min and indicate that the optimal texturing time is found.
- At 18 min the difference between G- and R-axis is large and the HC texture is already formed (see AFM measurement 5.15). This is an interesting point for further research because in absolute values

it can give even a better value than 24-26min of etching.

- If AFM measurements of 18 and 30 min are compared to each other (see figure 5.15), etching for 18 min introduces less defects compared to 30min. This makes 18 min of etching also an interesting point to investigate. Reducing the concentration of BHF can lead to HC-textures that remain defect free for longer etching times.

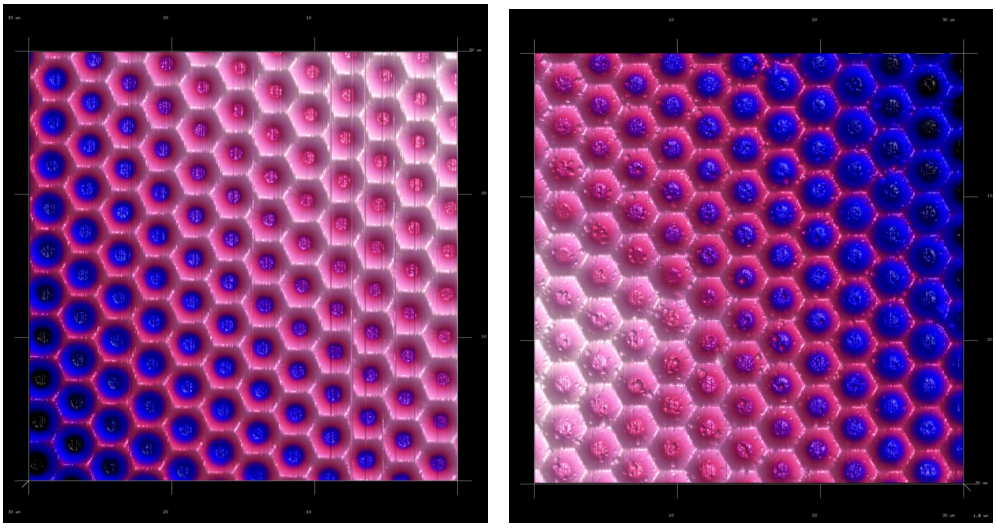

Figure 5.15: AFM measurments after 18 min (left figure) and 30 min (right figure) of etching (batch process) and shows the HC-texture is already created after only 18min of etching.

There is concluded 24-26 min of etching result in an optimal HC-texture but 18 min remains a point of interest. The definition saying that the difference between respective axes must be as large as possible and overetching resulting in a decrease in height along the R-axis is confirmed. Second, wafers must be processed individually because absolute values are affected. Last of all, decreasing the concentration of BHF (towards 9:1 etc.) is a point of interest for further research.

5.3.4. Optimal optical texturing

The different experiments performed to asses the parameters influencing the crater depth turned all out to negatively affect it (see table 5.1), which results in a poorer optical performance. Second, the S_{sk}- values could not be beaten by changing these parameters and resulted in more flat areas which is logical when crater depths are lower. All the different optical responses are not shown because they all lie close to each other because crater depths are low and S_{sk}-values are far from 0, all different responses are similar or lower to the red graph from figure 5.8 and **??**. Values for T_D at 370 nm (peak), lie between 14 - 18% and for 1200 nm between 1.5-2%. This implies that at these low crater depths the difference in depth between the different samples does not affect the light that much but only larger craters start to affect the diffusivity heavily.

The most optimal textures have a response shown in figure 5.16 and are created with PR 3012-2.1µm etching for 24 - 28 min. In this case T_D at 370 nm (peak) reaches values between 27.5 - 34% and for 1200 nm between 2.6 - 4.6%. This seems like a small value but compared to the previous samples, the diffusivity almost doubles. In section 5.3.3.6 is described that 28 min already shows signs of overetching, which is also the case here because its lower performance compared to 24 min. Nevertheless, this sample performs optically better than all the other samples created in the previous section. This means that in this work, the wafer with PR 3012 - 2.1µm etched in BHF (7:1) for 24 min is chosen as optimum. It must be kept in mind that further improvement is still required to reach S_{tr}- values of [0.2-0.25], which can be reached by changing the concentration of BHF or researching the effect of etching time further to obtain the absolute crater depths (S_c). In this work, only the relative trends are obtained for this because batch processing is performed. Second, other masks with different periodicities and hole sizes can be researched although for a 3 - 3.5 µm thick i-layer of nc-Si, a periodicity of 3 µm must be kept (according to Sai et al. [33]). Flat surface areas in the center of the HC decrease if the initial hole size decrease, which implies it must be minimized. It must also be kept in mind what the boundary of the photolithography machine is.

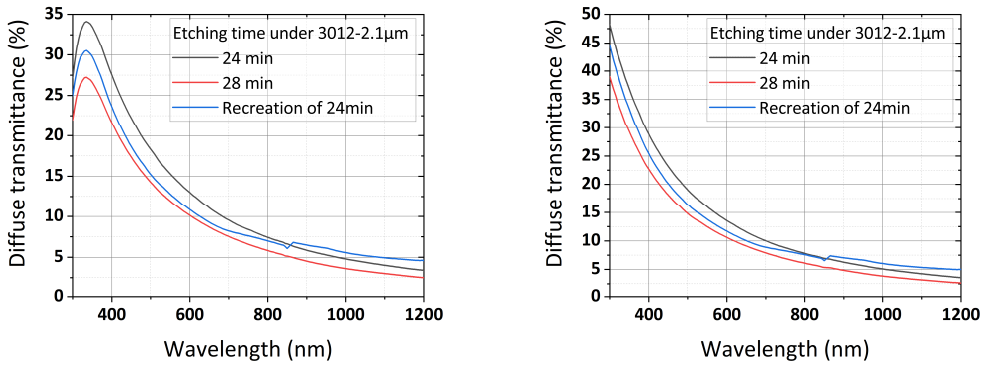

Figure 5.16: 3 best wafers created including the recreation of a wafer with PR 3012 - 2.1µm etched for 24 min, which shows the repeatability of the process.

5.3.5. Correlation between optical- and physical parametrisation

To reach a complete understanding of the process as in the previous chapter, it must be noted which parameters cause light scattering and are characteristic to high optical scatterers. Therefore, all the wafers processed in this work are taken together and plotted in different graphs. Chapter 4 already shows the depth of the crater determines its optical performance but the correlation to the diffusivity can be different here. Second, periodic structures are described by 2 axes (G- and R-axis) which means that the analysis for random textures is not completely transferable.

Parameters S_q, S_c and S_{tr} show a clear trend that describes an increased diffusivity is created due to an increased crater depth (shown in figure 5.17 and 5.18). The graph for S_c is not shown because S_{tr} holds this information and the periodicity is kept constant at 3 µm. The correlation for S_{tr} is more clear compared to S_q because it does not show the outliers that this measurements has. These outliers can be the result of a bad measurement or outliers that are the result of any experimental approach. For S_{tr}, the G-axis shows an asymptotic or exponential behaviour whereas the R-axis show a linear trends in function of the depth independent of the wavelength. The fit is described by the following R-square values:

- Exponential fit at 400nm = 0.56
- Exponential fit at 1000nm = 0.49
- Linear fit at 400nm = 0.93
- Linear fit at 1000nm = 0.87

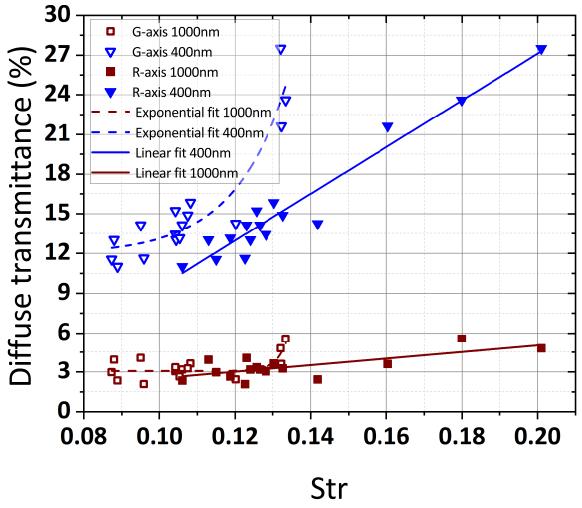

Figure 5.17: Scatter plot of the correlation between S_{st} and T_D for 400nm and 1000nm for HC texturing

The exponential fit is low which means that the fit provides limited explanation for the behaviour shown along the G-axis. Nevertheless, some type of asymptotic behaviour is observed. This implies that higher T_D-values are characterised by a low increase in S_{tr} along the G-axis. The linear fit provides an accurate explanation for the behaviour but the rate of increase differs between wavelengths. Smaller wavelengths are easier to affect, which results in a steeper linear curve while the opposite occurs for larger wavelengths that shows a lower response. Since the increase for larger wavelengths is more moderate, the R-square values for 1000nm are lower.

In section 5.3.1 is described that the high diffusivity is described by an increased difference between crater depths measured along the G- and R-axis. This behaviour is also confirmed in figure 5.17. The difference between both depths measured along the 2 axes increases which result in this higher diffusivity. Since the scattering behaviour along the G-axis is described by a exponential- or asymptotic behaviour and along the R-axis by a linear behaviour, the difference between both depths along the 2 axes increases. This results than in the increased scattering behaviour.

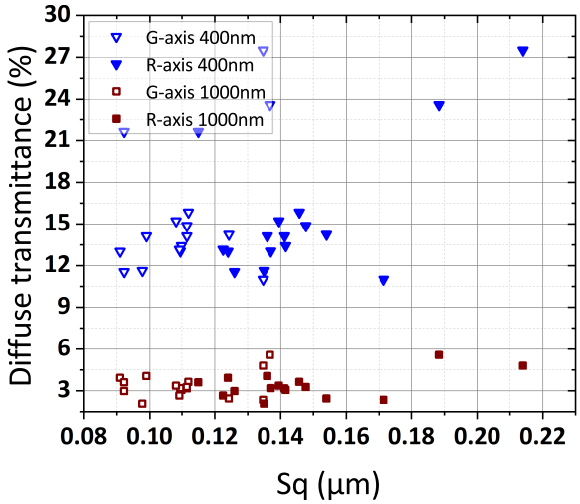

Figure 5.18: Scatter plot of the correlation between S_q and T_D for 400nm and 1000nm for HC texturing

The correlation to the diffusivity cannot be described by a sigmoid function and there is no indication that saturation occurs for increasing S_c/S_q. This implies that a further increase in diffusivity can still be created for this process, while also considering the electrical aspect. Since the depth can be changed independent from the width of the craters (different periodicity of the mask can be changed with different mask), a higher tunability is created which causes saturation effects seizing to occur. Second, it give a higher tunability in terms of creating the craters that match best with the deposited layers on top.

Parameter S_{sk} does not show a trend in figure 5.19 but high optically performing samples show characteristic values. Samples with a low optical response show along the R-axis S_{sk}-values (at 400nm: T_D [12-15]%) of around -0.4, which implies that the light interacts with a larger flat surface area so less light is diffused. The highest performing samples go towards values lying closer to 0 which means that more light can get diffused. Second, along the G-axis the inverse seems to occur. Increased diffusivity is characterised high S_{sk}-values, this seems counter-intuitive but because it represents the periodicity of the texture it does not show the absolute peak values. Since it does not show the peaks of the texture but the etching hemisphere keep increasing, this can be interpreted as an increase in flat surface area for the parameter. Every parameter values must be carefully interpreted otherwise it leads to wrong conclusions.

Parameter S_{ku} does not show any real trends B.4, all values though stay below 3 which implies that they are classified as smooth and no problems are predicted to occur for the electrical compatibility. Along the G-axis, high optically scattering samples have higher values than low scattering samples. Along the R-axis, no distinction can be made which seems logical because the sharpness of a texture from a macroscopic scattering point of view does only affect the angle where it scatters light too. This aspect of the light cannot be measured by the macroscopic R,T- measurements.

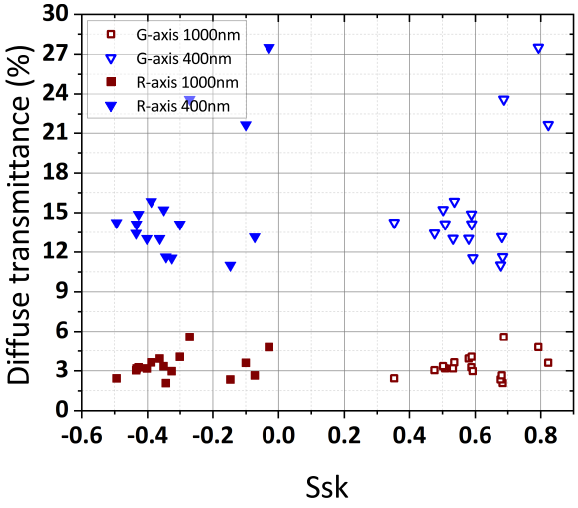

Figure 5.19: Scatter plot of the correlation between S_{sk} and T_D for 400nm and 1000nm for HC texturing

To conclude, parameters S_q and S_c are affecting the light the most but since periodic textures are considered S_{tr} is the most important parameter determining the optical performance. No trends are observed for S_{sk} or S_{ku} but for S_{sk} characteristic values towards 0 for the R-axis and towards 0.8 and higher for the G-axis accompany a higher performance.

5.3.6. Angular intensity distribution analysis

In section 5.3.4 is already established that the HC-texture scatters incident light. Since the macroscopic R,T measurements cannot distinguish the difference between random scattering phenomena (like Rayleigh-, Mie- or macroscopic scattering) and periodic scattering phenomena, an optical comparison is not justified between both. Second, it is unknown how these diffraction phenomena react in function of the wavelengths and what happens to a shift in scattering angle. To asses this, the wavelength interaction is measured at 400, 600, 800, 900 nm and to represent an actual solar cell better, 30nm of a-Si is deposited on top of the wafer.

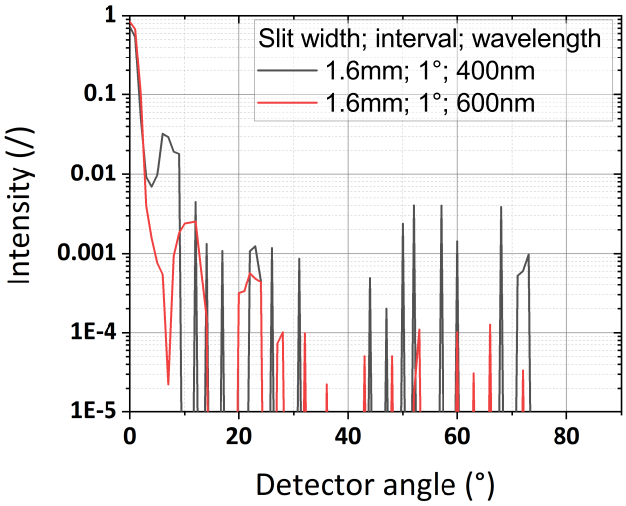

Figure 5.20: AID at 600nm and 400nm for HC-texture with PR 3012-2.1µm etching for a straight 24min.

One of the optical optimal wafers (3012-2.1µm straight etch for 24min) is chosen to asses the AID with and the response at 600nm is shown in figure 5.20. From a periodic structure is expected that diffraction

phenomena occur and with an AID this must be measured. The initial intensity is almost equal to 1 which is expected from a 0th order peak. From this point on, the 1st order peak is measured around 12° and the 2nd order around 22°. After this point, only noise is measured and the 3th or 4th order could not be measured because the 3th and 4th order are expected to occur around 30° and 40°. In section 2.3.2 is discussed that periodic textures do not show a symmetrical light distribution which means that only this measurement is not enough to describe the scattering spectrum. Therefore, the measurements must be performed again under a rotation of 30° around its center axis. This measurement is shown in figure 5.21. It shows a shift towards the right of around 1-2% and the first order peak describes a higher intensity while the second order shows a lower intensity. This measurement confirms the complete scattering behaviour requires 2 AID measurements.

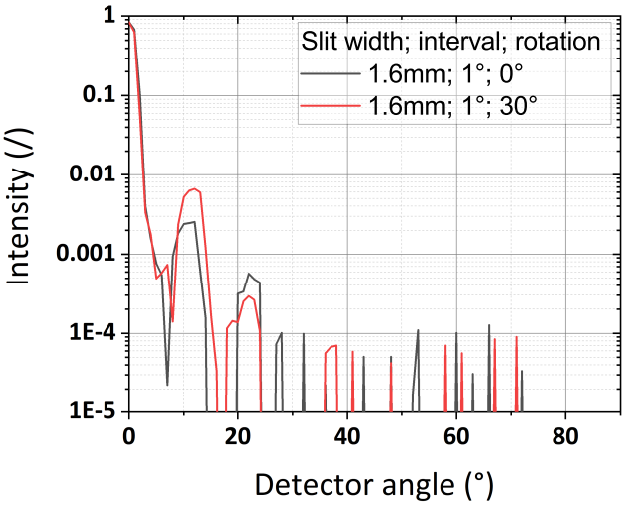

Figure 5.21: AID at 600nm for HC-texture rotated 30° around its center axis with PR 3012-2.1µm etching for a straight 24min.

If the wavelength is decreased to 400nm (shown in figure 5.20), a shift to the left of the 1st order is observed from 12° to 6°. Unfortunately, the 2nd or other orders are not accurately measured. The measurement at 800nm or 900nm shows a lot of noise which means the measurements cannot be used for analysis (shown in figure 5.22). The only noticeable point is the peak around 25° at 900nm which looks like a first order peak. If a simple extrapolation is performed for the shift between 400nm and 600nm, the first order peak must lie around 21° under the assumption that the shift shows a linear correlation to the wavelength. The deviation between 21° and 25° is still significant but it can show a clear trend if this is the actual 1st order peak at 900nm. This type of behaviour is very beneficial for a cell because the HC-texture has the purpose of scattering the higher wavelengths through the cell.

So far has been confirmed that in an air-glass-air interface a beneficial shift towards increasing angles is made for higher order peaks. To see, if these effects would also occur in a real solar cell a high refractive index material is put on top of it. Although an air interface is still used, this is the closest representation of reality possible. The deposition of 30nm a-Si resulted in a response of 600nm shown in figure 5.23. The initial intensity decreases again due to the increased reflectance but in general a vertical shift upwards is shown, which implies an increased optical performance is the result. The grating effect observed for the air-glass-air interface is removed and a smooth transition between different peaks is observed.

The response in the AID shown here, shows a grating effect but inside the cell this effect is small/ negligible and the response becomes more like an exponential decrease that stabilises at some point. The measurement radius is equal to 9cm which compared to a couple µm in a cell is negligible. With the introduction of a-Si, this grating effect is already avoided and inside the cell it is certainly negligible. The exponential decrease is vertically shifted upwards which indicates the HC has a better performance.

This section confirms that the created periodic textures create a periodic scattering profile that is not symmetrical. To form a complete scattering profile, the textures must be rotated 30° around its center.

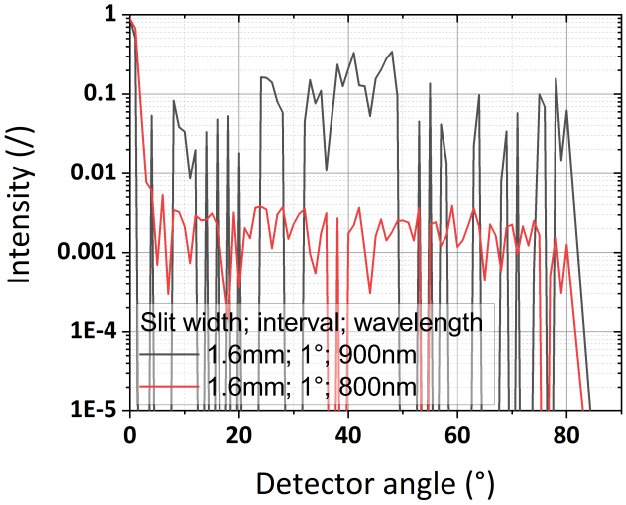

Figure 5.22: AID at 800nm or 900nm for HC-texture with PR 3012-2.1µm etching for a straight 24min

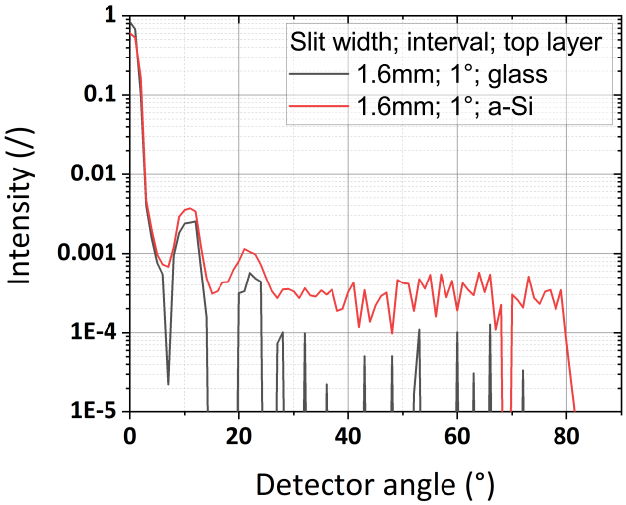

Figure 5.23: AID at 600nm while introducing an a-Si layer for HC-texture with PR 3012-2.1µm etching for a straight 24min

Second, higher wavelengths inside a cell benefits from the fact that the peaks shift towards higher angles which means that more light can be absorbed. From AID measurements is concluded that the HC structures matches optically good with the high refractive index layers because a vertical shift upwards in intensity is measured. In some of the measurements, noise is a dominant aspect in overshadowing the actual measurement. This can be avoided by increasing the measurement intervals to 2° (in this work 1° is used) and opening the slit widths a bit.

5.3.7. Electrical cell performance

In the previous section, there is determined what type of texture optimally scatters light. This resulted in a wafer with PR 3012-2.1µm etched straight for 24min, resulted in having the strongest diffraction response. This sample is used to process a nc-Si cell on with an identical stack as for the random textures superstrates 4.41. This results in the response shown in figure 5.24. The fill factor (FF) is significantly low and efficiencies are not able to be measured. This can be caused by a series resistance inside the cell that is too high, the deposition of the TCO was not the best which could have caused this problem. By applying a negative bias of -1V on the sample, the EQE gives the expected result.

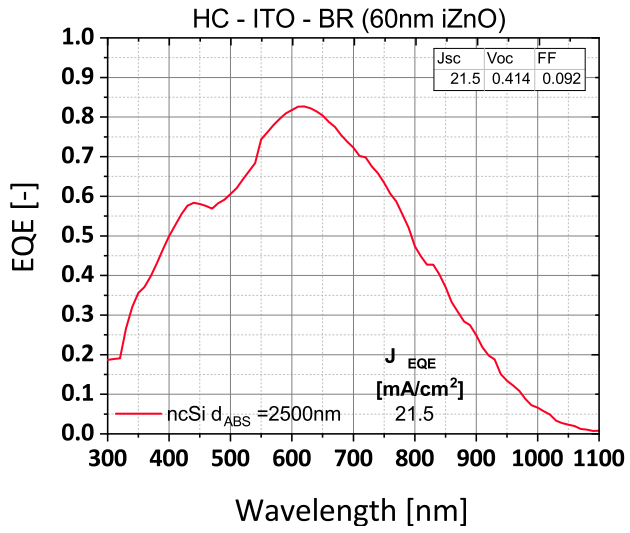

Figure 5.24: Nc-Si cells made on top of glass HC textured superstrates. d_{abs} determines the thickness of the silicon layer and J_{eqe} determines the produced current.

A current of 21.5 mA/cm² is measured which is a decent response although it does not exceed expectations. The dent in the graph between 450-550nm is an indication of a poor ITO deposition which has poor nano-texture and a bad electrical properties. From 700nm on, small dents are created which indicate that interference occurs for the high wavelength range. This can imply 2 things, the textures are not able to scatter the light enough or the absorber thickness is not large enough. In section 5.1 is stated that a bad match of the layer thickness with HC textures also create interference patterns which limits its performance. Since only 2.5µm of nc-Si is deposited, this is probably the cause of these small interference patterns. There is concluded that more cells must be processed to get a better assessment of the performance of these HC but this cell can be used as a proof of concept.

5.4. Results: Comparison random and periodic texturing

As stated before, periodic- and random textures cannot be compared to each other via the R,T measurements but the AID measurements give the option to already compare both types to each other. A comparison between these 3 types of textures is shown with and without an a-Si deposition on top in figure 5.25.

Without the a-Si deposition, the produced HC performs similar/ to slightly worse compared to the produced AZO sacrificial samples if there is an exponential decrease assumed (connecting the peaks of the diffraction orders). For the deposition of a-Si, ITO and AZO suffer both in their exponential decay while HC has an increased performance. In this case, the HC performs better than AZO for 20° on but still worse than ITO. This leads to the conclusion that with the current wafers, the performance of HC must exceed the one of AZO but ITO will remain dominant.

Since identical cell stacks are made for the different textures, a comparison is made possible. It must be noticed that cells processed on the HC texture, did not provide an efficiency and the EQE is measured on -1V. This results in a more optimistic look because aspects like series- and parallel restistances are taken out of the question. Considering this, the response of HC after 650nm is similar to the random textured cells and a comparison of the EQE's is visualised in table 5.2. Between 600-750nm, the HC-cell outperforms the random textures and where the AZO-cell shows the lowest response. After 800nm, the ITO-cell becomes the superior and the HC-cell performs 1% worse than the other cells from 900nm. This indicates that the created HC texture does not performs the worst, which lies conform with the optical predictions made before. It must be kept in mind that a bias voltage of -1V is used.

At 600nm, the HC-cell performs superior compared to the other textures but if this is compared to the macroscopic diffusivity measurement this does not match, which justifies the statement that for R,T measurements periodic and random textures cannot be compared to each other. If this is compared to

Table 5.2: The EQE for identical nc-Si solar cell stacks at different wavelengths using the best optical performing samples for each type of texture (shown in figure 4.41).

nc-Si stack	**Wavelength (nm)**								
Texture type	600	650	700	750	800	850	900	950	1000
HC	0.82	0.8	0.72	0.65	0.47	0.37	0.25	0.14	0.06
AZO	0.71	0.73	0.67	0.57	0.47	0.37	0.26	0.15	0.07
ITO	0.76	0.76	0.7	0.6	0.5	0.39	0.27	0.16	0.08

the AID measurements, there remains a mismatch in conclusions but the prediction is made that the HC texture would outperform the AZO texture is correct. The bias voltage of -1V could have affected the result in this case. Nevertheless, the performance has the same order of magnitude which confirms that the HC-texture contributes to the scattering of light in the cell.

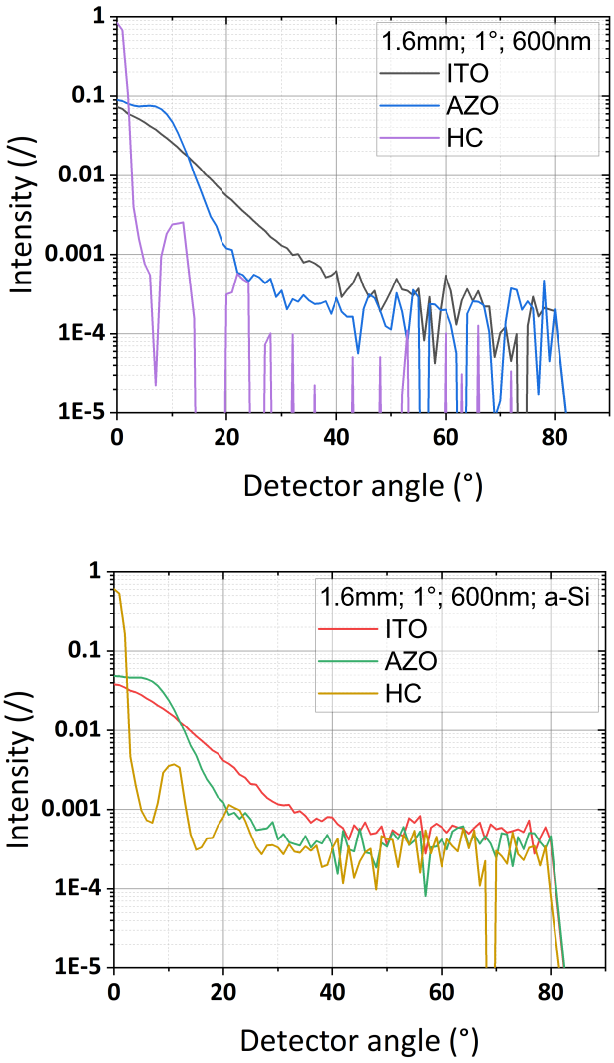

Figure 5.25: AID measurements compared between the 3 different samples at 600nm including or excluding an a-Si deposition.

5.5. Recommendations

For the HC texturing, the possible future work is more extensive. To reach the required aspect ratio, a time series must be created to obtain the absolute values. The focus must be put on 18, 26min because these are the most interesting points in this case. Based upon these results, the ratio of BHF (in this work 7:1 is used) can be changed towards 8:1 etc.

To fully avoid the large defects observed after processing on the wafers, higher quality Corning glasses must be used. This must only be opted for in case these defects affect the performance of the cell significantly.

There can also be opted for baking the PR more to increase the chemical resilience for thicker layers of PR and to be certain the layer is hardened out. This can also be performed as extra insurance for the current used thicknesses.

The cleaning procedure before and after processing must be further researched to increase adhesion with the PR. Afterwards, the cleaning procedure must be researched to obtain a particle free superstrate.

6

Conclusion

In the introduction 5 different research questions are stated to be solved:

1. Which process parameters create strong scattering random textures on glass superstates and how do these parameter influence the scattering performance at longer wavelengths?
2. Which profile parameters influence the light scattering performance (longer wavelengths) of the sample?
3. Is it possible to create reproducible periodic textures on glass superstrates? And how can their scattering performance be increased?
4. How does a texture scatter light on an angular level? And how are they different from each other?
5. Does periodic texturing lead to a higher optical- and/or electrical performance in comparison with random texturing?

For ITO sacrificial texturing, the optimal processing range of the sacrificial layer lies around P=190-210W; T=230-250°C; t=7200s; 5-10rpm. In this work, process parameters P=210W; T=230°C; t=7200s; 5rpm is chosen as optimum to asses further in depth to perform AID on and process cells on because it showed the highest Haze values between 92-86% for 300-1200nm. For AZO, the optimal process parameters are set at P=400W; T=400°C; t=7200s and similar characteristics influencing T_D are observed. The haze-values lie between 91-73% for 300-1200nm. If the optical response of both textures is compared to each other, ITO-textures are superior and must be used for future random textures.

The parameter determining the diffusivity of random textures the most, is the depth of the crater defined as S_q or S_c. The width S_{al} or aspect ratio S_{tr} show less of a trend. S_{al} and S_{ku} only show a characteristic value-range for samples showing high amounts of diffusivity. Second, sacrificial texturing methods show that a correlation exists between the depth- and width of the crater. This is important when thinking about growing nc-Si layers on top of it and when simulation of textures is involved in optical simulation software (such as GenPro4). The parameter determining the diffusivity of the periodic textures the most is the aspect ratio S_{tr}. Second, a higher diffusivity is correlated to lower S_{sk}-values (closer to 0) along the R-axis and higher values along the G-axis (further away from 0).

A stable methodology is designed to create periodic textures (honeycombs). This involves the use of photoresist on which the periodicity is created via a photolithography step. Afterwards, the periodicity and honeycombs are directly transfered into the superstrate with the use of BHF. Although some defects resulted out of this process, the optical response and physical parameters are able to be reproduced. The target of reaching aspect ratios between 0.2-0.25 is not reached and the maximum aspect ratio produced in this work lies between 0.18-0.2.

A more accurate representation of the scattering behaviour can be described by AID-measurements. With these types of measurement an overview or detailed information can be given about the scattering in different angles based on the settings of the measurement tool. An optical comparison between random and periodic textures is possible with these measurements which is the advantage of using this type of measurement. Random textures are characterised by an exponential decay for light scattering in small angles and Lambertian decay for light scattering in higher angles, for which ITO textures are superior in scattering light in higher angles. Periodic textures are characterised by diffraction pattern which inside the

cell acts more as a exponential decaying curve which stabilises at a certain point. The created periodic textures will have according to these measurements a similar performance inside an actual cell compared to the AZO textures. Out of all textures, ITO will perform the best because there is still extensive optimisation possible for the HC textures.

According to the made solar cells, the HC-textures performs in terms of J_{sc} slightly better than the random textures but because a bias of -1V is used in an a proper working cells (no efficiency could be measured), it will perform slightly worse. The scattering properties of the HC are proven but to exceed electrical performance inside a cell, the thickness of the nc-Si layer must be increased towards 3.5µm. Second, creating deeper craters can be required if this proves not to be enough.

References

[1] ADRIAN GIORDANI. “Cost of climate change in Europe could reach 4 % of GDP”. In: *Horizon* (). URL: https://ec.europa.eu/research-and-innovation/en/horizon-magazine/cost-climate-change-europe-could-reach-4-gdp.

[2] Planbureau voor de leefomgeving. “Correctie formulering over overstromingsrisico Nederland in IPCC-rapport”. In: *IPCC-rapport* (). URL: https://www.pbl.nl/correctie-formulering-over-overstromingsrisico.

[3] UCL. “Economic cost of climate change could be six times higher than previously thought”. In: *UCL* (). URL: https://www.ucl.ac.uk/news/2021/sep/economic-cost-climate-change-could-be-six-times-higher-previously-thought.

[4] U.S. Departement of Energy. “Top 6 Things You Didn’t Know About Solar Energy”. In: *Departement of Energy* (). URL: https://www.energy.gov/articles/top-6-things-you-didnt-know-about-solar-energy#:~:text=Solar%5C%20energy%5C%20is%5C%20the%5C%20most,the%5C%20world's%5C%20total%5C%20energy%5C%20use.

[5] Energydata. “Global Solar Atlas”. In: (). URL: https://globalsolaratlas.info/map?c=11.609193,8.4375,3.

[6] Arno Smets et al. *Solar Energy: The physics and engineering of photovoltaix conversion technologies and systems*. UIT Cambridge, 2016.

[7] Energydata. “Comprehensive Guide to Solar Panel Types”. In: (). URL: https://aurorasolar.com/blog/solar-panel-types-guide/.

[8] Thierry de Vrijer et al. “Advanced textured monocrystalline silicon substrates with high optical scattering yields and low electrical recombination losses for supporting crack-free nano- to polycrystalline film growth”. In: *Energy Science Engineering* 9.8 (2021), pp. 1080–1089.

[9] Indrajit Dutta et al. “Fundamentals of Glass Technology Applications for Advanced Semiconductor Packaging”. In: *2019 IEEE 69th ECTC* (). URL: https://www.corning.com/media/worldwide/csm/documents/Fundamentals%5C%20of%5C%20Glass%5C%20Technology%5C%20&%5C%20Applications%5C%20for%5C%20Advanced%5C%20Semiconductor%5C%20Packaging_ECTC%5C%202019.pdf.

[10] A. V. Shah et al. “Thin-film Silicon Solar Cell Technology”. In: *Progress in Photovoltaics: Research and Applications* 12.2-3 (2004), pp. 113–142.

[11] Ratno Sircar et al. “Design and Simulation of Thin-Film Silicon Quantum Well Photovoltaic Cell”. In: *Journal of Nano- and Electronic Physics* 3.2 (2011), pp. 11–18.

[12] Rajat Acharya. *Satellite Signal Propagation, Impairments and Mitigation*. Academic Press, 2017.

[13] Yu Zongfu et al. “Fundamental limit of light trapping in grating structures”. In: *Optics Express* 18.103 (2010), A366–A380.

[14] Olindo Isabella et al. “Modulated surface-textured substrates with high haze: From concept to application in thin-film silicon solar cells”. In: *Conference Record of the IEEE Photovoltaic Specialists Conference* (2011).

[15] Guantao Yang et al. “A novel way of texturing glass for microcrystalline silicon thin film solar cells application”. In: *Progress in Photovoltaics: Research and Applications* 23.10 (2015), pp. 1283–1290.

[16] Richard Leach. *Fundamental Principles of Engineering Nanometrology (Second Edition)*. William Andrew Publishing, 2014.

[17] Nicolas Duboust et al. “An optical method for measuring surface roughness of machined Carbon Fibre Reinforced Plastic composites”. In: *Journal of Composite Materials* 51 (2016).

[18] Franz Konstantin Fuss. “The effect of surface skewness on the super/postcritical coefficient of drag of roughened cylinders”. In: *Procedia Engineering* 13 (2011), pp. 284–289.

[19] Klaus Jäger et al. “Angular resolved scattering measurements of nano-textured substrates in a broad wavelength range”. In: *Measurement Science and Technology* 22 (2011).

[20] Guangtao Yang. “High-efficient n-i-p thin-film silicon solar cells”. In: (2015). URL: https://repository.tudelft.nl/islandora/object/uuid%5C%3A50a4a249-3373-48b4-90b9-5ed2b7098579.

[21] Hairen Tan et al. “Highly transparent modulated surface textured front electrodes for high-efficiency multijunction thin-film silicon solar cells”. In: *Progress in Photovoltaics: research and applications* 23.8 (2015), pp. 949–963.

[22] Ocal Tuna et al. “High quality ITO thin films grown by dc and RF sputtering without oxygen”. In: *Journal of Physics D: Applied Physics* 43.5 (2010).

[23] Sukanta Bose et al. “Sacrificial layer assisted front textured glass substrate with improved light management in thin film silicon solar cells”. In: *Journal of Materials Science: Materials in Electronics* 30.3 (2019), pp. 2622–2629.

[24] A. G. Aberle et al. “Glass texturing”. In: *International PCT patent application* WO 2004/089841 A1 (2004).

[25] Oliver Kluth et al. “Modified Thornton model for magnetron sputtered zinc oxide: film structure and etching behaviour”. In: *Thin Solid Films* 442.1 (2003), pp. 80–85.

[26] M. Python O. Madani et al. “Influence of the substrate geometrical parameters on microcrystalline silicon growth for thin-film solar cells”. In: *Solar Energy Materials and Solar Cells* 93.10 (2009), pp. 1714–1720.

[27] Matt Hughes. “What is Plasma Enhanced Chemical Vapor Deposition (PECVD)?” In: (2022). URL: https://www.semicore.com/news/118-what-is-plasma-enhanced-chemical-vapor-deposition-pecvd.

[28] Thomas Loef. “Periodic-Random Modulated Surface Textures For Efficient Light Trapping in Thin-Film Silicon Solar Cells”. In: (2018). URL: https://repository.tudelft.nl/islandora/object/uuid%5C%3Ad48a285f-cf84-40a3-b806-3211afa9c45e.

[29] Hitoshi Sai et al. “Enhanced photocurrent and conversion efficiency in thin-film microcrystalline silicon solar cells using periodically textured back reflectors with hexagonal dimple arrays”. In: *Applied Physics Letters* 101.17 (2012).

[30] Thierry de Vrijer et al. “The optical performance of random and periodic textured mono crystalline silicon surfaces for photovoltaic applications”. In: *EPJ Photovoltaics* 13 (2022).

[31] Park Hyeongsik et al. “Fabrication of honeycomb textured glass substrate and nanotexturing of zinc oxide front electrode for its application in high efficiency thin film amorphous silicon solar cell”. In: *Journal of Photonics for Energy* 7.2 (2017).

[32] D. Eisenhauer et al. “Honeycomb micro-textures for light trapping in multi-crystalline silicon thin-film solar cells”. In: *Optics Express* 26.10 (2018), A498.

[33] Hitoshi Sai et al. “Relationship between the cell thickness and the optimum period of textured back reflectors in thin-film microcrystalline silicon solar cells”. In: *Applied Physics Letters* 102.5 (2013).

[34] Jicheng Zhou et al. “Effect of front surface light trapping structures on the PERC solar cell”. In: *SN Applied Sciences* 2.5 (2020).

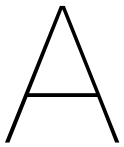

Appendix

CORNING

EAGLE XG®

Glass Substrates

Material Information

CORNING

Glass Type – Alkaline earth boro-aluminosilicate
Forms Available – Fusion-drawn sheet
Principal Uses – Substrates for active-matrix flat panel displays

Properties

Where applicable, units are stated in Metric and English

Mechanical

	Metric	English
Density (20°C, 68°F)	2.38 g/cc	148.5 lb/ft^3
Young's Modulus	73.6 GPa	10.7 x 10^6 psi
Shear Modulus	30.1 GPa	4.4 x 10^6 psi
Poisson's Ratio	0.23	
Vickers Hardness (200 gm load, 25 sec dwell)	640	

Thermal Expansion

0 - 300°C	31.7 x 10^{-7}/°C (0 - 300°C)	17.7 x 10^{-7}/°F (32 - 572°F)
Room Temperature	35.5 x 10^{-7}/°C	19.7 x 10^{-7}/°F
To Setting Point	(25 – 675°C)	(77 – 1247°F)

Thermal Conductivity

Thermal conductivity is a calculated value, and is equal to the product of the thermal diffusivity multiplied by specific heat multiplied by the density of the glass.

Temp (°C)	Specific Heat (J/gm- °K)	Thermal Diffusivity (cm^2/sec)	Thermal Conductivity (W/cm-°K)
23	0.768	0.00601	0.0109
100	0.896	0.00572	0.0122
200	0.998	0.00546	0.0129
300	1.067	0.00530	0.0134
400	1.110	0.00522	0.0137
500	1.154	0.00518	0.0142

Viscosity

Working Point (10^4 poises)	1293
Softening Point (10$^{7.6}$ poises)	971
Annealing Point (10^{13} poises)	722
Strain Point (10$^{14.5}$ poises)	669

Electrical

Log_{10} Volume Resistivity (ohm-cm)

12.9 (250°C, 482°F)
8.8 (500°C, 932°F)

Dielectric Constant

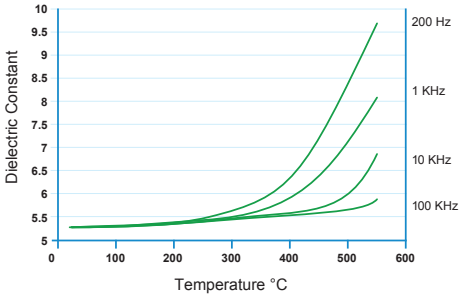

Dielectric Constant: 5.27
(20°C/68°F – 1 kHz)

Dissipation Factor (Loss Tangent)

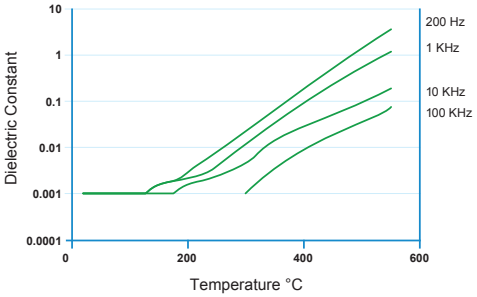

Loss Tangent: 0.30%
(20°C/68°F – 1 kHz)

Chemical

Weathering: 1
Weathering is defined as corrosion by atmospheric-borne gases and vapor such as water and carbon dioxide. Glasses rated 1 will almost never show weathering effects; those rated 2 will occasionally be troublesome, particularly if weathering products cannot be removed; those rated 3 require more careful consideration.

Durability:
Durability is measured via weight loss per surface area after immersion. Values are highly dependent upon actual testing conditions. Unless otherwise noted, concentrations refer to weight percent.

Reagent	Time	Temp	Weight Loss (mg/cm²)
HCl – 5%	24 hrs	95°C	0.79
HNO_3 – 1M	24 hrs	95°C	0.49
HF – 10%	20 min	20°C	5.18
NH_4F: HF – 10%	20 min	20°C	0.84
1HF: 10HNO_3	3 min	20°C	1.48
1HF: 100HNO_3	3 min	20°C	0.16
DI H2O	24 hrs	95°C	0.00
Na_2CO_3 – 0.02N	6 hrs	95°C	0.16
NaOH – 5%	6 hrs	95°C	1.83

Total alkali content is approximately: 0.1 wt%
(Typical < 0.05 wt%)

Optical Wavelength	Refractive Index
435.8 nm	1.5198
467.8 nm	1.5169
480 nm	1.5160
508.6 nm	1.5141
546.1 nm	1.5119
589.3 nm	1.5099
643.8 nm	1.5078

Birefringence Constant

331 (nm/cm)/(kg/mm²)

Transmittance

UV Transmission

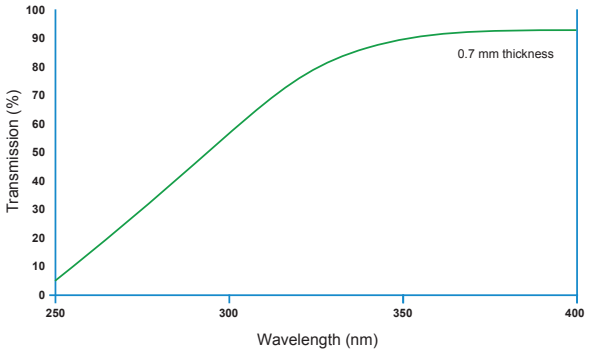

Optical Transmission

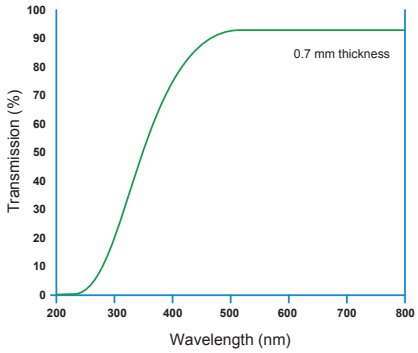

North America and all other countries
Corning Display Technologies
MP-HQ-W1
Corning, NY 14831
United States
Telephone: +1 607-974-9000
Fax: +1 607-974-7097
Internet: www.corning.com/displaytechnologies

Japan
Corning Japan K.K.
Main Office
Akasaka Intercity 7th floor
1-11-44, Akasaka
Minato-ku, Tokyo 107-0052 Japan
Telephone: +81 3-5562-2260
Fax: +81 3-5562-2263
Internet: www.corning.co.jp

Nagoya Sales Office
Nihon Seimei Sasashima Bldg., 15th floor,
27-2 Meieki minami 1-chome, Nakamura-ku,
Nagoya 450-0003 Japan
Telephone: +81-52-561-0341
Fax: +81-52-561-0348

China
Corning China (Shanghai)
Regional Headquarters
31/F, The Center
989 Chang Le Road
Shanghai 200031
P.R. China
Telephone: +86 21-5467-4666
Fax: +86 21-5407-5899
Internet: www.corning.com/displaytechnologies/sc

Corning Display Technologies (China) Co., Ltd.
No. 22, South Tongji Road
Beijing Economic & Technology Development
Area (BDA), Beijing
Beijing 101102, China
Telephone: +86-10-67873838
Fax: +86-10-67856653
Internet: www.corning.com/displaytechnologies/sc

Taiwan
Corning Display Technologies Taiwan Co., Ltd.
Room #1203, 12F, No. 205
Tun Hua North Road,
Taipei 105, Taiwan
Telephone: +886 2-2716-0338
Fax: +886 2-2716-0339
Internet: www.corning.com.tw

Korea
Samsung Corning Precision Glass Co., Ltd.
20th Floor, Seocho HQ Building, Samsung
Electronics
1320-10, Seocho-dong, Seocho-gu, Seoul, Korea
Telephone: +82 2-2255-2777
Fax: +82 2-2255-2739
Internet: www.samsungscp.co.kr

CORNING

PIE 301 | 4

CORNING

EAGLE XG® Glass

Exceptional Dimensional Stability and Surface Quality in Thin, Large-Size Sheets

Corning® EAGLE XG® Glass is considered the most widely used and trusted glass by the world's leading panel makers, and was the first glass composition to include no heavy metals. Available in the widest variety of form factors, EAGLE XG® Glass can be made as thin as 0.25 mm up to Gen 5.5, 0.3 mm up to Gen 6, 0.4 mm up to Gen 8.5, and 0.5 mm up to Gen 10.5 to enable thinner, lighter, and curved display panels.

Product & Material Information

Corning® EAGLE XG® Glass is produced to the following type specifications:

Material Information		
Glass Type	Alkaline Earth Boro-Aluminosilicate	
Forms Available	Fusion Drawn Sheet	
Principle Uses	Substrates for active-matrix flat panel displays	
Mechanical Properties	Density (20°C)	2.38 g/cc^3
	Young's Modulus	73.6 GPa
	Shear Modulus	30.1 GPa
	Poisson's Ratio	0.23
Thermal Expansion	Coefficient of Thermal Expansion (0 - 300°C)	31.7x10^{-7} / °C
	Room Temperature to Setting Point	35.5x10^{-7} / °C (25-675°C)
Viscosity	Working Point (10^4 poises)	1293°C
	Softening Point (10$^{7.6}$ poises)	971°C
	Annealing Point (10^{13} poises)	722°C
	Strain Point (10$^{14.5}$ poises)	669°C
Electrical Properties	Log^{10} Volume Resistivity	*12.9 ohm- cm* at 250°C
		8.8 ohm- cm at 500°C
Optical Properties	Birefringence Constant	331 (nm/cm) /(kg/mm^2)

Electrical

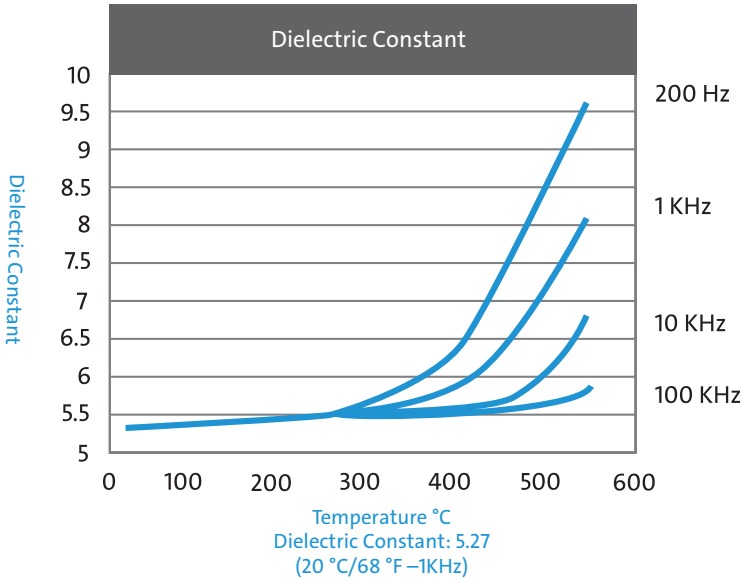

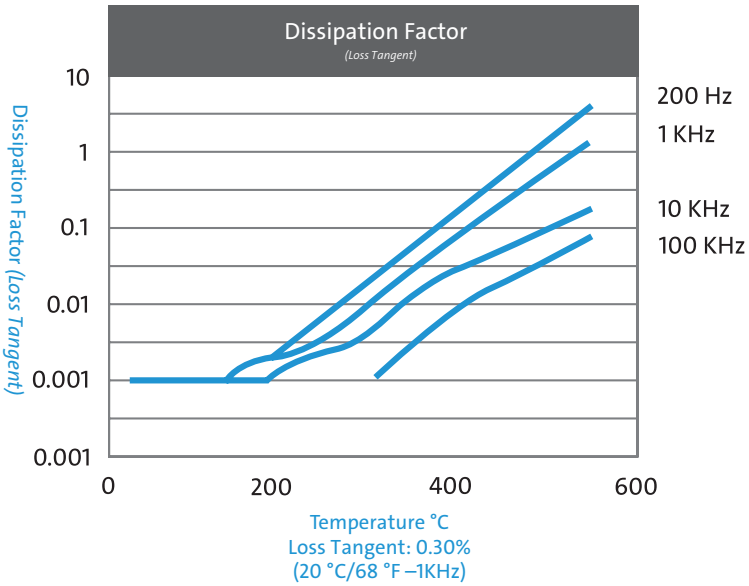

Issued: December 2021

Chemical Durability

Chemical durability is measured via weight loss per surface area after immersion. Values are highly dependent upon actual testing conditions. Unless other- wise noted, concentrations refer to weight percent

Reagents	Time	Temp	Weight Loss (mg/cm^2)
HCl - 5%	24 hrs	95°C	0.79
HNO_3 - 1M	24 hrs	95°C	0.49
HF - 10%	20 min	20°C	5.18
NH_4F:HF - 10%	20 min	20°C	0.84
1HF:10HNO_3	3 min	20°C	1.48
1HF:100HNO_3	3 min	20°C	0.16
DI H_2O	24 hrs	95°C	0.00
Na_2CO_3 - 0.02N	6 hrs	95°C	0.16
NaOH - 5%	6 hrs	95°C	1.83

Total alkali content is approximately: 0.1wt% (Typical <0.05wt%)

Weathering: 1

Weathering is defined as corrosion by atmospheric-borne gases and vapor such as water and carbon dioxide. Glasses rated 1 will almost never show weathering effects; those rated 2 will occasionally be troublesome, particulary if weathering products cannot be removed; those rated 3 require more careful consideration.

Optical Wavelength	Refractive Index
435.8nm	1.5198
467.8nm	1.5169
480nm	1.5160
508.6nm	1.5141
546.1nm	1.5119
589.3nm	1.0599
643.8nm	1.5078

Transmittance

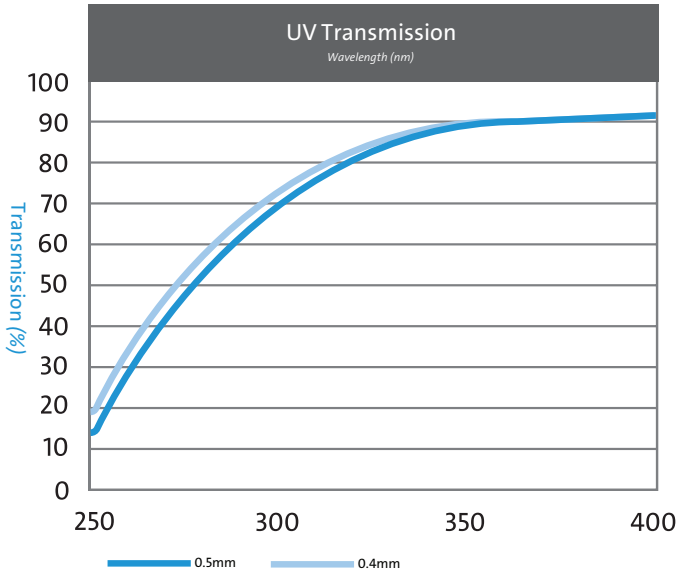

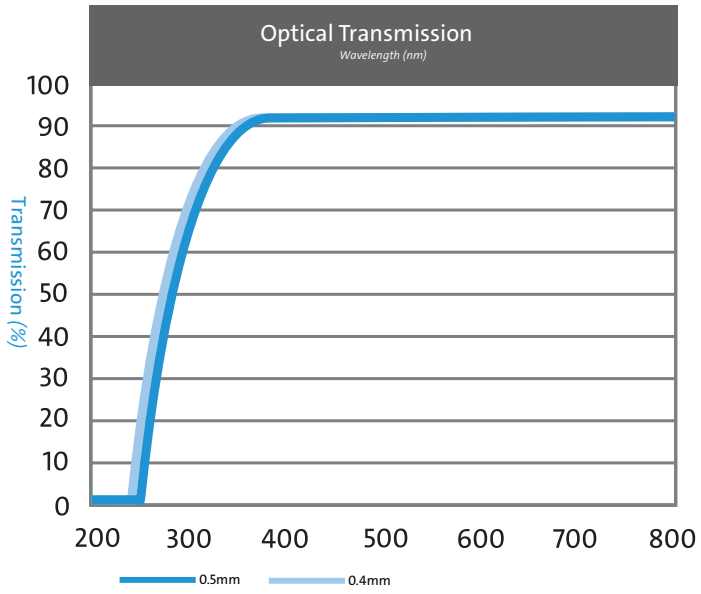

Thermal Conductivity

Thermal conductivity is a calculated value, and is equal to the product of the thermal diffusivity multiplied by specific heat multiplied by density of the glass.

Temp (°C)	Diffusivity (cm^2/sec)	Specific Heat(J/gm-°K)	Conductivity (W/cm -°K)
23	0.00601	0.768	0.0109
100	0.00572	0.896	0.0122
200	0.00546	0.998	0.0129
300	0.00530	1.067	0.0134
400	0.00522	1.110	0.0137
500	0.00518	1.154	0.0142

For additional product or technical information, please visit www.corning.com/worldwide/en/products/display-glass.html. To obtain additional technical information, an engineering sample, or to place an order for this product, please contact us at: Tel: +1-607-974-9000 mail: display@corning.com

Issued: December 2021

B

Appendix

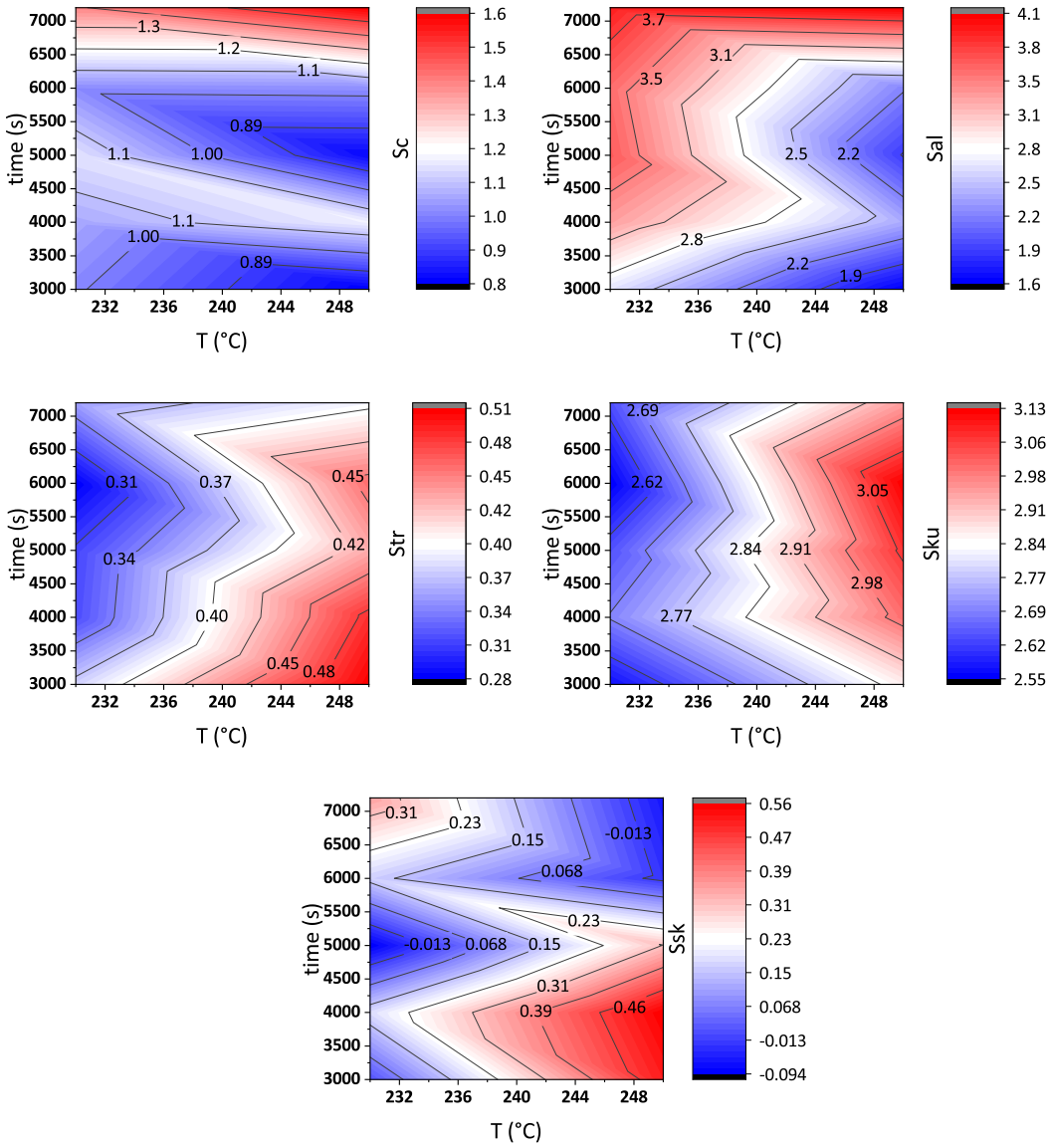

Figure B.1: Contour plots describing the influence of deposition time and T for S_c, S_{al}, S_{tr} for ITO-sacrificial texturing

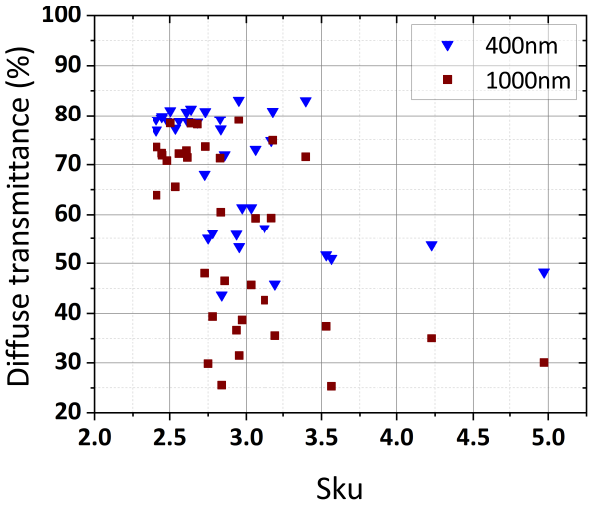

Figure B.2: Scatter plot of the correlation between S_{ku} and T_D for 400nm and 1000nm for ITO-sacrificial texturing

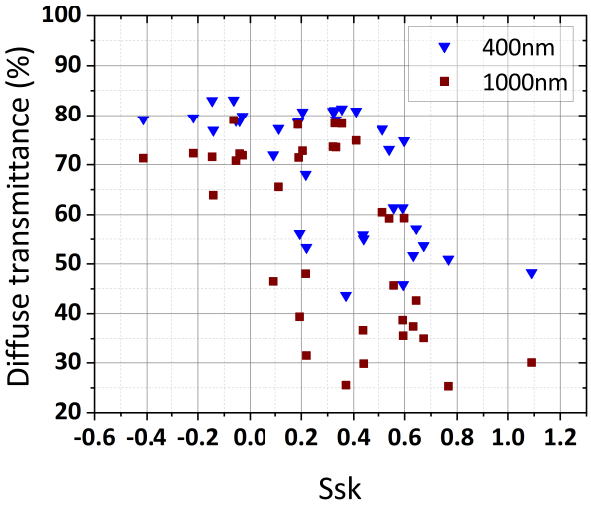

Figure B.3: Scatter plot of the correlation between S_{sk} and T_D for 400nm and 1000nm for ITO-sacrificial texturing

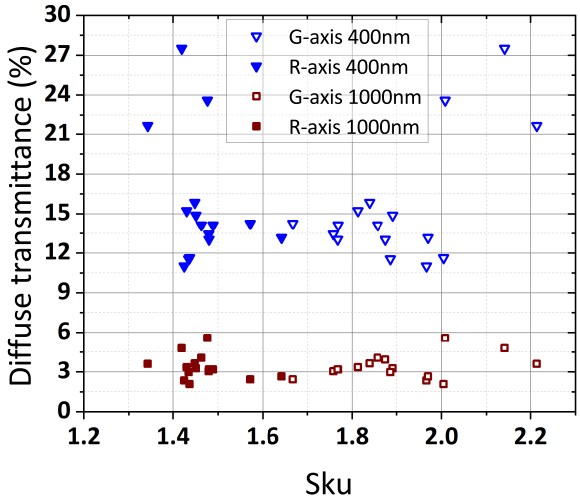

Figure B.4: Scatter plot of the correlation between S_{ku} and T_D for 400nm and 1000nm for HC texturing